DEPOSITIONAL SETTING AND CONTROLS ON POROSITY DEVELOPMENT IN THE MARMATON GRANITE WASH, SOUTHWESTERN ANADARKO BASIN, WESTERN OKLAHOMA AND TEXAS PANHANDLE

By

AUTUMN M. GRAF

Bachelor of Science in Geology

Oklahoma State University

Stillwater, Oklahoma

2021

Submitted to the Faculty of the
Graduate College of the
Oklahoma State University
in partial fulfillment of
the requirements for
the Degree of
MASTER OF SCIENCE
May 2023

DEPOSITIONAL SETTING AND CONTROLS ON POROSITY DEVELOPMENT IN THE MARMATON GRANITE WASH, SOUTHWESTERN ANADARKO BASIN, WESTERN OKLAHOMA AND TEXAS PANHANDLE

Thesis Approved:

Dr. James O. Puckette

Thesis Adviser

Dr. Mary Hileman

Dr. Jack Pashin

ACKNOWLEDGEMENTS

I would like to extend my sincere appreciation to my thesis advisor, Dr. Jim Puckette, for allowing me to work under his guidance, wholeheartedly supporting my academic career, and sharing his incredible knowledge and passion for geology with me. This thesis would not have been possible without his encouragement and patience. I am also grateful to my committee members, Dr. Mary Hileman and Dr. Jack Pashin, for their helpful suggestions and insight.

I would also like to thank the many others who supported and assisted me throughout this project: Chase Watkins and Dylan Morton for providing invaluable advice about geologic processes and software, careers, and life as a young geologist; Keith Edmonds for financially sponsoring this project and my graduate research assistantship; Lisa Whitworth and Brent Johnson at the OSU Microscopy lab for their assistance with SEM; Vital Energy (formerly Laredo Petroleum) for loaning OSU the Kicking Bird #1-20 core used in this study and allowing us to use and publish proprietary data from their analyses; LMKR for allowing the use of GVERSE GeoGraphix software for this project through their University Grant Program; and both MJ Logs and Enverus for providing wireline logs.

Lastly, I would like to thank my family and friends for their love and encouragement. I could not have undertaken this journey without my fiancé, Jared, who has provided an endless amount of both emotional and IT support throughout the development of this project, and has always been there to check my math (whether solicited or not). A special “thank you” is due to my parents, Michael and Chandra, and my older sister, Elizabeth, who instilled in me a love for the natural world at a young age and who have been my biggest supporters since day one.

Name: AUTUMN M. GRAF

Date of Degree: MAY 2023

Title of Study: DEPOSITIONAL SETTING AND CONTROLS ON POROSITY DEVELOPMENT IN THE MARMATON GRANITE WASH, SOUTHWESTERN ANADARKO BASIN, WESTERN OKLAHOMA AND TEXAS PANHANDLE

Major Field: GEOLOGY

Abstract: The Middle Pennsylvanian (Desmoinesian) Marmaton Granite Wash is a tight gas sandstone reservoir in western Oklahoma and the Texas Panhandle that can economically produce natural gas, condensate, and natural gas liquids (NGLs). Despite being developed for years using vertical wells with varying degrees of success, the constituent low-permeability arkosic sandstones and conglomerates have become a significant gas play due to recent advancements in both hydraulic fracturing and horizontal drilling. Examination of the depositional and diagenetic processes that influence porosity development leads to a better understanding of reservoir evolution and improves targeting wells for the Marmaton Granite Wash and similar tight gas sandstone reservoirs as a whole.

This study examined three Marmaton Granite Wash cores at variable distances from the Amarillo-Wichita Uplift source area: two in Buffalo Wallow Field in Hemphill County, Texas (Dominion Grant Meek #236-1 and Fillingim #88-2) and one in Roger Mills County, Oklahoma (Laredo Kicking Bird #1-20). Sedimentary and biogenic structures as well as grain size trends in core were compared to wireline log data. Thin section analysis, scanning electron microscopy (SEM), and x-ray diffraction (XRD) were conducted to examine variations in depositional and diagenetic features and their effects on porosity development. Cross sections as well as structure and thickness maps were constructed to understand depositional trends by dividing the formation into distinct wash intervals using regionally-extensive shale markers. Porosity was not observed in thin section in Kicking Bird samples, but pores are evident in SEM images with sizes <10 μm and commonly <5 μm. The Buffalo Wallow wells displayed higher amounts of porosity and more evidence of dissolution. It is concluded that the abundant detrital clay matrix in the Kicking Bird protected grains from secondary porosity generation through dissolution. This study indicates that the wash in Buffalo Wallow wells was deposited in a middle submarine fan environment while the wash in the Kicking Bird well was deposited in a distal submarine fan environment and is likely too distal from the source area to possess ideal reservoir properties.

TABLE OF CONTENTS

Chapter Page

Chapter Page

LIST OF TABLES

LIST OF FIGURES

Figure Page

Figure Page

CHAPTER I

INTRODUCTION

1.1 Background

The Middle Pennsylvanian (Desmoinesian) Marmaton Granite Wash is a tight gas sandstone play located in the southwestern Anadarko Basin in western Oklahoma and the eastern Texas Panhandle. The formation is a known producer of natural gas, oil, condensate, and natural gas liquids (NGLs) with total cumulative production reaching 15.3 million barrels of oil (MMBO) and 351 billion cubic feet of gas by June 30, 2011 (Mitchell, 2011). The stacked-pay reservoir has been explored for hydrocarbons since the 1950s, with early vertical wells aiming to come into contact with as many stacked-pay horizons as possible by drilling through the Granite Wash while primarily targeting the deeper Early Pennsylvanian Morrow Formation and/or the Early Silurian to Early Devonian Hunton Group. Of the over 2,000 vertical wells drilled into the formation prior to 2007, most had inefficient recovery and poor economic performance due to the low permeability of the arkosic sandstones, carbonate wash, and boulder-bearing conglomerates that make up the Granite Wash (Mitchell, 2011). This low permeability encountered in vertical wells leads to the conclusion that the reservoir cannot produce volumes of natural gas at an economical rate without the use of horizontal wellbores and/or stimulation by hydraulic fracturing methods, thus classifying the Granite Wash as an unconventional reservoir. The reservoir is further classified as a liquids-rich tight gas sandstone, which are typically defined as having a

matrix permeability value of less than 0.1 milidarcy (mD) and less than 10% matrix porosity (Bahadori, 2014). Although it has been steadily developed since the early 1970s using conventional vertical wells with varying degrees of success, recent advancements in both horizontal drilling and multi-stage hydraulic fracturing that provide the ability to drill laterally into preferential zones have resulted in the play's resurgence as a significant play for petroleum production. The Marmaton Granite Wash has become a perfect model for employing novel horizontal drilling and completion technologies for targeting individual zones and consequently turning mature tight gas formations into promising plays.

Despite usually being referred to as a single play, the Granite Wash is a series of stacked deposits containing detritus sourced from eroded older Paleozoic and Precambrian granitic basement rock exposed on the rising Amarillo-Wichita Uplift throughout the Pennsylvanian and into the early Permian (**Figure 1.1**). The Granite Wash is a catch-all term for the combination of Atokan, Desmoinesian, Missourian, and Virgilian Granite Wash sediments, which are fine to very coarse-grained, poorly sorted, arkosic and lithic sands with a composition reflective of the source lithology that were shed off the Amarillo-Wichita Uplift and accumulated as a thick wedge of sediment in the deep Anadarko Basin to the northeast, adjacent to the uplift (Rothkopf et al., 2011) (**Figure 1.2**). Active tectonism and frequent changes in eustatic sea level throughout the Pennsylvanian led to cyclic sedimentation of the Granite Wash deposits. Comprised of arkosic and lithic sandstones, conglomerates, and shales, detritus shed from the uplift was deposited in stacked layers of alluvial fan, fan delta, slope, and submarine fan channel deposits with intermittent marine shales and carbonates (Wei and Xu, 2016). Granite Wash sediments deposited adjacent to and just to the northeast of the Amarillo-Wichita Uplift source area tend to be coarse conglomerates with minor amounts of sandstone, limestone, and shale, whereas sandstone and shale lithologies become more dominant going northeast further into the basin. The more proximal sediments are believed to be deposited as alluvial fans, fan deltas, proximal turbidites,

and debris flows while the more distal sandstones and shales are thought to be medial- to distal-turbidite and debris flow lobe deposits (Mitchell, 2011). While the term "Granite Wash" refers to sediments ranging in age from Atokan (Early Pennsylvanian) to Virgilian (Late Pennsylvanian), this study focuses on the Desmoinesian (Middle Pennsylvanian) Marmaton Granite Wash, also known as the Marmaton Wash or the Marmaton Group (**Figure 1.3**).

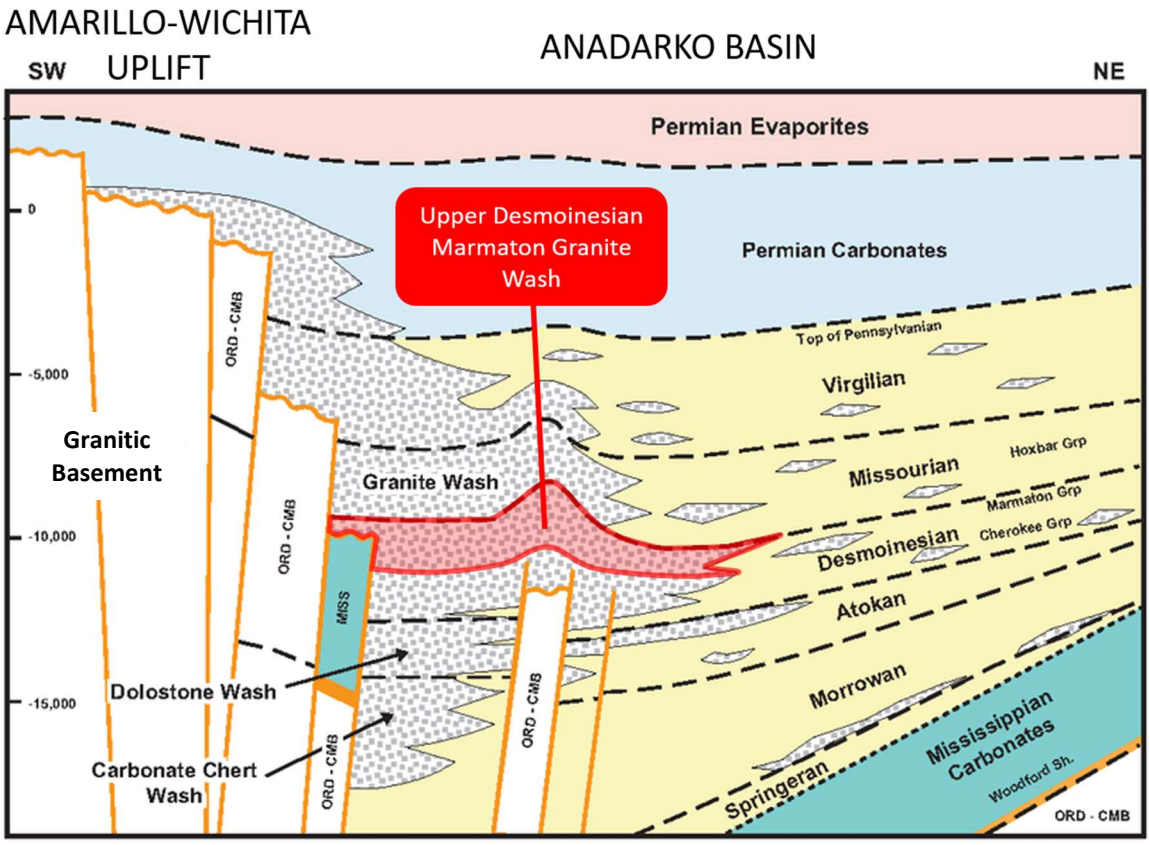

Figure 1.1: SW-NE schematic cross section of the Anadarko Basin. The Upper Desmoinesian Marmaton Granite Wash, the focus of this study, is highlighted in red above the Lower Desmoinesian Cherokee Group (modified from Wei and Xu, 2016).

Stratigraphic correlation and mapping wash distribution can prove difficult proximal to the uplift due to the overwhelmingly massive conglomerates and sandstones, while more distal Granite Wash intervals (about 10 to 20 miles from the mountain front) are interbedded with marine shales that can be excellent stratigraphic markers (Mitchell, 2011). These shale markers are commonly widely extensive and can be seen in **Figure 1.4**, a type log for the Desmoinesian-

age Granite Wash, including the Marmaton Group. Adding to the difficulty of correlating the Granite Wash is the wide array of terminology given to Granite Wash packages and marker beds by industry professionals over the years, with a multitude of different names being given to the same wash package. Further still, the radioactive feldspars within the eroded granitic sandstones of the formation make well log analysis and correlation even more complicated, as sandy intervals can have higher gamma-ray signatures than expected and can be mistaken for shale by those unfamiliar with arkosic washes. The varied mineralogy, complex stratigraphy, and changing depositional patterns of the Granite Wash mean that a thorough understanding of its depositional and diagenetic history as well as geological variation across the play area are crucial for successful well completion and play development.

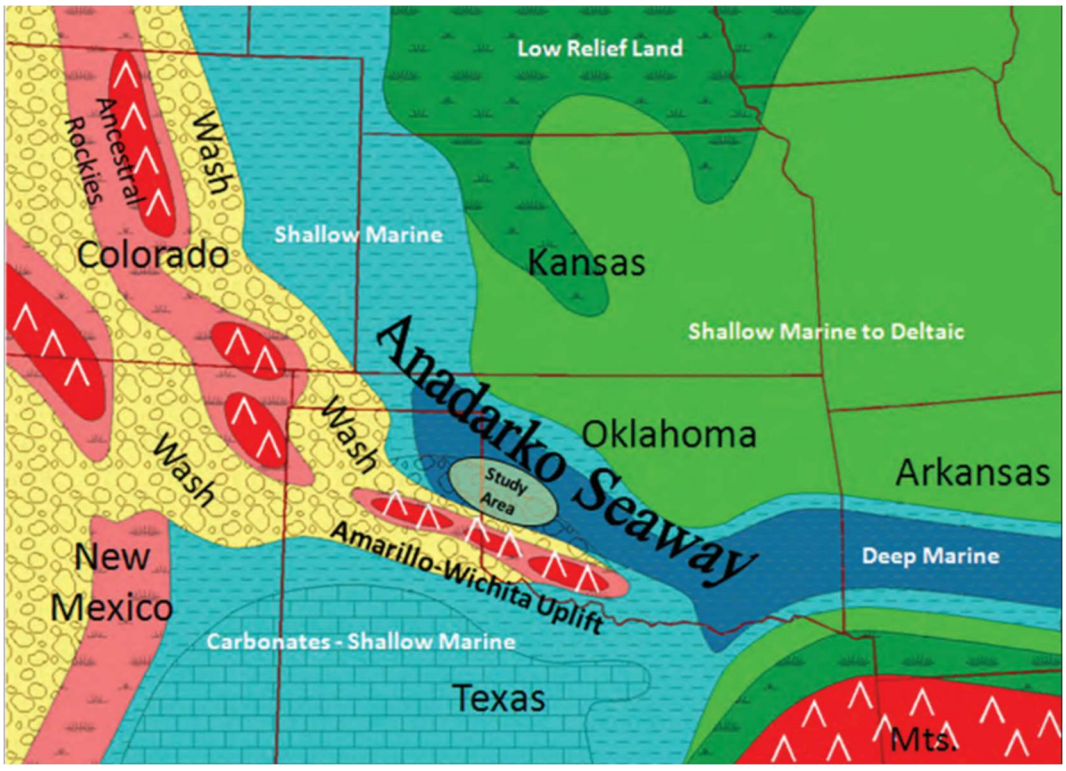

Figure 1.2: Desmoinesian (Middle Pennsylvanian) paleogeography of the Mid-Continent region, USA from Mitchell (2011). The Marmaton Granite Wash study area is circled.

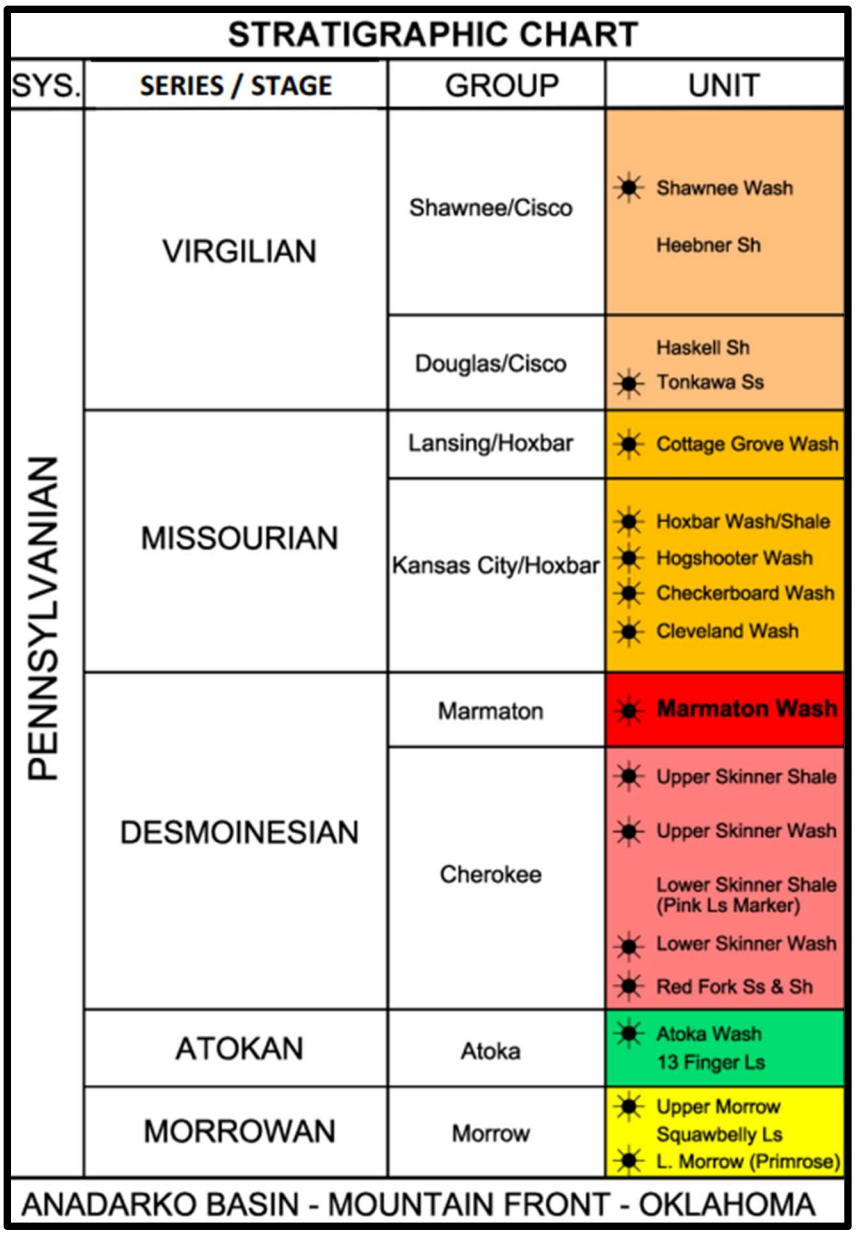

Figure 1.3: Pennsylvanian stratigraphic column, southwestern Anadarko Basin, western Oklahoma and Texas Panhandle (Mitchell, 2011).

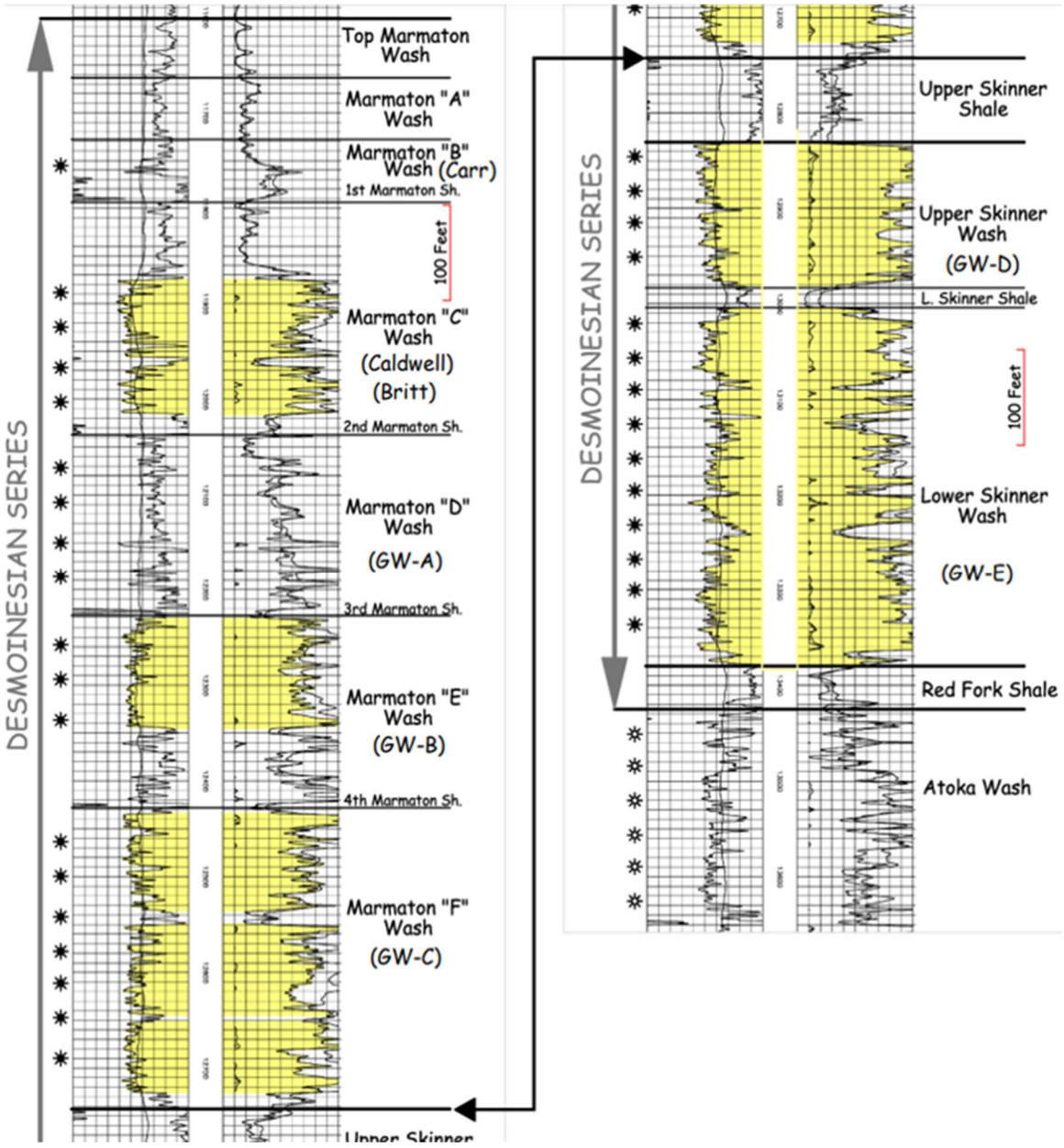

Figure 1.4: Gamma-ray and resistivity curves for the Desmoinesian Granite Wash section, deep Anadarko Basin, in the Devon #16-4 Truman-Zybach well, Sec. 16, Block R&E Survey, Wheeler County, Texas. The Pennsylvanian strata in the study area are separated into operational informal stratigraphic units including the Atoka Wash, the Desmoinesian Cherokee Wash, and the Marmaton Wash. The Cherokee Wash is comprised of the Red Fork Sandstone and Shale, Lower Skinner Wash, Lower Skinner Shale, Upper Skinner Wash, and the Upper Skinner Shale and the Marmaton Wash. The Upper Desmoinesian Marmaton Granite Wash is the focus of this study. It is commonly divided into five intervals, the Marmaton "A" through "F" Wash intervals, each of which is separated by a marine shale (the 1st through 4th Marmaton Shales) as shown (Mitchell, 2011).

1.2 Study Area

The Marmaton Granite Wash extends across the southwestern portion of the Anadarko Basin in western Oklahoma and the eastern Texas Panhandle. The play is over 130 miles long and about 30 miles wide, covering portions of Beckham, Roger Mills, Custer, and Washita counties in Oklahoma and Hemphill, Roberts, and Wheeler counties in the Texas Panhandle. This southwestern portion of the basin is also known as the deep Anadarko Basin, as it lies along the northern flank of the Amarillo-Wichita Uplift and encompasses the deepest reaches of the basin with over 40,000 feet of sedimentary rock at its deepest point. Given the sizable extent of the play, the focus area of this study is the central region of the Marmaton Granite Wash, which concentrates on portions of Hemphill and Wheeler counties in the Texas Panhandle and Roger Mills County in western Oklahoma (**Figure 1.5**). A small number of wells were added to the dataset from Roberts County, Texas as well as from Dewey and Beckham counties in Oklahoma to facilitate correlation and mapping, but the major focus was on Hemphill, Wheeler, and Roger Mills counties. This study area allows for the investigation of Marmaton Granite Wash deposition, diagenesis, and structure in more proximal areas closer to the Amarillo-Wichita source area and extends to the northeast to more distal environments. The southwestern extent of the study area is defined by the Mountain View Fault System along the northern edge of the Amarillo-Wichita Uplift, while the northeastern extent is in the southwestern corner of Dewey County, Oklahoma. The northern boundary was determined based primarily on well control and the generalized distribution pattern of recognized granite wash. Several productive Granite Wash fields are included in the study area, including Buffalo Wallow, Stiles Ranch, Mills Ranch, and Reydon Field. Marmaton Granite Wash reservoir depths within this study area range from 8,000 to 16,500 feet (Mitchell, 2011).

1.3 Purpose of Study

The Marmaton Granite Wash was chosen as the focus of this study, as it is known to produce high volumes of oil, gas, and condensate and hosts the majority of both vertical and horizontal well completions within the Pennsylvanian washes of the Anadarko Basin (Mitchell, 2011). However, little research has been devoted to the depositional and diagenetic processes that influence the porosity development and overall reservoir quality of the Marmaton Granite Wash, which is a key component of the play's successful development. Further, few published studies have attempted to create regionally extensive stratigraphic cross sections, structure maps, and thickness maps from the mountain front northeastward to more distal wash areas, past the extent of ideal porosity and permeability for productive reservoirs. By analyzing how the lithological, mineralogical, and structural characteristics of the formation vary across the study area, this study will provide a greater understanding of how depositional and diagenetic events affected porosity development in the Marmaton Granite Wash from proximal environments northeast towards the distal reaches of the play.

This study examined depositional features and differentiated them from those of diagenetic origin in order to better understand the effects of rock composition and fabric on porosity enhancement and/or reduction during burial and diagenesis. Additionally, this study examined the lateral extent and thickness trends of the Marmaton Granite Wash, which is essential to identifying ideal drilling locations within and around the study area. The ultimate goal of this study was to provide insight into where the Marmaton Granite Wash play becomes too distal and thus displays too low of porosity to be economically produced using horizontal wells and to determine the depositional and diagenetic processes that cause these spatial trends in reservoir quality. This primary goal included two key objectives: (1) to develop a regional stratigraphic framework for the Marmaton Granite Wash, and (2) to provide a greater understanding of depositional and diagenetic processes and how they influence porosity

development in the play across the study area. This analysis will ultimately provide a basis for targeting drilling locations and identifying productive trends within the Granite Wash and similar reservoirs, and lead to a greater understanding of tight gas sandstone reservoirs as a whole.

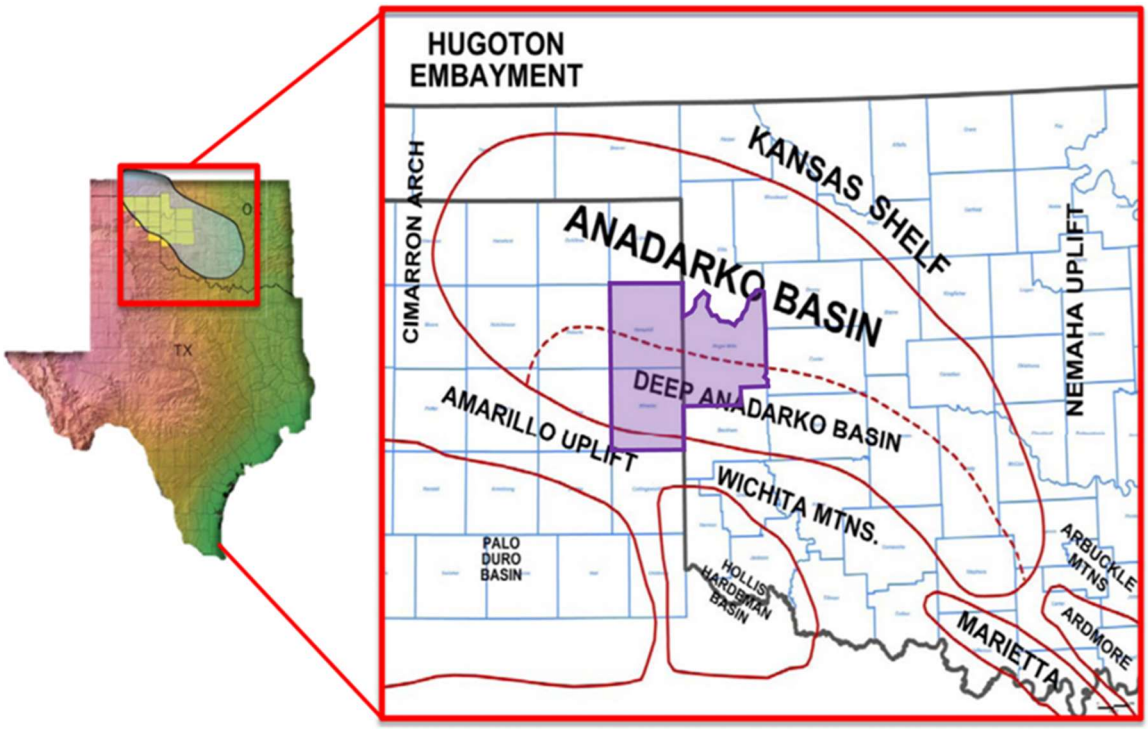

Figure 1.5: Map showing the location of the general study area, highlighted in purple, within the Anadarko Basin. The Marmaton Granite Wash extends to the counties marked in yellow on the topographic map to the left, but this study focuses on the central portion of the Marmaton Granite Wash play in Hemphill and Wheeler counties in Texas and Roger Mills County, Oklahoma (modified from LoCricchio, 2012).

CHAPTER II

METHODOLOGY

In order to analyze the structure, depositional and diagenetic history, and porosity development within the Marmaton Granite Wash, several methods of data collection were utilized: literature review, stratigraphic correlation and subsurface mapping, core analysis, thin section petrography, scanning electron microscopy, x-ray diffraction analysis, x-ray fluorescence (XRF) analysis, and porosity analysis using well logs. At the outset of this study, an extensive literature review was conducted involving previous studies of the Granite Wash formation, the development and structure of the Anadarko Basin, and fan delta and submarine fan depositional environments.

2.1 Stratigraphic Correlation and Subsurface Mapping

In order to develop a thorough understanding of the stratigraphic and structural framework of the Marmaton Granite Wash, stratigraphic tops for four Marmaton Granite Wash "hot shale" stratigraphic markers (as well as other helpful stratigraphic markers like the underlying Upper Skinner Shale) in 576 wells across the study area were correlated using LMKR GVERSE GeoGraphix software. These hot shale markers represent flooding surfaces that have a high API reading on gamma-ray logs and can be used to package the various Marmaton Granite Wash intervals into distinct mappable units. While 1,692 wells are present within the study area,

well logs could only be obtained for around 600 wells due to monetary constraints and limitations in data availability.

The gamma-ray log is a measurement of a formation's natural radioactivity, measured in API units (standard units designated by the American Petroleum Institute). This radioactivity can be attributed to potassium, uranium, and thorium as well as uranium and thorium daughter products. In the Marmaton Granite Wash, gamma-ray log values for sandstone often range from 90 to over 120 API. Given that the typical gamma-ray cutoff for shale is around 110 to 120 API units, these Marmaton sandstones would normally be interpreted as shales (Asquith et al., 2004). However, the granitic detritus of the Granite Wash is especially high in potassium feldspar, making sandstone intervals show a much higher gamma-ray value than would typically be expected to indicate sandstone. For this reason, the gamma-ray curve is not a viable shale indicator for the Marmaton Granite Wash. However, gamma-ray logs (along with resistivity and SP logs) serve as a reliable tool for dividing the Marmaton Granite Wash into distinct wash intervals through the identification of the Marmaton hot shale flooding surfaces, which often exceed 150 API units proximal to the mountain front. These marine shale markers read higher than a typical shale interval on gamma-ray logs because they are reading the uranium associated with the organic matter in the shale. Uranium is not water soluble in reducing environments, and therefore adsorbs and remains attached to the organic material in these environments. It should be noted that potash formed in evaporitic environments, a common cause of hot shale gamma-ray spikes in other parts of the Mid-Continent region, is not known to be found in the study area.

The identification of the Marmaton hot shale stratigraphic tops using gamma-ray and resistivity logs allowed for the creation of regional cross sections as well as structure and thickness maps. Cross sections were constructed to correlate hot shale marker beds in order to illustrate stratigraphic and structural trends across the study area. Structure maps were constructed at the top of the four Marmaton hot shale markers to establish the structural attitude

of the region and to better understand the major tectonic features prominent at the time of deposition. Thickness maps of the individual wash packages between the shale marker beds were also constructed to gain a better understanding of depositional trends and reservoir geometry. Structure and thickness maps as well as cross sections were constructed in GVERSE GeoGraphix, an LMKR Geological and Geophysical Interpretation software suite. Well logs in the dataset were acquired from both Enverus (formerly DrillingInfo) and MJ Logs and consist of both LAS (Log ASCII Standard) digital logs and depth-registered raster logs. Landgrid data for both Texas and Oklahoma as well as all well data were acquired from LMKR.

In order to better understand Marmaton Granite Wash fan lobe deposition, a net sand thickness map of the Marmaton "D" Wash interval in Buffalo Wallow Field in Hemphill County, Texas was constructed by hand (not computer generated) based on the stratigraphic top picks for the Second and Third Marmaton Shales in GVERSE GeoGraphix. A gamma-ray shale baseline was established on a well-to-well basis by finding the average between a typical marine shale (disregarding hot, radiogenic shales) and a typical clean sandstone. In and around Buffalo Wallow Field, the gamma-ray log appears to be indicating shale intervals effectively. Two cores utilized in this study are from Buffalo Wallow Field, and core calibration further indicates that the gamma-ray log is an effective shale indicator in this area. In other parts of the Granite Wash play area such as Elk City Field in Beckham and Washita Counties in Oklahoma, feldspar content in the sandstone is high enough to cause the gamma-ray curve in sandstone to read as high as the gamma-ray readings in adjacent shales. For this reason, many geologists in these areas use the SP curve as a shale baseline indicator rather than the gamma-ray curve. When available, neutron porosity logs as clay mineral indicators are also useful in identifying shale and are valuable in delineating arkosic sandstones from shale on wireline logs when the gamma-ray curve is not a reliable shale indicator.

2.2 Core Analysis

Conventional cores from the Marmaton "D" Wash interval of three wells within the study area were analyzed for depositional, biogenic, and diagenetic features to better understand the depositional system. The easternmost core was from the Laredo Kicking Bird #1-20 well located in Reydon Field in Roger Mills County, Oklahoma. The two additional cores were the Dominion Grant Meek #236-1 and the Dominion Fillingim #88-2, both located in Buffalo Wallow Field in Hemphill County, Texas. All three cores are housed at the Gary F. Stewart Core Research Facility on the Oklahoma State University campus in Stillwater, Oklahoma. The Kicking-Bird #1-20 core was generously donated to the Oklahoma State University Boone Pickens School of Geology by Laredo Petroleum, while the Grant Meek #236-1 and the Fillingim #88-2 cores were generously donated by Linn Energy. Each core was photographed, examined, and described to identify and record lithology, color, sorting, grain size variations, bedding contacts, sedimentary structures, and biological features. Grain size was measured and reported using the Wentworth scale (Wentworth, 1922).

Conventional core analysis data for the Kicking Bird #1-20 was provided by Laredo Petroleum, while porosity and permeability data derived from conventional core plugs from the Fillingim #88-2 core originally provided by Linn Energy was acquired from Parks (2011).

2.3 Sandstone Petrography

Sandstone petrography was conducted on thin sections taken from the Marmaton "D" Wash interval. Samples were taken from the Kicking Bird #1-20 core at the 15 highest available porosity values (excluding those taken for scanning electron microscopy (SEM) analysis), as determined from the core analysis data provided by Laredo Petroleum. Each sample was made into a standard 30 micron thick thin section, and analyzed using a Nikon Optiphot-POL Research Microscope to evaluate the abundance and type of detrital and authigenic constituents as well as

porosity. Both qualitative descriptions and quantitative point counts using the Gazzi-Dickinson method were recorded. Point count data taken from the Grant Meek #236-1 (7 thin sections) and Fillingim #88-2 (10 thin sections) cores were acquired from Parks (2011), a study that used similar methodology, and were compared to the results of the Kicking Bird #1-20. An Olympus BX51 Petrographic Microscope with image analysis software was used to capture photomicrographs of the thin sections from all three wells.

A paragenetic sequence of diagenetic events for the Marmaton "D" Wash interval was created based on petrographic observations such as cross-cutting relationships, packing density and grain deformation, dissolution and cementation patterns, and diagnostic fabrics and morphologies seen in thin section. This paragenetic sequence allowed for better understanding and visualization of the order of events that occurred in the diagenetic history of the Marmaton Granite Wash.

2.4 Scanning Electron Microscopy (SEM)

Scanning electron microscopy (SEM) was performed on three samples from the Marmaton "D" interval of the Kicking Bird #1-20 core and three samples from the Marmaton "D" interval of the Fillingim #88-2 core. This was done in order to evaluate the pore structure (pore type, shape, and distribution) of selected intervals in each core at a micro- to nano-meter scale and compare the pore structure between the two cores, with the Kicking Bird #1-20 being more distal from the Amarillo-Wichita Uplift source area. SEM samples in the Kicking Bird #1-20 core were chosen at depths with the highest porosity values recorded in the core analysis data provided by Laredo Petroleum, while samples in the Fillingim #88-2 were chosen at depths with the highest porosity values seen on the density-neutron porosity log.

After being extracted from the core, the samples were taken to the Oklahoma State University Microscopy Laboratory where they were cut to the appropriate size for mounting and

then cleaned, dried, polished, and mounted on a specimen holder. They were subsequently coated with a thin layer of gold/palladium alloy to increase electrical conductivity before being examined with a FEI Quanta 600 Field-emission Gun Environmental Scanning Electron Microscope (FESEM). Photomicrographs were taken with the attached digital camera system. The FESEM at the Oklahoma State University Microscopy Lab has a resolution of 1.2 nm at 30 kV, 1.5 nm at low vacuum mode, and 1.5 nm at ESEM mode.

2.5 X-ray Diffraction (XRD) Analysis

Semi-quantitative x-ray diffraction (XRD) analysis was performed on samples from three depths in the Kicking Bird #1-20 well in order to determine sandstone mineralogy, including clay species. Bulk mineral analysis was performed on samples at all three depths, and samples at two of the three depths were also chosen for extracted clay mineral analysis. Samples chosen for powder XRD diffraction were powdered using a ball mill, and powder holders were lightly packed with the sample sediment using a metal spatula. Clay minerals were extracted from samples designated for clay mineral analysis and treated using procedures outlined by Poppe et al. (2001): an acetic acid treatment for the removal of carbonates and a hydrogen peroxide treatment to remove organic matter, separation of silt and clay particles from larger grains in solution by centrifugation, mounting of the clay smear on a glass slide, the addition of ethylene glycol to the clay smear to expand swelling clays (e.g. smectites, mixed-layer clays, and vermiculite), and heating of the mounted clay smear to aid in the identification of clay minerals by revealing structural changes in mineral species that collapse or lose their crystal structure when dehydrated.

Samples were analyzed using a Philips PW 3710 X-ray Diffractometer located in the Noble Research Center (NRC) on the Oklahoma State University campus. Bulk mineralogy analysis was performed using Cu-Kα radiation at 45 kV and 40 mA from 5 to 60 degrees 2Θ at a

step of 0.02 degrees 2Θ for either 0.5 or 1.0 seconds per step. Clay smears were subsequently analyzed using the same settings on the diffractometer but were run from 2 to 40 degrees 2Θ in order to better identify clay minerals with lower angle reflections. XRD peak positions were recorded by the diffractometer and the d-spacing of each peak was determined and compared to the d-spacing of known minerals.

XRD data for the Grant Meek #236-1 and the Fillingim #88-2 cores were originally provided by Linn Energy and acquired from Parks (2011).

2.6 X-ray Fluorescence (XRF) Analysis

In order to measure and determine variability in the elemental composition across the Marmaton "D" Wash cored interval, semi-quantitative energy-dispersive x-ray fluorescence (XRF) measurements were collected for the Kicking Bird #1-20 core using a handheld Thermo Scientific™ Niton™ XL3t GOLDD+ XRF Analyzer without helium. The instrument measures the concentration of 35 elements (the lightest able to be distinguished being magnesium) within each sample in a non-destructive manner. Each chosen core depth point was sampled for 180 seconds to obtain maximum accuracy. Two depth points were analyzed for each foot for all 54 total feet of core, making for 108 separate measurements (not including calibration). As the samples were placed in a Niton™ XL3 portable test stand due to the large number of measurements and long sampling time, depth points were chosen partially based on ease of fitting a core piece into the test stand for analysis. Care was taken to ensure the highest range of varying lithology and grain size was obtained when choosing two depth points per foot for analysis. The system was calibrated to check analysis quality every 10 to 15 samples using the USGS Cody Shale standard (SCo-1), which is known to have a similar chemical composition to the average shale and is considered to be an excellent reference standard for geochemical studies involving shales and other sedimentary rocks (McLennan and Taylor, 1980).

CHAPTER III

LITERATURE REVIEW

While multiple studies have been dedicated to the lithological and structural history of the various Granite Wash intervals of Atokan through Virgillian age shed off the Amarillo-Wichita Uplift and into the Anadarko Basin, only a portion of those have been dedicated to the Late Desmoinesian-age reservoirs that host the majority of Granite Wash completions. The Granite Wash was first targeted in 1947 with the discovery of Elk City Field in Beckham County, Oklahoma and produced modestly from various intervals for decades using conventional wells, but was largely characterized by poor recovery efficiency (Mitchell, 2011). Before horizontal drilling practices and hydraulic fracturing took off in the 1990s to early 2000s, the Late Desmoinesian Granite Wash was largely considered sub-economical due to low permeability and was largely bypassed in favor of units with histories of better recovery such as the Red Fork and Hunton Groups (Mitchell, 2011). Because of this, the Late Desmoinesian Marmaton Granite Wash received little attention by researchers until the mid-2000s to 2010s, and this lack of interest is reflected heavily in the early Granite Wash literature.

Prior research on the Marmaton Granite Wash has focused on general stratigraphy and lithology in order to better understand the depositional environment, but studies that provide chronostratigraphic correlation of Marmaton Granite Wash units are typically proprietary to industry members and are not made public. Further, few published studies have focused on

diagenetic variability and its effects on mineralogy and porosity across the play from proximal to more distal environments.

One of the earliest mentions of the Granite Wash is by Edwards (1958), who examined the lithological variation in Pennsylvanian clastics along the northern flank of the Wichita Mountains in southwestern Oklahoma. He determined that the Pennsylvanian-age sediments adjacent to the Wichita Mountains were largely coarse-grained granitic washes derived from the uplift of the Wichita Mountains and composed of igneous rock fragments (primarily granophyre and micrographic granite) with varying amounts of detrital carbonate and chert (Edwards, 1958). Edwards (1958) observed a basinward shift in facies from conglomerate to sandstone that eventually interfingers with marine sandstones, shales, and limestones, and concluded that the Granite Wash is representative of a transitional environment between continental and shallow marine conditions. He asserts that adjacent to the Wichita Mountains, Granite Wash sediments were deposited in a complex system of alluvial fans and deltas (Edwards, 1958). He then suggests that the best porosity and permeability in the region is seen in the coarser crystalline granitic washes rather than in sediments derived primarily from rhyolite or carbonate (Edwards, 1958).

Several more classic studies investigated the composition and depositional environment of the various Granite Wash intervals or the Granite Wash as a whole, including Sahl (1970), Brown (1979), Dutton (1982), Carroll, (1986), Alberta (1987), and Mitchell (2011). Focusing on Mobeetie Field in Wheeler County, Texas, Sahl (1970) found that Atokan rocks in Mobeetie Field derived from the erosion of Early Paleozoic rocks on the Amarillo-Wichita Uplift contain a significant amount of detrital carbonate and are poorer in porosity and permeability than the overlying Desmoinesian granitic sandstones that consist primarily of unaltered granitic rock fragments, quartz, and feldspars. Brown (1979) asserted that the Granite Wash sandstones and conglomerates found along the flanks of the Amarillo-Wichita Uplift were deposited principally in fan delta environments and associated braided streams into the Anadarko Basin. Fan deltas are

gravel-rich deltas that form when alluvial fans deposit sediment directly into a body of water from an adjacent highland (McGowen, 1971a; McPherson et al., 1987). Through extensive well log analysis and subsurface mapping, Brown (1979) provides typical well log patterns and generalized depositional models for various fan delta and fluvial sandstones in the Mid-Continent region, including the Pennsylvanian Granite Wash fan deltas of the Anadarko Basin. Brown (1979) described the geometry of the Pennsylvanian Granite Wash fan deltas coming off the Amarillo-Wichita Uplift as "elongate to lobate", indicating that the Anadarko Basin was characterized by low marine energy at the time. McGowen (1971a) studied modern alluvial fans and fan deltas in both arid and humid environments around the world to create depositional models, and explains that fan delta deposits are consistently reworked by marine processes.

Also focusing on Mobeetie Field in Wheeler County, Texas, Dutton (1982) describes fan deltas of terrestrial sandstones and carbonates that repeatedly prograde onto a shallow carbonate shelf in the Anadarko Basin in the Missourian (Late Pennsylvanian). Dutton (1982) relates the facies seen in the Mobeetie Field cores to those observed by McGowen (1971b) in the Holocene Gum Hollow fan delta off the Texas coast in order to subdivide the depositional environments, but it is noted that the Gum Hollow is not a proper analog in regards to fan size, source area relief, or sediment size. Dutton (1982) explains that the clastic sequence seen in the Missourian-age Mobeetie Field cores is representative of the distal portion of a fan-delta system. A north-south trending regional cross section from the Amarillo-Wichita Uplift into the Anadarko Basin presented by Dutton (1982) is frequently utilized in subsequent granite Wash literature.

Dutton (1984) provides a detailed description of alluvial fan and fan delta depositional processes and distinguishes four main fan delta depositional environments: fan plain, distal fan, main channels, and prodelta. Dutton (1984) also asserts that the Pennsylvanian- Lower Permian Fountain, Maroon, Hermosa-Cutler, and Sangre de Cristo Formations in Utah and Colorado are both stratigraphic and genetic equivalents to the Granite Wash. Dutton and Land (1985) describe

the mineralogy of Granite Wash sandstones and their distribution, then outline their diagenetic and paragenetic history based off of cores from Mobeetie Field. They discuss the reduction of porosity through the precipitation of authigenic minerals such as quartz, feldspar, clays, and carbonates (Dutton and Land, 1985). They then suggest that the Granite Wash sediments in Mobeetie Field were under the influence of meteoric fluids flowing down-dip from the Amarillo-Wichita Uplift throughout their early burial history, and that these meteoric fluids are responsible for the majority of Granite Wash diagenesis (Dutton and Land, 1985).

In their study of the Early Pennsylvanian Morrow sandstones of the Anadarko Basin, Al-Shaieb and Walker (1986) state that most porosity in the Morrow sandstones is secondary and that the development of this secondary porosity is directly related to: (1) the availability of H^+ ions produced by the maturation of organic matter in adjacent shales, and (2) original composition and texture of the sandstone. They outline a complex diagenetic history for the Morrow sandstones (including the development of secondary porosity resulting from the dissolution of clay matrix, carbonates, glauconite, and quartz) that they attribute to a combination of organic and inorganic reactions taking place as the Anadarko Basin subsided (Al-Shaieb and Walker, 1986). Alberta (1987) described the depositional facies, mineralogy, diagenetic history, and porosity development of the "Puryear" Member of the Upper Morrow Chert Conglomerate in Roger Mills and Beckham Counties, Oklahoma. After providing a detailed description of Early Pennsylvanian fan delta deposition in the Anadarko Basin, Alberta (1987) used core-linked well logs to develop characteristic neutron-density porosity log signatures for various fan delta depositional facies, including: distributary channels, crevasse splay, overbank, delta front, delta plain, swamp/marsh, and prodelta facies.

Puckette (1990) outlined the depositional setting and facies as well as the stratigraphic framework for the Cabaniss Group in Beckham, Dewey, Custer, Ellis, Roger Mills, and Washita Counties in Oklahoma. The Cabaniss Group is commonly referred to as the "Upper Cherokee" by

the petroleum industry and is of Desmoinesian age, consisting of (in ascending order) the Pink Limestone, Lower and Upper Skinner Sandstones, Verdigris Limestone, Prue Sandstone, and the "Cherokee Hot Shale" (Puckette, 1990). The Cabaniss/Upper Cherokee Group was deposited primarily on the relatively stable shelf area in the northern Anadarko Basin during the Desmoinesian (Puckette, 1990). Similarities between the stratigraphic framework of the Cabaniss/Upper Cherokee Group on the shelf in the north central Anadarko Basin and the hot shales of the Marmaton Granite Wash in the southwestern Anadarko Basin are discussed in Section 4.3.

A few published studies have tackled establishing a stratigraphic framework for the Desmoinesian Marmaton Granite Wash. The industry standard for mapping and deciphering the stratigraphy of the Marmaton Granite Wash is to divide it into wash "packages" or sandstone reservoir intervals separated by regionally-correlative black marine shales that represent regional flooding surfaces (Mitchell, 2011; LoCricchio, 2012; Karis, 2015). While providing detailed descriptions of Granite Wash depositional processes, lithology, and production trends, Mitchell (2011) establishes a stratigraphic framework for the Marmaton Granite Wash by dividing it into seven different wash packages: the Marmaton "A" through "F" Washes, in descending stratigraphic order. Parks (2011) established a local stratigraphic framework for the Marmaton Granite Wash in Buffalo Wallow Field in Hemphill County, Texas by correlating the hot shales seen in Buffalo Wallow field to known, age-dated flooding surfaces (in ascending stratigraphic order: Verdigris Marker, Excello Shale, Marmaton Flooding Surface 1, and Marmaton Flooding Surface 2) on the shelf of the Anadarko Basin to the northeast. LoCricchio (2012) also established a stratigraphic framework, dividing the Desmoinesian Granite Wash (including both the Marmaton Group and the underlying Cherokee Group) into eleven stacked sandstone wash "horizons" divided by regionally correlative shale flooding surfaces. Karis (2015) utilized these regionally correlative hot shales to create regional structure and isochore maps for the Marmaton

Granite Wash as a whole, and then developed 3-D lithology models for the Marmaton Group using core-linked electrofacies.

Philp and his associates (2016) examined the geochemical characteristics of 14 oils from various intervals of the Granite Wash across western Oklahoma and the eastern Texas Panhandle. They analyzed the maturity of the samples and concluded that maturity increased with depth, with deeper reservoir samples being condensate while shallower samples were a mixture of oil and condensate (Philp et al., 2016). The condensate in both the shallow and deep samples were determined to be derived from the same source, which was found to be primarily a marine shale likely of Pennsylvanian age (Philp et al., 2016).

Koch and his associates (2017) evaluated 49 cores across the Granite Wash play area, identifying 31 lithofacies across seven different facies associations: alluvial fan, fluvial channel, estuarine, proximal/distal delta front, prodelta, and offshore. By combining detailed core analysis with well log analysis and the construction of isopach and facies maps, the researchers determined that the Granite Wash can be divided into generally coarsening-upward, 100-300 feet thick (on average) depositional cycles that are bounded by marine shales (Koch et al., 2017). It was established that Granite Wash depositional cycles resulted from a combination of eustatic and tectonic processes, with the lower part of the cycle (early HST) being a prograding fluvial-deltaic system followed by normal regression (late HST) that is overlain by a transgressive marine shale (Koch et al., 2017).

In general, Granite Wash sediments are thought to be deposited adjacent to the Amarillo-Wichita Uplift in alluvial fan, fan delta, and proximal turbidites and debris flows, then grade into medial- to distal-turbidite and debris-flow lobes going basinward towards the northeast (Mitchell, 2011; LoCricchio, 2012). While much of the early Granite Wash literature (Sahl, 1970; Dutton, 1982; Alberta, 1987; etc.) focuses on these proximal alluvial fan and fan delta environments in

the Granite Wash, the more distal submarine fan (turbidite system) environments have received significantly less attention. This is likely attributed to the especially low economic performance of distal Granite Wash wells compared to their proximal counterparts using conventional drilling practices. Still, a great deal of general submarine fan literature is available and is of great use to this study.

The submarine fan model outlined by Walker (1978) combines previous models from earlier studies of modern and ancient submarine fans. The model consists of 1) a deep feeder channel that supplies sediment, 2) an upper fan leveed channel, 3) a middle fan consisting of suprafan lobes that grade outward from shallow braided channels into turbidity deposits, and 4) a topographically smooth lower fan and basin plain that display parallel bedding and distal turbidites (Walker 1978; Anderson, 1992). Using this submarine fan model outlined by Walker (1978), Anderson (1992) was able to determine the submarine fan facies distribution and fan morphology of the Desmoinesian Upper Red Fork Sandstone of the Cabaniss (Uppper "Cherokee") Group (stratigraphically below the Marmaton) of the Anadarko Basin.

Bouma (2000) details and compares both fine-grained, mud-rich submarine fans and coarse-grained, sand-rich submarine fans and provides depositional models for both. While mud-rich submarine fans are typically found on passive margins and are usually characterized by long fluvial transport, a wide shelf, and are delta-fed, sand-rich submarine fans are most often found on active margins and are characterized by a short terrestrial transport distance, a narrow shelf, and are canyon-fed (Bouma, 2000). Also highlighted is that in sand-rich submarine fans, the proximity to source and short terrestrial transport often do not allow ample time for the breakdown of unstable minerals (Bouma, 2000).

CHAPTER IV

GEOLOGIC SETTING

4.1 General Stratigraphy and Paleogeography

The sedimentary sequence in the Anadarko Basin contains a wide assortment of lithologic units ranging in age from Cambro-Ordovician to Permian (**Figure 4.1**). In general, the lower Paleozoic was dominated by marine inundation and carbonate sedimentation while upper Paleozoic rocks are primarily terrigenous clastics. Noteworthy exceptions to this generalization include the quartz sandstones of the middle Ordovician Simpson Group and the limestones and dolomites of the lower Permian (Wolfcampian) Chase Group.

At the base of the Anadarko Basin stratigraphic sequence, the transgressive Late Cambrian Reagan Sandstone lies unconformably above rift volcanics of the granitic basement. Consisting largely of reworked detritus shed from the volcanic basement rocks, the Reagan is feldspathic and glauconitic (Johnson, 1991). Deposited on a moderately mature erosional surface of low relief throughout the region, the Reagan marks the start of a lengthy period of subsidence for the Southern Oklahoma Trough (precursor to the Anadarko Basin) and a resulting marine transgression (Wickham, 1978; Perry, 1989). Transgression and subsidence continued to flood the entirety of the continental margin, allowing for the widespread deposition of Cambro-Ordovician Arbuckle Group limestones and dolomites on the “Great American Bank”, an expansive carbonate ramp that formed the southern margin of the North American craton (Gaswirth and

Higley, 2014). The cyclic platform interior carbonates of the Arbuckle Group were deposited throughout the Mid-Continent region and range in thickness from around 400 to 8,000 feet (Ball et al., 1991.

The middle Ordovician Simpson Group lies unconformably above the Arbuckle Group. Consisting of clean quartzose sandstones that are interbedded with shallow marine limestones and greenish-grey shales, Simpson Group strata signify a change from predominantly carbonate deposition to a dominant influx of clastic sediment. The quartz-rich sands of the Simpson were transported across the exposed shelf during periods of relative lowstand into early transgression, with basal lowstand sands being deposited along the margin of the Southern Oklahoma Trough and transgressive sands accumulating as discontinuous shoreface complexes (Candelaria and Handford, 1995). These sandstone units of the Simpson Group are the only significant coarse siliciclastics of lower Paleozoic age in the Anadarko Basin.

Overlying the Simpson Group is the Late Ordovician Viola Limestone. After a short marine withdrawal, a broad, shallow, transgressive epicontinental sea covered the Anadarko Basin region, resulting in the deposition of the Viola on a carbonate platform (Gaswirth and Higley, 2014). The Viola is a dense, tight limestone that contains nodular chert and is highly fossiliferous. Before the end of the Late Ordovician, Viola carbonate deposition ended abruptly as clays began to flood the system and form the overlying greenish-gray Sylvan Shale. The Sylvan becomes more calcareous from east to west as its thickness increases, and it locally grades into argillaceous, skeletal carbonate to the northwest (Johnson, 1991).

The mid-continent region saw widespread marine-carbonate deposition on a broad carbonate ramp throughout the Silurian and Devonian, forming the nearly pure limestones, limely marlstones, and marly shales that dominate the Late Ordovician to Early Devonian Hunton Group. The top of the Hunton is marked by the regional pre-Woodford (post-Hunton)

unconformity, which developed as the Mid-continent emerged and Hunton strata were eroded during lowstand conditions. Transgression of the Devonian-Mississippian Woodford Sea followed, with inundation initially being confined to erosional channels that would fill with sediment and organic material that would become Woodford Shale (Gaswirth and Higley, 2014). The Viola Limestone, Sylvan Shale, and Hunton Group all have similar thicknesses in the Anadarko Basin region as they do on the North American Craton, indicating that the basin and craton were subsiding at similar rates throughout the Devonian (Alberta, 1987).

Hunton Group strata are unconformably overlain by either the Late Devonian-Early Mississippian dark, organic-rich Woodford Shale or locally by the Late Devonian Misener Sandstone. The Misener (the basal unit of the Woodford) consists of fine-grained quartzose sandstone with minor amounts of dolomite and was deposited on top of the pre-Woodford unconformity as incised-valley fill (Kuykendall and Fritz, 2001). The deposition of the dark, organic-rich Woodford Shale indicates a change in depositional environment from shallow marine conditions to restricted, anoxic, deeper waters beginning in the Late Devonian.

Superimposing the Woodford Shale is the Mississippian section, which signifies a transition from the predominant carbonate deposition of the lower Paleozoic to the clastic deposition that dominated in the Pennsylvanian (Hill, 1984). By the end of the early Mississippian, the broad, often anoxic to euxinic seas of the Late Devonian-Early Mississippian that resulted in Woodford Shale deposition were replaced by well-oxygenated shallow-marine environments. Kinderhookian (early Mississippian) dark shales grade upward into massive fossiliferous, cherty limestones and dolomites of Osagean (early middle Mississippian) and Meramecian (early middle Mississippian) age (Rascoe and Adler, 1983). The Kinderhookian-Meramecian section above the Woodford Shale consists of multiple alternating limestone and shale units including the Sycamore Limestone, Mayes Shale, and the Caney Shale, and is commonly collectively referred to as the “Mississippian Lime”. The shales (including the

Goddard Shale), thin carbonates, and sandstones of Chesterian (Late Mississippian) age indicate a major marine regression and mark an end to the predominantly carbonate depositional cycle of the Lower Paleozoic. This marine regression caused the deposition of the Chesterian-Morrowan (Early Pennsylvanian) Springer Formation, which is typified by shale with interbeds of sandstone. To the northeast, the top of the Springer grades into deltaic and shallow marine sediments from the exposed shelf (Ball et al., 1991). Webster (1980) found that basin subsidence outpaced that of the craton during the Mississippian, demonstrated by the presence of 5,500 feet of Mississippian shale in the deep basin but only 500 feet on the northern shelf (Alberta, 1987).

Clastics dominated Anadarko Basin sedimentation during the Pennsylvanian. Morrowan (early Pennsylvanian) strata are mostly gray shales that were deposited during marine transgression, with intermittent discontinuous sandstones, conglomerates, and limestones that were deposited during brief regressive phases of the overall transgressive period (Alberta, 1987; Ball et al., 1991). The Morrowan unit forms a thick wedge of sediment that is thickest adjacent to the Amarillo-Wichita Uplift and thins onto the shelf to the northeast. The Morrowan series is commonly divided into upper and lower sections. Lower Morrow sands trend northwest-southeast and were likely deposited in shallow marine shelf and beach environments, while upper Morrow sands were likely deposited in tidal-dominated fluvio-deltaic environments (Rascoe and Adler, 1983; Al-Shaieb and Walker, 1986). Orogenic activity initiated the rise of the Amarillo-Wichita Uplift in the late Morrowan, causing extensive erosion of Mississippian Meramec-Osage cherty limestones, bedded cherts, and dolomites on top of the uplift and their subsequent deposition in the southwestern Anadarko Basin along the uplift's northern flank (Evans, 1979; Shelby, 1980). These discontinuous, coarse-grained, cherty washes are commonly referred to as the "Upper Morrow Chert Conglomerate" and were deposited in a fan delta type complex just north of the Lips Fault Zone, along the northern edge of the uplift (Evans, 1979). Following the erosion of

Mississippian-age rocks from the uplift, Devonian, Silurian, and Ordovician rocks were eroded and the subsequent detritus was deposited in the basin in order of inverted geological age.

The gray shales of the Morrowan Series are overlain by the Atokan (early Pennsylvanian) "Thirteen Finger" Limestone across most of the basin. The "Thirteen Finger" comprises a cyclic sequence of thin marine limestones and shales, suggesting that there was a discontinuous supply of clastic sediment influx into the basin during its deposition (Rascoe and Adler, 1983; Alberta, 1987). The Wichita Orogeny continued into the Atokan, with sediment shedding off the rising Amarillo-Wichita Uplift continuing to be the primary sediment influx to the Anadarko Basin. The Cambro-Ordovician Timbered Hills and Arbuckle Groups were eroded off the exposed top of the uplift in pulses, producing a thick wedge of detrital dolomite wash in the basin. Minor amounts of siliciclastic material also contributed to the dolomite wash through the erosion of limited exposures of granitic basement (Lyday, 1985).

Following the erosion of the Cambro-Ordovician Arbuckle Group in the Atokan, the granitic core of the Amarillo-Wichita Uplift was fully exposed from the Desmoinesian (middle Pennsylvanian) through the early Permian. During this time, coarse arkosic sediment up to boulder-size was shed from the exposed Precambrian granite and was transported into the Anadarko Basin. This arkosic sediment is commonly referred to as "Granite Wash". The continual uplift, erosion, and deposition of sediment into the basin throughout the Pennsylvanian and Early Permian led to more than 13,000 feet of synorogenic detritus with an inverted vertical age sequence: detritus of older material is superimposed on younger material (Lyday, 1985). Morrowan cherty conglomerates derived from Mississippian-age carbonates are superimposed by Atokan detrital carbonates derived from the Arbuckle group, which are in turn superimposed by Desmoinesian sandstone and conglomerates derived from the granitic basement. Differential uplift, erosion, or a combination of both caused varying lithologies of various ages to intermix within the washes (Lyday, 1985).

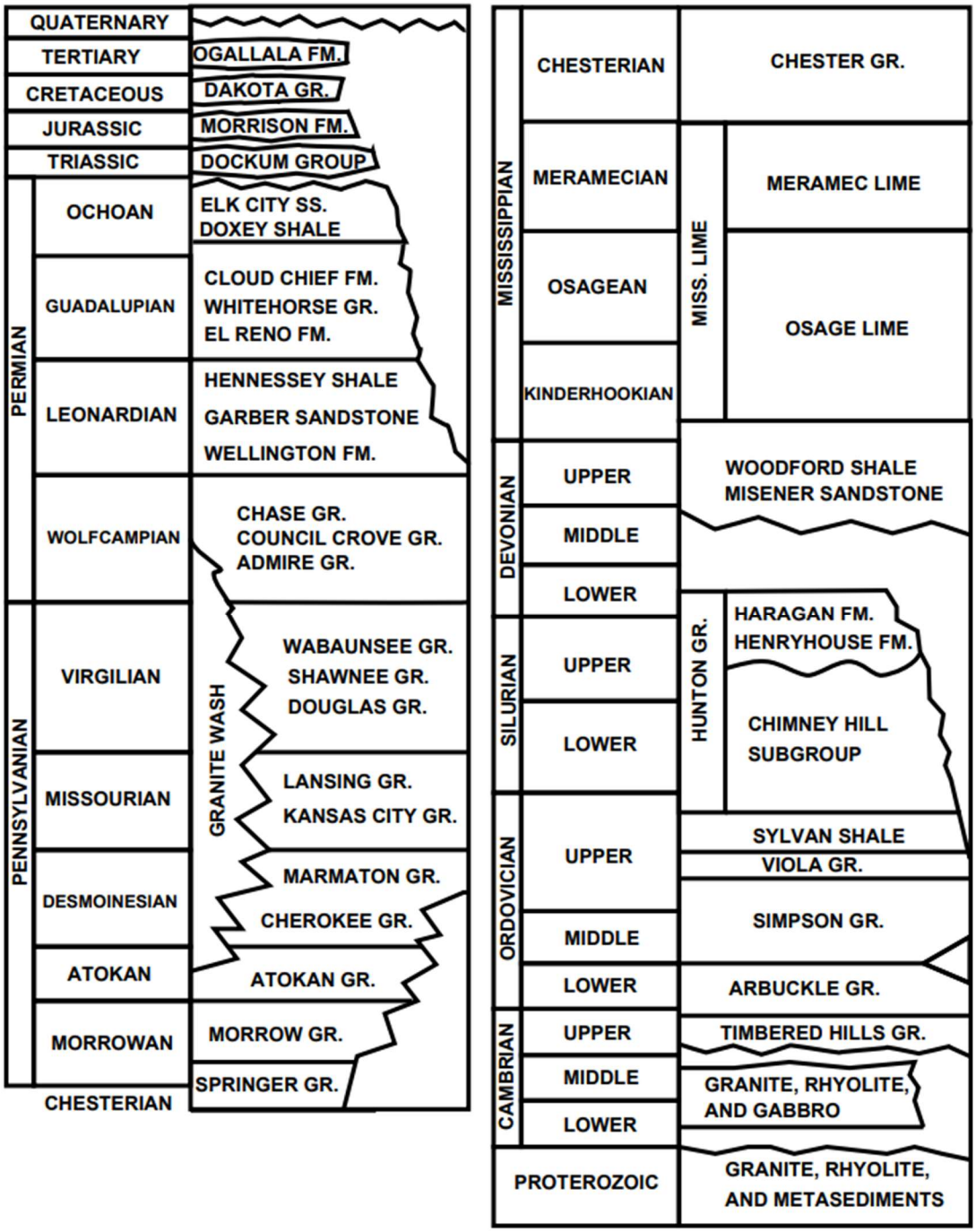

Figure 4.1: Generalized stratigraphic column for the Anadarko Basin. Height of formation or group box is not related to unit thickness (Carter, 1998).

An overall marine transgression with intermittent regressions typify Desmoinesian sedimentation throughout the Anadarko Basin. While the Granite Wash continued to develop in the south and southwest from arkosic detritus being shed off the Amarillo-Wichita Uplift, some

Desmoinesian sediment was sourced from other sides of the basin as the Nemaha Uplift to the east and the Arbuckle Mountains to the southeast had become defined basin boundaries by this time (Hill, 1984). Alluvial fans and fan deltas consisting of Granite Wash sediment prograded northward from the Amarillo-Wichita mountain front, with deposits in the proximal wash being largely coarse-grained and upwards fining, while deposits of the distal wash were typically finer-grained and interfingered with marine muds and silts. By the end of the late Desmoinesian, the majority of the Mid-Continent was blanketed in marine carbonates.

In the Missourian (middle to late Pennsylvanian), sedimentation in the Anadarko Basin looked similar to that of the Desmoinesian. Transgressive shales and thick, intermittent nearshore and valley fill sandstones formed, with noteworthy sands being the Cleveland, Cottage Grove, and Marchand (Hill, 1984). Granite Wash sediments continued to be deposited along the Amarillo-Wichita mountain front, in much the same fashion as in the Desmoinesian.

Virgilian (Late Pennsylvanian) sediments are typified by terrigenous clastic wedges deposited in deltaic environments that alternate with shallow marine carbonates deposited on the shelf (Alberta, 1987). Granite Wash deposition was still taking place as the granitic basement continued to be eroded off the uplift, but decreased tectonic activity had slowed the rate of deposition (Rascoe and Adler, 1983).

The Anadarko Basin was entirely filled in the early Permian. Lower Wolfcampian (Early Permian) sediments consist of transgressive marine limestones and shales, and the upper Wolfcampian is composed of a transgressive sequence of red and green shales, grayish yellow mudstones, limestones, and cherty limestones as well as a regressive sequence of the same lithologies in reverse vertical order (Moore, 1979). Leonardian (Early to Middle Permian) and Guadalupian (late Permian) consist of cyclic red beds and evaporites, which mark the final

withdrawal of Paleozoic seas from the southern Mid-continent and the termination of tectonic activity in the Amarillo-Wichita Uplift (Moore, 1979; Alberta, 1987).

4.2 Regional Structural Setting and Tectonics

Bounded on the south by the Amarillo-Wichita Uplift, on the east by the Nemaha Uplift, on the north and west by broad gentle shelf areas, and on the southeast by the Arbuckle Mountains and the Ardmore Basin, the Anadarko Basin is the deepest Phanerozoic sedimentary basin in the cratonic interior of the United States (**Figure 1.5**). The basin is elongated and asymmetrical, with thick accumulations of Paleozoic sedimentary strata reaching as much as 40,000 feet in its structurally deepest southern margin grading into thin coeval accumulations on the northeastern shelf, where basement depths are less than 5,000 feet (Ball et al., 1991). Rates of subsidence hardly ever exceeded rates of deposition, and the basin was rarely a topographic basin (Perry, 1989). It is separated from the Amarillo-Wichita Uplift on its southern margin by the Amarillo-Wichita Mountain Front Fault System, which is characterized by great vertical block uplift, regional left-lateral strike-slip movement, and up to 12 km of structural relief (Evans, 1979; Ye et al., 1996).

The Anadarko Basin did not exist as an independent structural feature until the Early Pennsylvanian as a result of the Late Paleozoic Pennsylvanian Orogeny. Faulting associated with the uplift of the Amarillo-Wichita Uplift to the south and the Arbuckle Mountains to the southeast, which partially define the basin's present shape, peaked in the Early Pennsylvanian and had largely ceased by the close of the Permian. However, the basin was an active subsiding tectonic feature throughout the Paleozoic, and its long and complex structural and tectonic history begins long before late Paleozoic tectonism developed its current configuration.

The structural and tectonic history of the Anadarko Basin can be divided into three major episodes: (1) an igneous (rifting) episode, or the Late Precambrian-Middle Cambrian

emplacement of intrusive and extrusive basement rocks and the development of the Southern Oklahoma Aulacogen (failed rift), (2) an epeirogenic episode, or the Middle Cambrian-Late Ordovician (post-Hunton) subsidence that formed the Southern Oklahoma Trough due to cooling that followed the emplacement of the large igneous province, and (3) a deformation episode, or Late Paleozoic tectonism, in which the Amarillo-Wichita Uplift and the adjacent Arbuckle Mountains were uplifted and the subsequent processes of thrust and sediment loading, oblique transpression, and regional flexure formed the present-day Anadarko Basin on the northwestern flank of the Southern Oklahoma Trough and the Ardmore Basin to the southeast (Wickham, 1978; Johnson, 1989; Perry, 1989; Turko, 2019).

Late Precambrian to Cambrian rifting resulted in the emplacement of a NW-SE oriented large igneous province across southern Oklahoma and into Texas. Recent work based on the igneous petrology and geochemical analysis of rocks in the Wichita Mountains support that the large igneous province is the result of an aulacogen (failed rift) that was initiated due to the opening of the southern Iapetus Ocean during the break-up of the supercontinent Rodinia (Hanson et al., 2013; Brueseke et al., 2014; Turko, 2019). While two of the three arms in the triple junction became sites of seafloor spreading as the Iapetus Ocean opened and would develop into Paleozoic continental margins, the third arm would extend into the continent and become an inactive rift zone termed the Southern Oklahoma Aulacogen (Hanson et al., 2013). During rifting, large amounts of igneous rocks were intruded (gabbros and granites) and extruded (basalts and rhyolites). An alternative hypothesis to the Southern Oklahoma Aulacogen being the failed arm of a radial-rift triple junction is that the Southern Oklahoma fault system is instead a transform-parallel intracratonic fault system associated with the Iapetan rift system (Thomas, 2014). Proponents of the interpretation that the Southern Oklahoma Aulacogen is not really an aulacogen but rather a system of transform faults point to the large volume of igneous rocks along the fault

system as evidence for a mantle thermal anomaly that is consistent with a leaky transform fault (Thomas, 2014).

Following rifting and the emplacement of the large igneous province, the aulacogen began to cool and subside, forming a passive continental margin and the Southern Oklahoma Trough. The axis of the Southern Oklahoma Trough is coaxial with the Southern Oklahoma Aulacogen, extending northwest from the paleocontinental margin (southeast of the present-day Ardmore Basin), through the Ardmore Basin, Arbuckle Mountains, and the modern Wichita Mountains and into the northern Texas Panhandle. Subsidence and the accompanying marine transgression is represented by the thick, largely shallow-marine carbonate sedimentary sequence from the Late Cambrian through the Early Mississippian, beginning with the deposition of the transgressive marine Late Cambrian Reagan Sandstone. Feinstein (1981) modeled the thermally-controlled isostatic subsidence by constructing subsidence curves for the Anadarko Basin. They depict a clear exponential curve with initially high subsidence rates that greatly slow and almost flatten in the Early Silurian through Early Devonian, with the craton being relatively stable into the Middle Mississippian (Feinstein, 1981; Turko, 2019).

The Late Mississippian marked the start of great tectonism, renewed subsidence, and the growth of the asymmetric Anadarko Basin due to the collision of Paleozoic North America with Gondwana. Some researchers advocate that stresses from this collision (which created the Appalachian and Ouachita-Marathon Fold and Thrust Belts) are responsible for the structural inversion of the core of the Southern Oklahoma Aulacogen into the Wichita Uplift, which caused thrust loading of the region that would develop into the Anadarko Basin (Perry, 1989). More recently, some geologists have proposed that the inversion of the Southern Oklahoma Aulacogen was a result of intraplate tectonics caused by tectonic activity along the western (Nevada) and southwestern (Sonora) of the North American Plate (Turko, 2019). Some have suggested that deformation was driven by stresses along the Sonora Margin by flat-slab subduction (Ye et al.,

1996) or as a result of the combined compressional forces from the Sonora, Ouachita-Marathon, and Antler margins (Leary et al., 2017).

The Late Paleozoic tectonism that caused the deformation of the Southern Oklahoma Aulacogen can be divided into two tectonic events. The first event, the Wichita Orogeny, occurred from the Late Mississippian to the Atokan (Early Pennsylvanian) and marks the significant inversion and uplift of the Amarillo-Wichita Uplift horst block along a series of W-NW-trending reverse faults (Johnson, 1989). The basin continued to subside throughout the duration of Pennsylvanian orogenic activity, and major thrust faults with maximum vertical displacement reaching 40,000 feet have been identified on the Amarillo-Wichita Uplift-Anadarko Basin boundary (Ball et al., 1991).

The second Late Paleozoic tectonism event is the Arbuckle Orogeny, which occurred from the Late Desmoinesian (Middle Pennsylvanian) through the Virgilian (Late Pennsylvanian). This orogenic event includes the uplift of the Arbuckle Mountains and the folding and subsidence of the Ardmore Basin. By the end of the Pennsylvanian, the majority of tectonic activity had ceased in the region and the Anadarko Basin was fully developed. The deposition of Permian red beds, dolomites, shales, and evaporites on top of Pennsylvanian arkosic sands represents the end of Paleozoic deposition and active tectonism in the Anadarko Basin (Webster, 1980).

4.3 Marmaton Granite Wash Stratigraphic Framework

Given the massive nature of the largely conglomerate and sandstone debris that was rapidly shed off the Amarillo-Wichita Uplift into the deep Anadarko Basin, the formation can appear homogenous on wireline logs. Subdividing these massive wash packages, particularly immediately proximal to the uplift, is a daunting, if not impracticable, task. As the subaqueously deposited granitic wash packages do not exhibit characteristics of subaerial unconformities, the Exxon Sequence Stratigraphic Model is not an applicable method of subdividing the Marmaton

Granite Wash. Sequence boundaries in the formation are typically considered to be the erosional bases of fining upward sequences and the tops of shales. While it is not feasible to recognize depositional sequence boundaries and develop a sequence stratrigraphic framework for the formation, the various wash packages of the Marmaton Granite Wash examined in this study can be correlated using regionally extensive transgressive shale markers.

Around 10 to 20 miles to the northeast of the mountain front where the accumulation of detritus was less pervasive, four "hot" (high API reading on gamma-ray logs) marine shales are found to be interbedded between wash packages and can be easily observed and correlated on wireline logs (Mitchell, 2011). These four hot shale marine flooding surfaces represent transgression and inundation of the expansive northern shelf and narrow southern shelf of the basin and are known to be regionally extensive with unique and characteristic log signatures, while the intervening sandstone/conglomerate wash packages are representative of periods of massive deposition of the uplift-derived detritus. The hot shales are identified on well logs by a prominent high-magnitude and short-duration increase in radioactivity (spike) in gamma-ray value greater than 150 API units, increased neutron porosity, an accompanying decrease in deep resistivity, and an increase in density porosity (Mitchell, 2011). Names of these hot shale marker beds and wash packages are highly variable across the petroleum industry (e.g. Hendrickson et al., 2001; Mitchell, 2011; LoCricchio, 2012) with terminology not only varying from company to company, but being especially variable on either side of the Texas-Oklahoma border.

This study utilizes the stratigraphic nomenclature and correlation framework developed by Mitchell (2011) to identify these hot shale markers and construct a stratigraphic framework for the Marmaton Granite Wash interval. This stratigraphic framework was essential for correlation, constructing regional cross sections, and mapping. The stratigraphy as proposed by Mitchell (2011) is shown in an example wireline-log section from Wheeler County, Texas (**Figure 1.4**). Under this correlation scheme, the four hot shales that subdivide the Marmaton Granite Wash are,

in ascending stratigraphic order, the Fourth through First Marmaton Shales. Between the underlying Upper Skinner Shale and the Fourth Marmaton Shale is the Marmaton "F" Wash, between the Fourth and Third Marmaton Shales is the Marmaton "E" Wash, between the Third and Second is the Marmaton "D" Wash, and between the Second and First is the Marmaton "C" Wash.

The Marmaton "A" and "B" Washes lie above the First Marmaton Shale, but these wash intervals lack shale marker beds and are rather homogenous on wireline logs, making these two packages and the top of the Marmaton Wash difficult to distinguish and define. Further, the Upper Skinner Shale that underlies the Marmaton "F" interval and serves as the base of the entire Marmaton Granite Wash interval proved difficult to correlate across the region. Due to these reasons as well as limitations in time and data, this study focuses primarily on the Marmaton "C", "D", and "E" Washes which are separated by the four Marmaton hot shales. Of particular interest to this study is the Marmaton "D" wash interval, of which three cores were extensively analyzed.

A regional cross section was constructed across the study area to trace the extents of the four Marmaton hot shales (First through Third Marmaton Shales) from the Mountain View Fault System in south-central Wheeler County, Texas southwest into the Anadarko Basin and to the northeastern extent of the study area in southwestern Dewey County, Oklahoma (**Figure 4.2**). The cross section was flattened on the top of the First Marmaton Shale as it is the most consistent and reliable marker across the study area. Between the four Marmaton hot shales are the Marmaton "C" through "E" Washes, and the Marmaton "F" wash lies between the Fourth Marmaton Shale above and the Upper Skinner Wash below. Also depicted on the cross section are the underlying Upper Skinner Wash, Lower Skinner Shale, and the top of the Lower Skinner Wash in order to better understand and compare depositional trends prior to the Marmaton. The left-most (farthest to the southwest) well in **Figure 4.2** is located within the fault system and is situated on an up-thrown fault block. As depicted in this well, all formations appear to be

substantially thinner within the fault system. Moving southwest into the fault system, the Marmaton Shales quickly become indiscernible as the wash intervals rapidly thin and shallow on the up-thrown fault block.

A cross section consisting of the same wells as in **Figure 4.2** but with only the depth tracks visible is shown in **Figure 4.3** in order to provide a better visual representation of changes in formation thickness across the study area. This cross section is also flattened on the top of the First Marmaton Shale, the most consistent and reliable stratigraphic marker. The First (stratigraphically highest) through Third Marmaton Shales are widespread and traceable across the entirety of the study area and likely extend even further to the northeast (only limited here by data availability). In western Roger Mills County, Oklahoma, the hot shale marker at the top of the Fourth Marmaton Shale becomes indistinguishable from the surrounding wash and is unable to be traced any farther northeast. The top of the underlying Upper Skinner Shale (the base of the Marmaton "F" Wash) becomes indistinguishable to the northeast even sooner, reaching its traceable extent away from the fault system in southwestern Roger Mills County. However, the tops of the Middle Desmoinesian (Cabaniss "Cherokee" Group) Upper Skinner Wash, Lower Skinner Shale, and Lower Skinner Wash below are traceable a little farther than the top of the Fourth Marmaton Shale, becoming indiscernible in central Roger Mills County. The tops of the Skinner interval are picked back up in east-central Roger Mills County and become increasingly more discernable to the northeast, likely extending beyond the northeastern extent of the study area. The tops of both the Fourth Marmaton Shale and the Upper Skinner Shale are not clearly distinguishable to the northeast and are not picked back up again, reaching their final extents within the study area in western Roger Mills County.

This correlation indicates that the four Marmaton hot shale markers (the First through Fourth Marmaton Shales) observed by Mitchell (2011) in the deep Anadarko Basin are correlative to the Marmaton and Cabaniss (Upper "Cherokee") Group on the Anadarko Shelf to

the northeast recognized by Puckette (1990), Boyd (2008), and others. Further, it is likely that the Lower Skinner Wash observed by Mitchell (2011) adjacent to the mountain front is time equivalent to the Desmoinesian Upper Red Fork, Pink Limestone, and Lower Skinner Sandstone that are well established stratigraphic sections on the Anadarko Shelf.

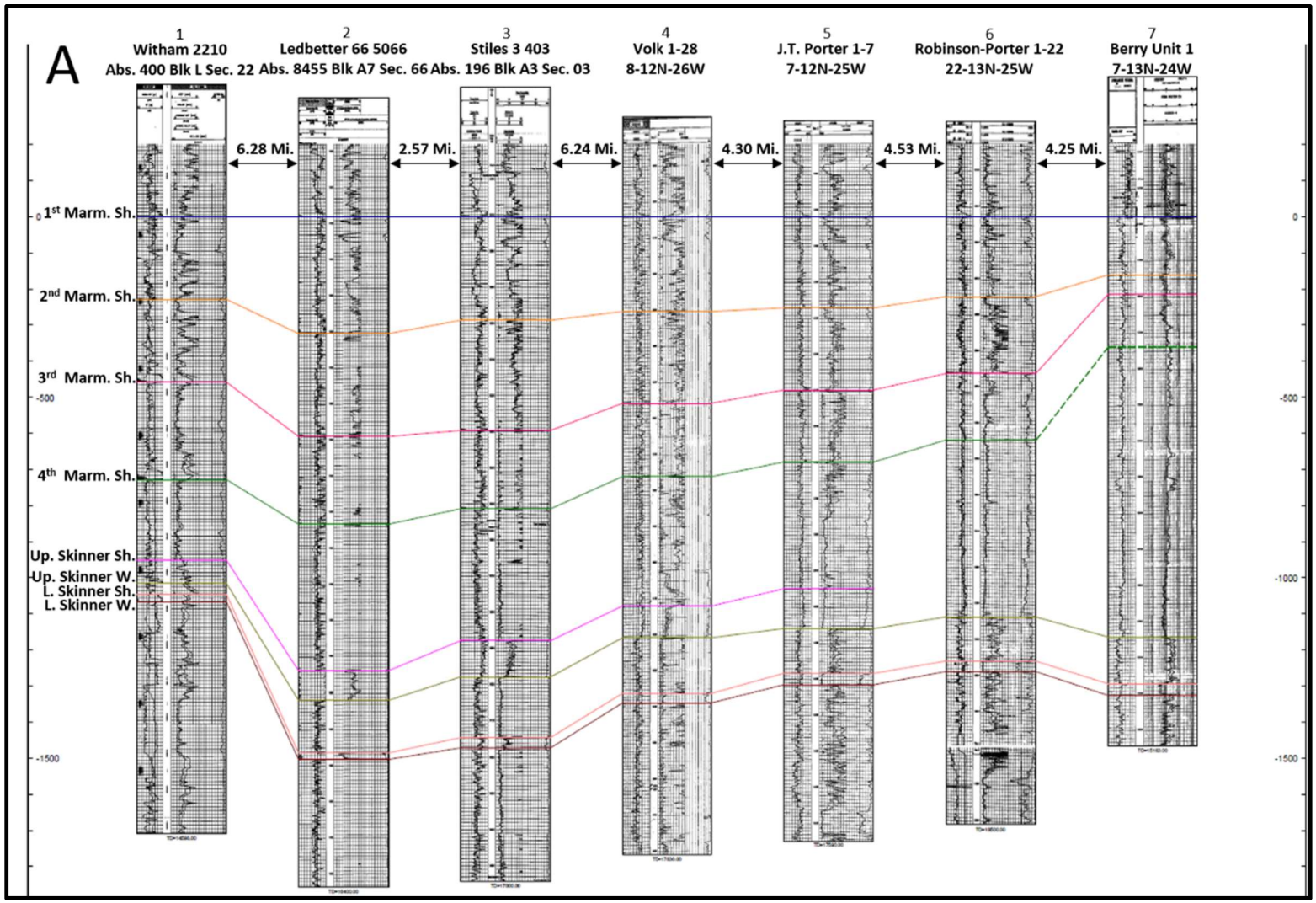

Figure 4.2: Regional SW-NE cross section across the study area from the Mountain View Fault System to the northeastern extent of the study area in Dewey County, Oklahoma, flattened on the First Marmaton Shale. Section location is shown in **Figure 4.4**.

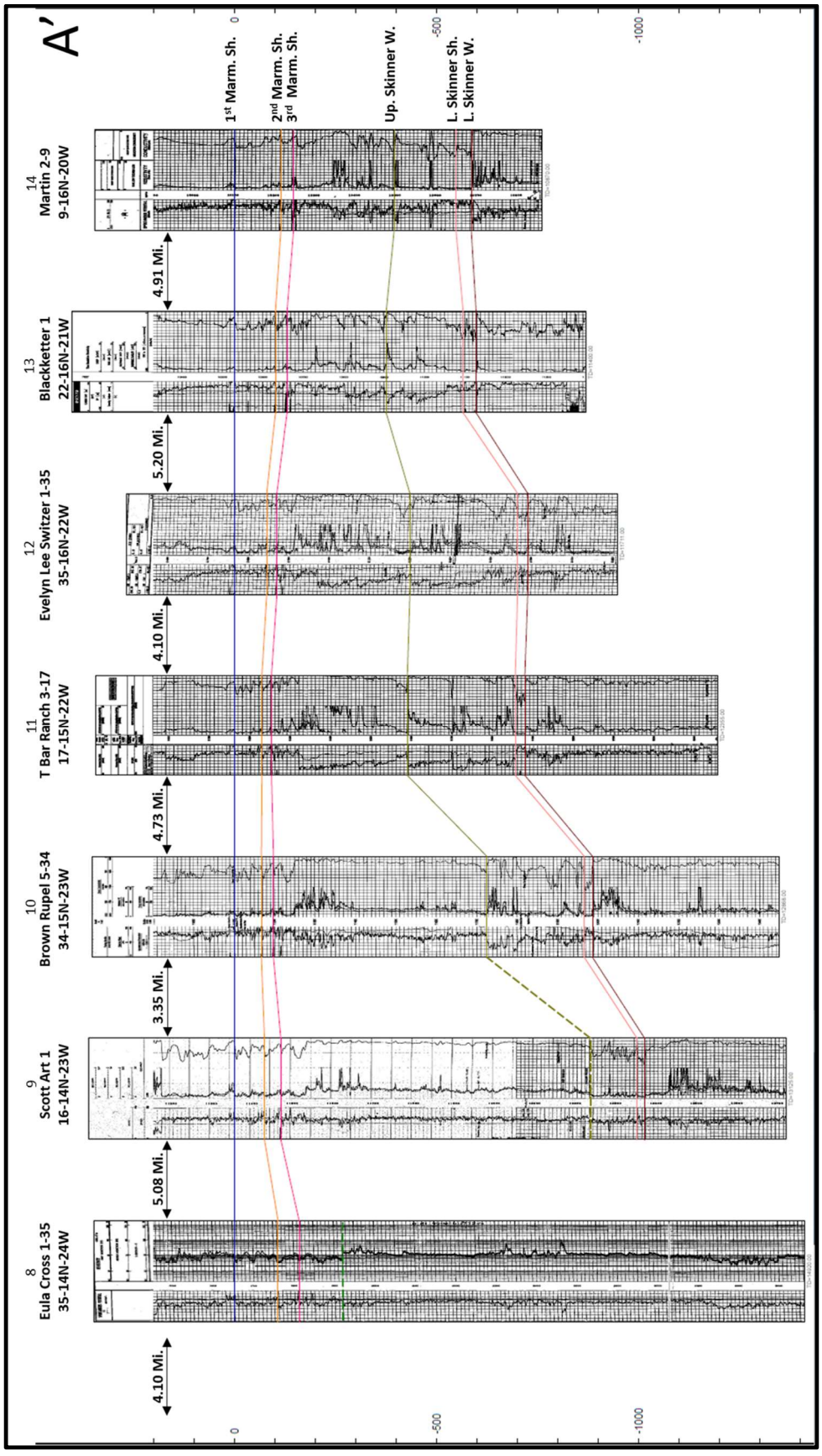

Figure 4.2 continued.

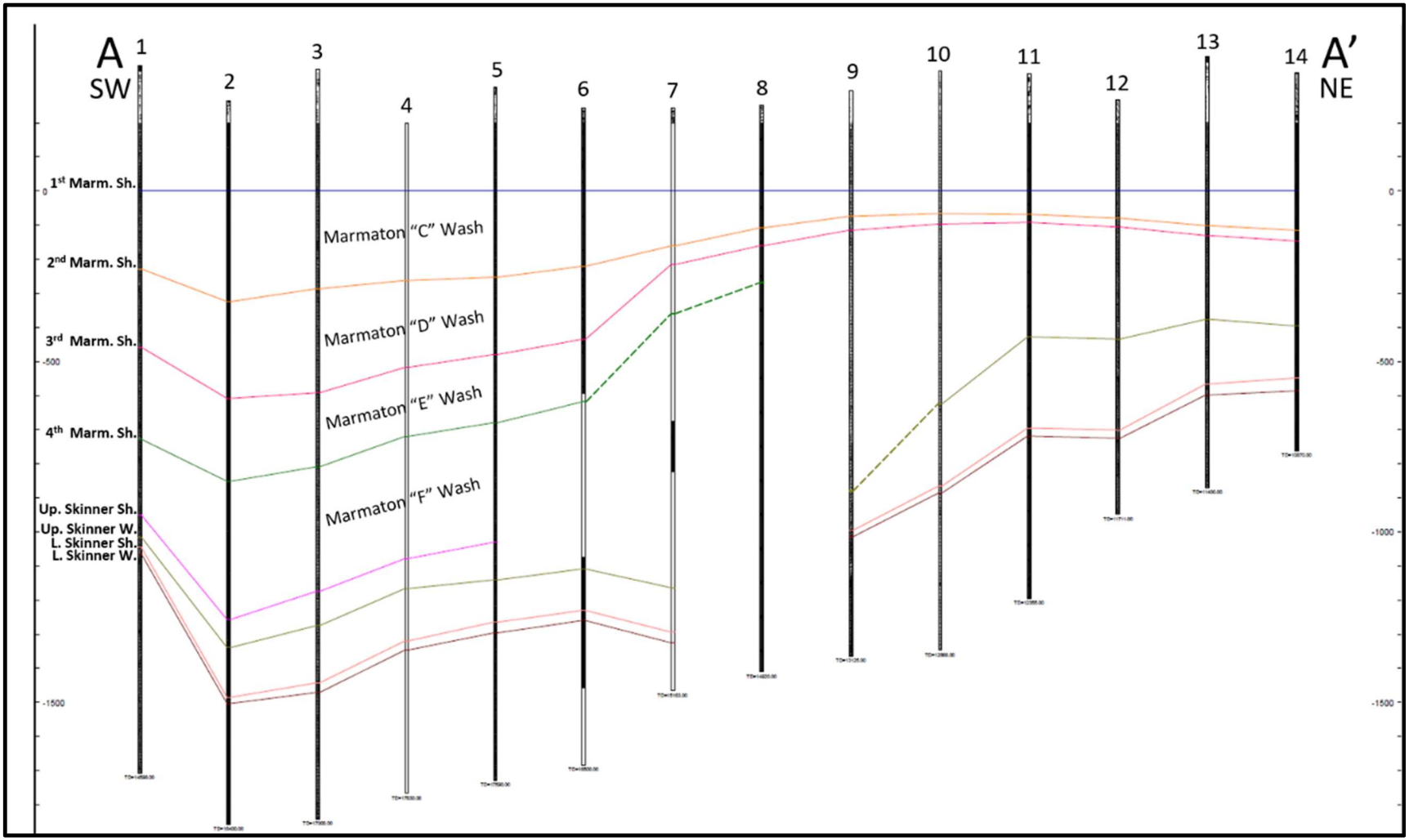

Figure 4.3: Regional SW-NE cross section shown in Figure 4.2 but with only depth tracks visible for better visualization of thickness trends across the study area. Section is flattened on the First Marmaton Shale as it is the most consistent and reliable stratigraphic marker across the study area. Section location is shown in **Figure 4.4**.

4.4 Marmaton Granite Wash Structure

A structure map referenced to a sea level datum was generated on the top of each of the four Marmaton hot shale flooding surfaces (**Figures 4.4**, **4.5**, **4.6**, and **4.7**). Further, a structural cross section showing the same wells on the same datum as in **Figure 4.2** but with only the depth tracks visible is shown in **Figure 4.8** in order to provide a better visual representation of structural trends. The First through Third Marmaton Shales are regionally extensive across the study area, but the hot shale marker at the top of the Fourth Marmaton Shale is not able to be correlated to the full study area extent and becomes indistinguishable in western Roger Mills County, Oklahoma. For this reason, the Fourth Marmaton Shale structure map was cut off at the Texas-Oklahoma border and does not extend any further east (**Figure 4.7**).

The depth below sea level of the top of the First Marmaton Shale reaches 10,878 feet at its deepest point in the study area in southwestern Roger Mills County, Oklahoma (**Figure 4.4**). The top of the Marmaton shale shallows from this point to the north, west, and northwest, reaching around 7,565 feet below sea level in the northwest in western Hemphill County, Texas and around 7,930 feet below sea level at the far northeastern extent of the study area in southwestern Dewey County, Oklahoma. The Mountain View Fault System is located at the southwestern edge of the study area, along the southwestern boundary of the Anadarko Basin and the northern flank of the Amarillo-Wichita Uplift. The Mountain View Fault System displays left-lateral transpression. The top of the First Marmaton Shale is at its shallowest within the fault system at about 6,390 feet below sea level, but quickly deepens to over 9,000 feet below sea level along the northern side of the fault system. In general, dip is to the southeast in the Texas Panhandle portion of the study area but is to the south-southwest in Western Oklahoma. The other three Marmaton Shale markers display very similar structural trends and follow largely the same contour pattern.

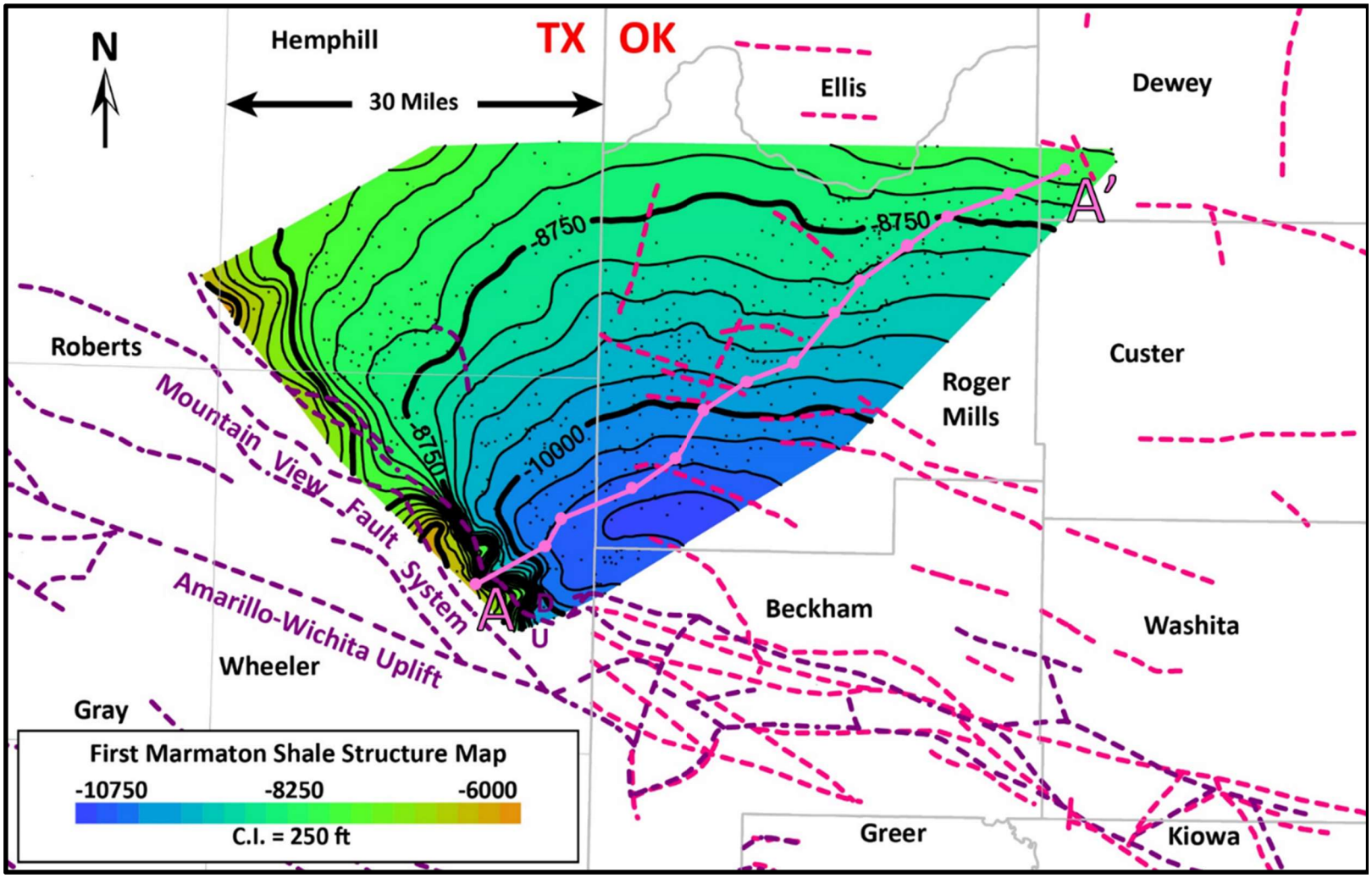

Figure 4.4: Structure map on the base of the First Marmaton Shale. Contour interval is 250 feet. All depth values are subsea (SS). Pink fault lines are from Oklahoma Geological Survey (OGS) (Marsh and Holland, 2016) and purple fault lines are from the Bureau of Economic Geology (BEG) (Ewing, 1990). Cross section A-A' is shown in **Figure 4.2**.

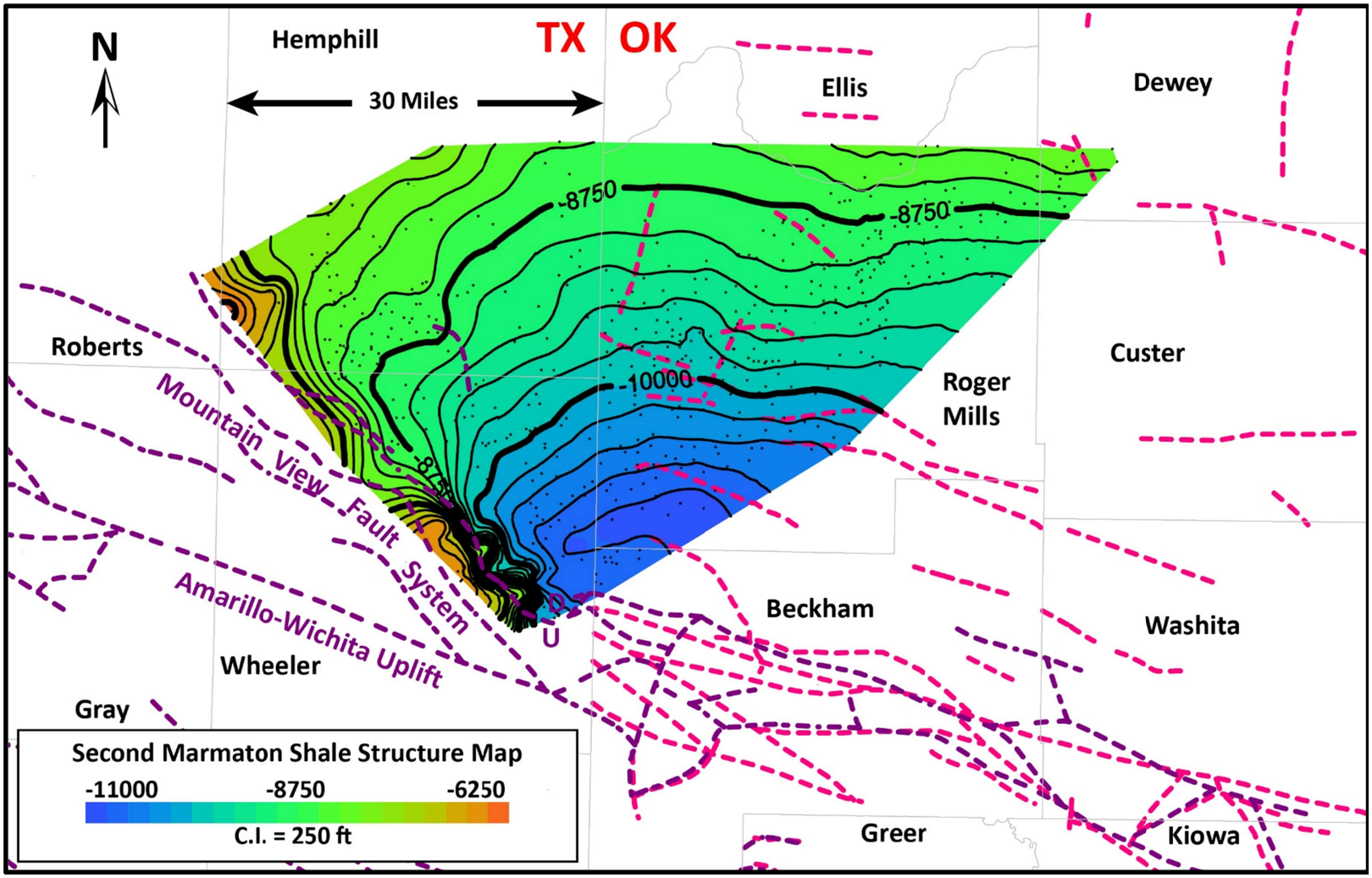

Figure 4.5: Structure map on the base of the Second Marmaton Shale. Contour interval is 250 feet. All depth values are subsea (SS). Pink fault lines are from Oklahoma Geological Survey (OGS) (Marsh and Holland, 2016) and purple fault lines are from the Bureau of Economic Geology (BEG) (Ewing, 1990).

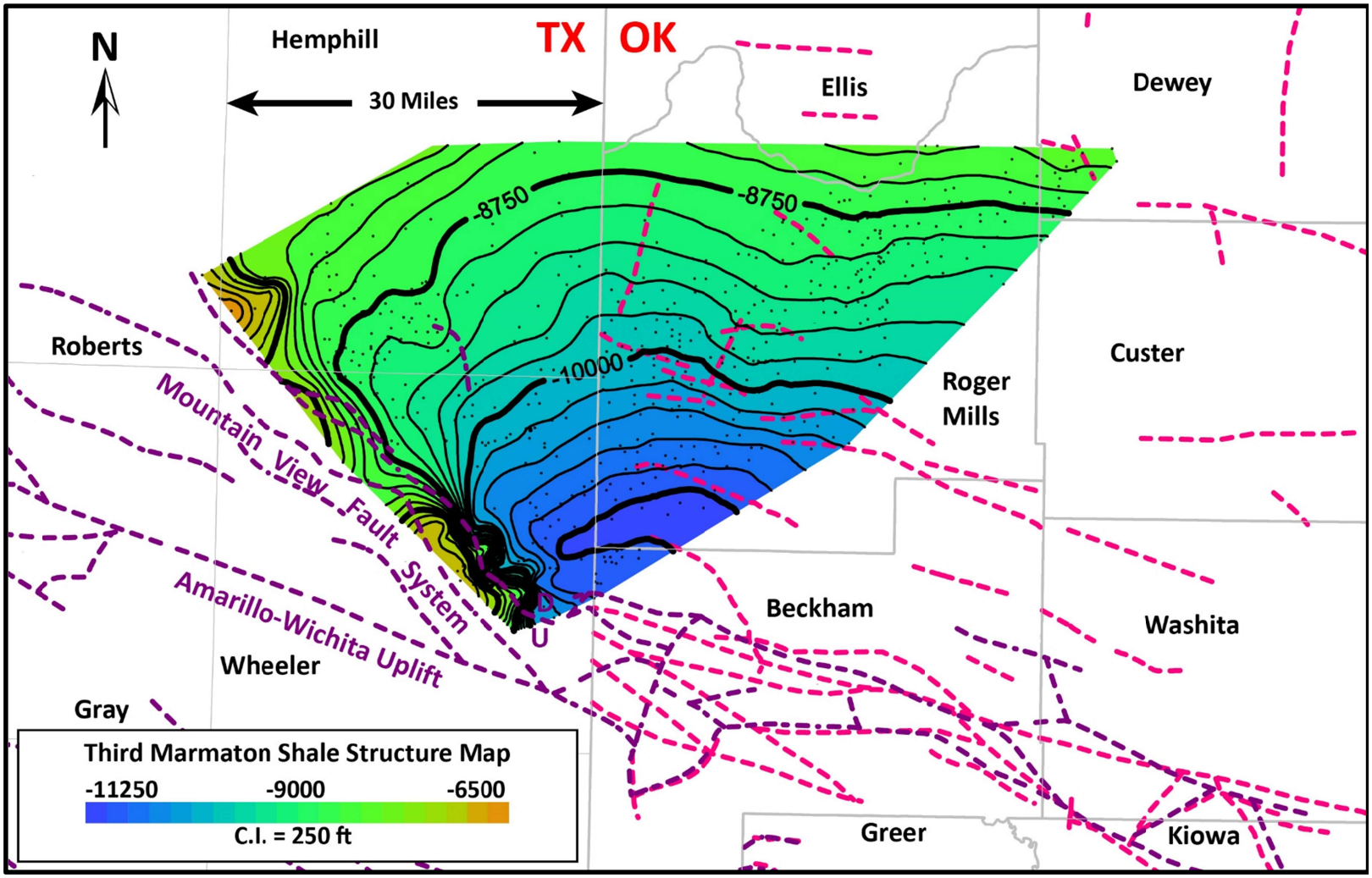

Figure 4.6: Structure map on the base of the Third Marmaton Shale. Contour interval is 250 feet. All depth values are subsea (SS). Pink fault lines are from Oklahoma Geological Survey (OGS) (Marsh and Holland, 2016) and purple fault lines are from the Bureau of Economic Geology (BEG) (Ewing, 1990).

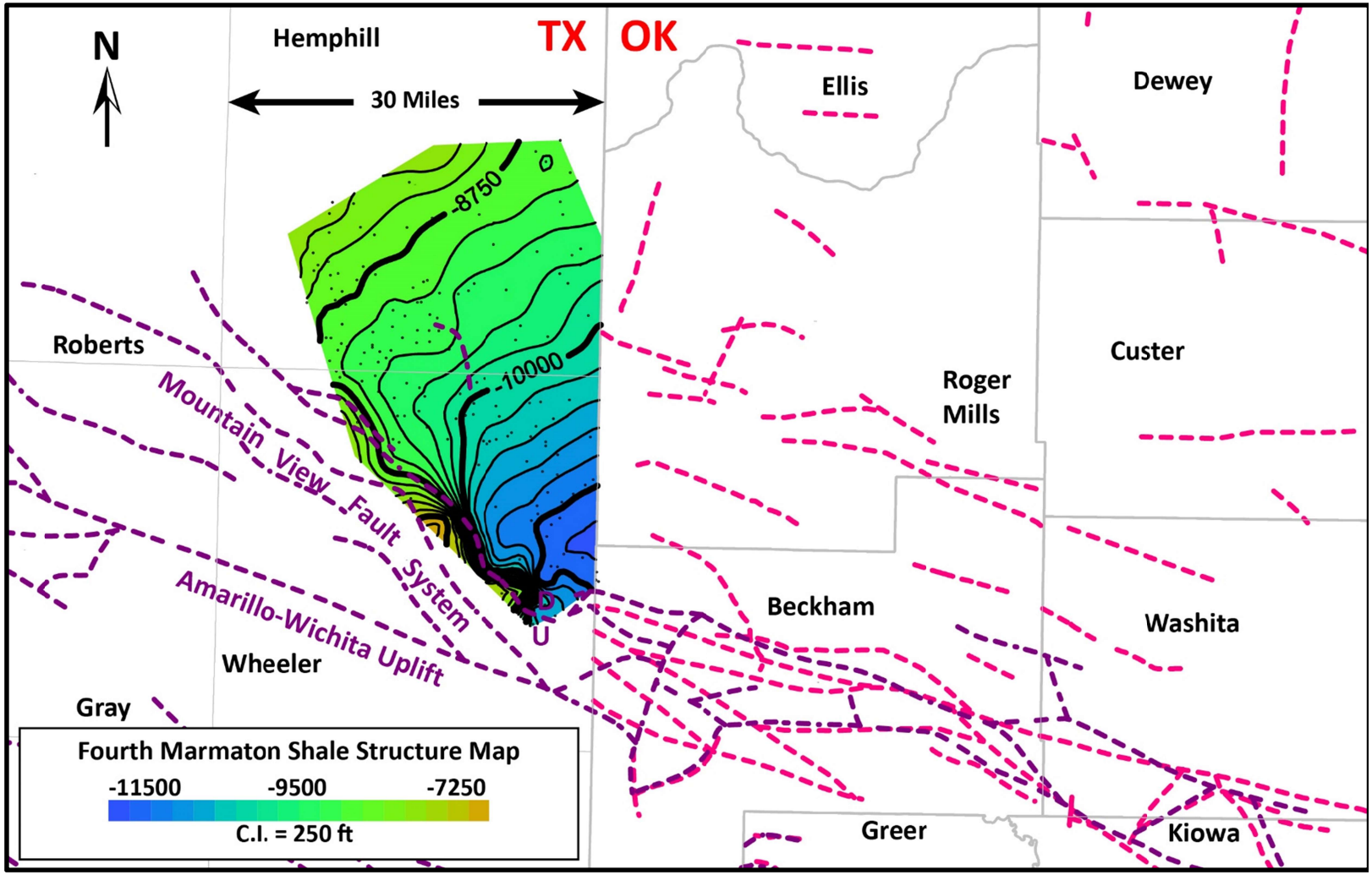

Figure 4.7: Structure map on the base of the Fouth Marmaton Shale. Contour interval is 250 feet. All depth values are subsea (SS). Pink fault lines are from Oklahoma Geological Survey (OGS) (Marsh and Holland, 2016) and purple fault lines are from the Bureau of Economic Geology (BEG) (Ewing, 1990).

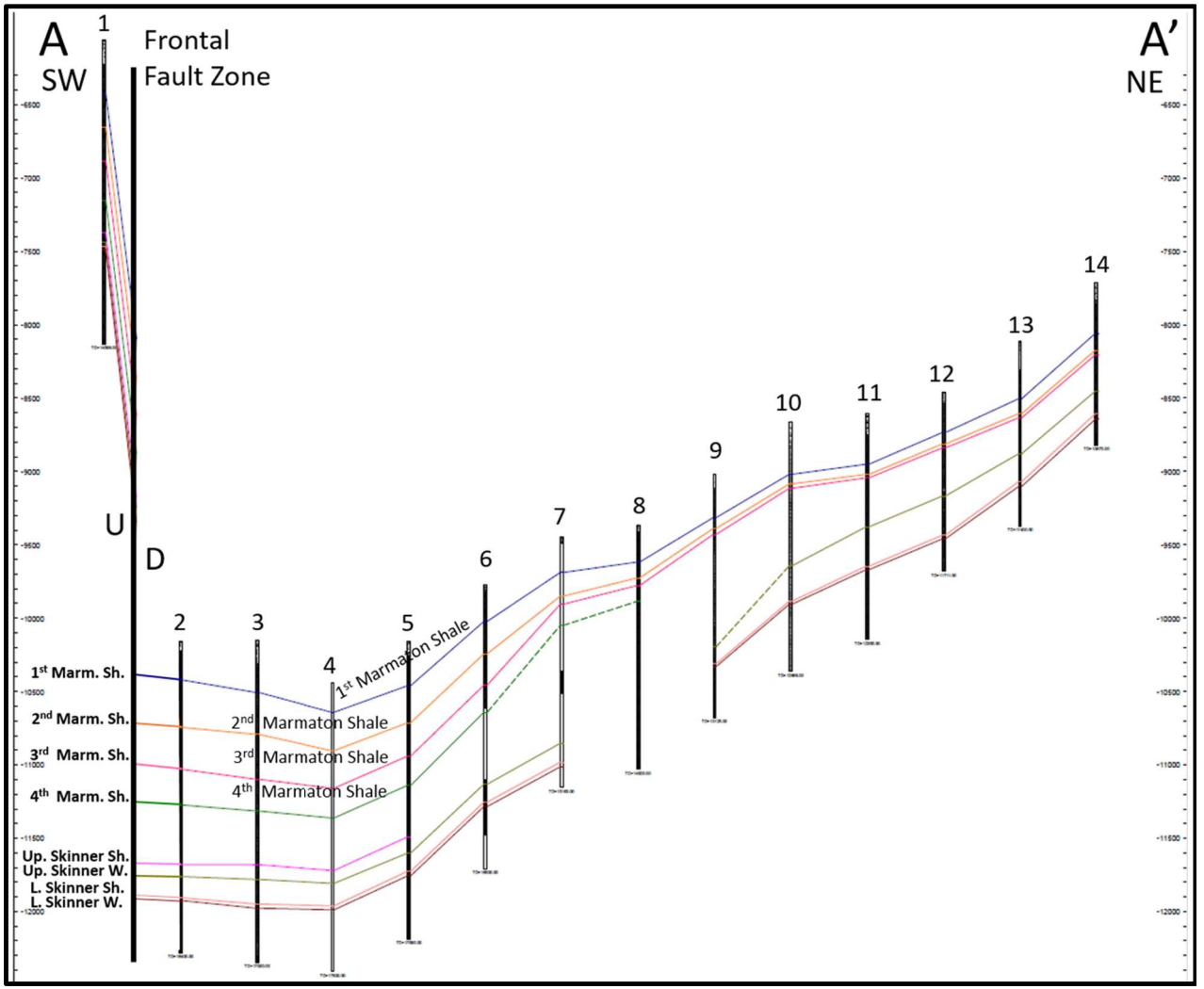

Figure 4.8: Regional SW-NE structural cross section shown in Figure 4.2 with only depth tracks visible for better visualization of structural trends across the study area. Section location is shown in **Figure 4.4**.

CHAPTER V

DISTRIBUTION AND GEOMETRY OF MARMATON GRANITE WASH

5.1 Introduction to Depositional Trends

The granitic sediments of the Marmaton Granite Wash were sourced from the crystalline basement rocks on top of the Amarillo-Wichita Uplift and were deposited into the deep Anadarko Basin in response to tectonic uplift. The study area was located around 10° south of the paleoequator during the Middle Pennsylvanian, meaning that the region was characterized by a humid equatorial climate (Kushner et al., 2022). The associated high precipitation in the region would have facilitated a high weathering and erosion rate atop the Amarillo-Wichita Uplift, leading to a high volume of granitic detritus being rapidly deposited into the subsiding Anadarko Basin to the north and northeast during Marmaton time. Subsidence rates in the southern Anadarko Basin are thought to have been similar to rates of deposition, which allowed for a clastic wedge of granitic sediment greater than 5,000 feet thick to accumulate in the basin just north of the Amarillo-Wichita Frontal Fault System (Dutton, 1982).

The Marmaton Granite Wash is considered to be of similar depositional origin as the Early Pennsylvanian washes of the Anadarko Basin described by Dutton (1984), Lyday (1985), Dutton and Land (1986), and Alberta (1987). These early studies on the Early Pennsylvanian washes described proximal alluvial fan and fan delta environments of deposition. However, given the fact that the Middle Pennsylvanian Marmaton Granite Wash was deposited later than these

early washes during a period of marine transgression and continued basin subsidence (and given that the study area described in this study extends further away from the mountain front source area than those described in these early studies), the Marmaton Granite Wash is largely associated with submarine fan environments. While these early Anadarko Basin wash studies are helpful in understanding the depositional processes seen in the Marmaton Granite Wash, it is necessary to look into generalized submarine fan (both modern and ancient) studies in order to develop a better understanding of wash deposition into the deep Anadarko Basin (i.e. Walker 1978; Shanmugam and Moiola, 1988; Anderson, 1992; Bouma, 2000).

Shanmugam and Moiola (1988) define submarine fans as "channel and lobe (or sheet sand) complexes formed from sediment gravity flows in the deep-sea environment, commonly beyond the continental shelf" and do not consider fan deltas (that develop in shallow-water environments) to be a type of submarine fan. Sediment gravity flows are the primary deep marine process associated with the development of submarine fans, transporting sediment that has bypassed the shelf through submarine canyons and gullies (Shanmugam and Moiola, 1988). Fan size and shape is highly variable, with some modern fans being elongate (e.g., Bengal Fan in the northeastern Indian Ocean), some being trapezoidal (e.g., the Astoria Fan, about 10 miles offshore from the mouth of the Columbia River in the northwestern United States), and others being even more complex in shape. While some submarine fans are less than 10 miles across in total length, the Bengal Fan is more than 1,500 miles long. This high variability in fan morphology can be contributed to a range of factors including (but certainly not limited to) shelf-to-basin relief, slope gradient, and local tectonic features on the sea floor (Shanmugam and Moiola, 1988). Howell and Normark (1982) identify the primary controls on submarine fan morphology as (1) size and shape of the basin the sediment is being deposited into, and (2) the volume, rate of deposition, and grain-size distribution of the sediment supply.

Grain size distribution of sediment is an important aspect of submarine fan architecture. It is a primarily control on reservoir quality, and can also reflect the distribution of particulate organic matter across the fan. In general, submarine fan lobes typically display a linear fining grain-size trend away from the sediment source due to decreasing energy of deposition. Conglomeratic sediment is expected proximal to the Amarillo-Wichita Uplift source area as coarser bedload material requires more energy to be transported than finer-grained bedload and suspended sediments, which are expected to be found in more distal fan environments where they prograde into the basin and interfinger with deeper marine mudrocks.

5.2 Thickness Trends of Marmaton Granite Wash Intervals

In order to help determine the distribution, geometry, and depositional trends of the Marmaton Granite Wash across the study area, thickness maps were constructed for the Marmaton "C", "D", and "E" Wash intervals using the distinctive, regionally-distinguishable high gamma-ray response of the hot shale markers that define them. A thickness map of the Marmaton "F" Wash was not included as its base, the Upper Skinner Shale, is not widely extensive across the study area and reaches its northeastern extent in southwestern Roger Mills County, Oklahoma. Thickness trends of the uppermost Marmaton Granite Wash intervals (the Marmaton "A" and "B" Washes) are also not mapped as these intervals do not have a defining hot shale marker as their upper limit and lack a sharp, uniform boundary at their stratigraphic tops.

A thickness map of the Marmaton "C" Wash, which lies between the First and Second Marmaton Shales, is shown in **Figure 5.1**. Source direction appears to be from the west-southwest, which supports that the Amarillo Wichita Uplift is the primary source of sediment. Multiple prominent lobate features are observed extending from the Amarillo-Wichita Uplift to the southwest and west of the study area, trending towards the northeast. The individual lobes are thickest along their central axis, which run perpendicular to the uplift. Marmaton "C" Wash

thickness reaches just shy of 350 feet thick along the central axis of a lobe located in the northeastern corner of Wheeler County, Texas. The lobes are separated by interlobe areas proximal to the uplift, but they increasingly blend together and become less distinct from one another going away from the source area. These interlobe areas are 200 feet thick or less proximal to the uplift. The lobes themselves are commonly 100 to 150 feet thicker than the interlobe areas. In general, wash thickness wanes to the northeast. Contour density rapidly increases along a northwest-southeast trend in western Roger Mills County, indicating a sudden decrease in thickness from about 200 feet to 125 feet thick in just over 2.5 miles. The thickness of the Marmaton "C" Wash remains more consistent to the northeast of this trend, gradually decreasing to 60 feet thick in north-central Roger Mills County and then gradually increasing again to 130 feet thick in southwestern Dewey County, Oklahoma.

A thickness map of the Marmaton "D" Wash, which is bounded by the Second Marmaton Shale above and the Third Marmaton Shale below, is shown in **Figure 5.2**. All three cores analyzed in this study (and described in detail in Chapter 6) belong to this interval. The locations of these three cores are represented on the Marmaton "D" Wash thickness map in **Figure 5.2** as colored polygons. As with the Marmaton "C" Wash above it, the wash forms lobes that are typically thickest and more discrete in shape in the west and southwest, adjacent to the uplift. Thickness decreases to the northeast away from the uplift, and the same linear trend of increased contour density is observed in western Roger Mills County. Thickness decreases more than 100 feet in only 2.5 miles across this trend. The wash is thickest along the central axis of individual lobes, reaching almost 350 feet thick in the center of one lobe in southwestern Hemphill County, Texas. The two Buffalo Wallow Field cores from Hemphill County described in this study are found within this discrete lobe and have thickness values around 275 feet (**Figure 5.2**). The location of the third core described in this study, the Kicking Bird of Roger Mills County, is shown in **Figure 5.2** and has a Marmaton "D" Wash thickness value of 233 feet. It is located too

far from the uplift for discrete lobes to be observed and identified, and appears instead to be situated where the distal fringes of individual lobes have merged together. Interlobe areas adjacent to the uplift are as low as 200 feet thick. Thickness remains more constant to the northeast of the linear trend that runs northwest-southeast across western Roger Mills County, gradually decreasing from 90 feet thick in south-central Roger Mills County to 30 feet thick in southwestern Dewey County.

The Marmaton "E" Wash, which is bounded by the Third Marmaton Shale above and the Fourth Marmaton Shale below, is the deepest of the three thickness maps and displays similar thickness trends to the Marmaton "C" and "D" Washes (**Figure 5.3**). The map does not extend further northeast than the extent of the Forth Marmaton Shale and is therefore cut off in western Roger Mills County. The lobate structure seen adjacent to the uplift is not as defined as on the two shallower thickness maps, but is still evident. Thickness within lobes reaches over 300 feet thick immediately adjacent to the uplift, whereas interlobe areas just as close to the uplift have thickness values as low as 160 feet.

5.3 Net Sandstone Thickness Trends at Buffalo Wallow Field

A net sandstone thickness map of the Marmaton "D" Wash interval in Buffalo Wallow Field in Hemphill County, Texas and the surrounding area was developed in order to better understand sandstone depositional trends across individual fan lobes (**Figure 5.4**). The thickness of the sandstone (specifically excluding the interbedded shales) within the Marmaton "D" wash interval of each well in the area was determined from wireline logs. A shale baseline was established using gamma-ray logs on a well-to-well basis by finding the average between a typical marine shale and a typical clean sandstone. An explanation of why the gamma-ray log is a reliable indicator of shale intervals in this region of the Marmaton Granite Wash study area even though the formation is notoriously high in potassium feldspar is provided in Chapter 2.

Marmaton “D” Wash net sandstone thickness across Buffalo Wallow Field and the surrounding area ranges from 125 feet to 250 feet. The overall geometry depicts lobate structures similar to those seen on the total Marmaton “D” Wash thickness map, but at a larger scale. In this region of the Marmaton Granite Wash study area, the Marmaton “D” Wash appears to form discrete lobes, unlike in the more distal areas seen in the total thickness map where the lobes begin to overlap and discrete lobes are not identifiable. Source direction appears to be coming from the southwest, as net sandstone thickness values are highest along a central linear trend coming from the southwest and running perpendicular to the uplift before branching off to the northeast and northwest. Net sandstone thickness contour density is greatest along a central axis running southwest-northeast, but lessens in each direction away from this central axis. The two cores from Buffalo Wallow Field described in this study are located in this central area of higher net sandstone thickness, with the Grant Meek #236-1 having a Marmaton “D” Wash net sandstone thickness of 150 feet and the Fillingim #88-2 having a net sandstone thickness of 185 feet.

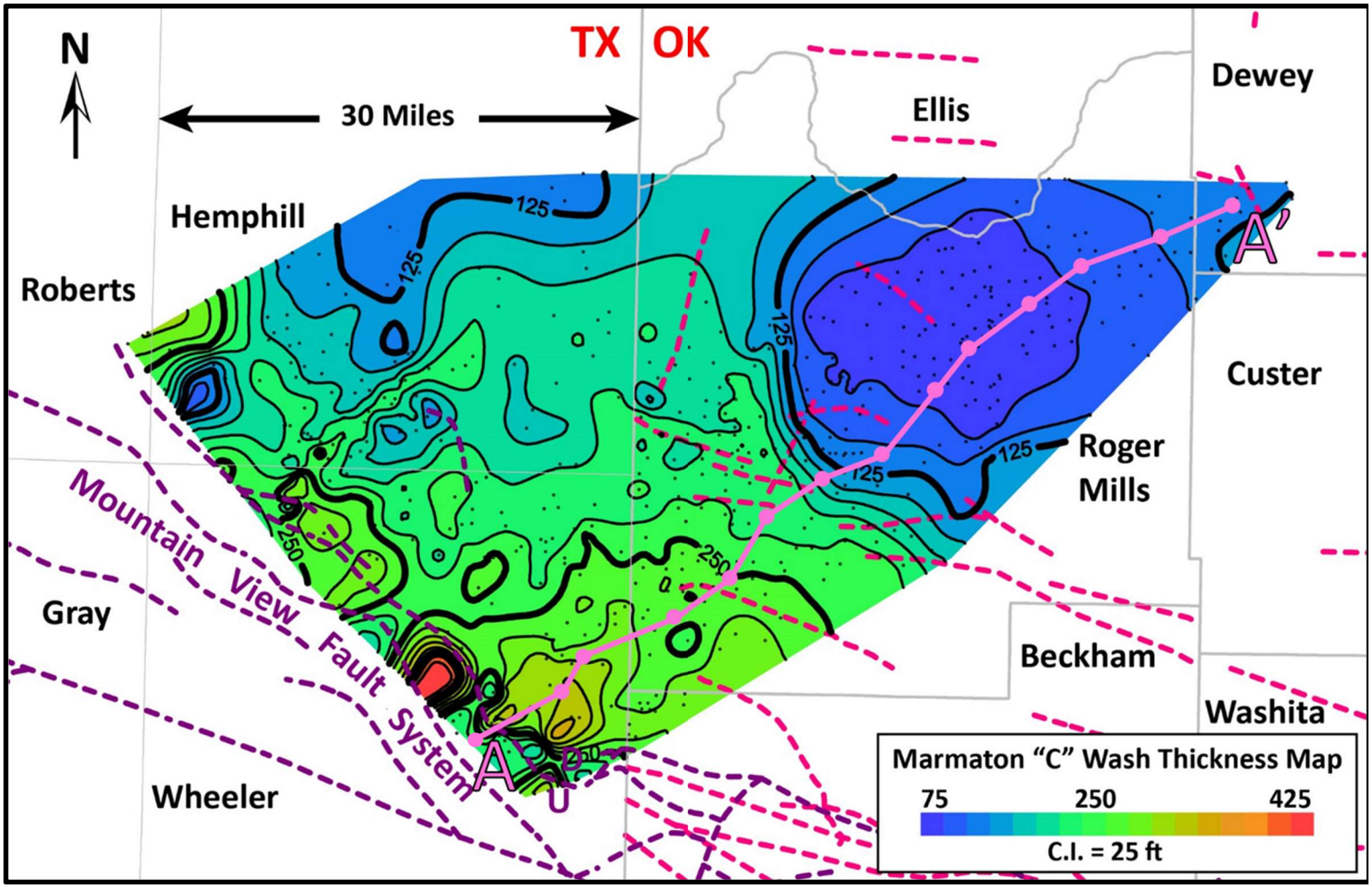

Figure 5.1: The Marmaton "C" interval is thickest adjacent to the uplift and thins northeastward. The evident trends in thickness are southwest to northwest. Two more prominent trends are in eastern Wheeler County, Texas, and southern Hemphill County, Texas. Contour interval is 25 feet. Pink fault lines are from Oklahoma Geological Survey (OGS) (Marsh and Holland, 2016) and purple fault lines are from the Bureau of Economic Geology (BEG) (Ewing, 1990). Cross section A-A' is shown in **Figure 4.2**.

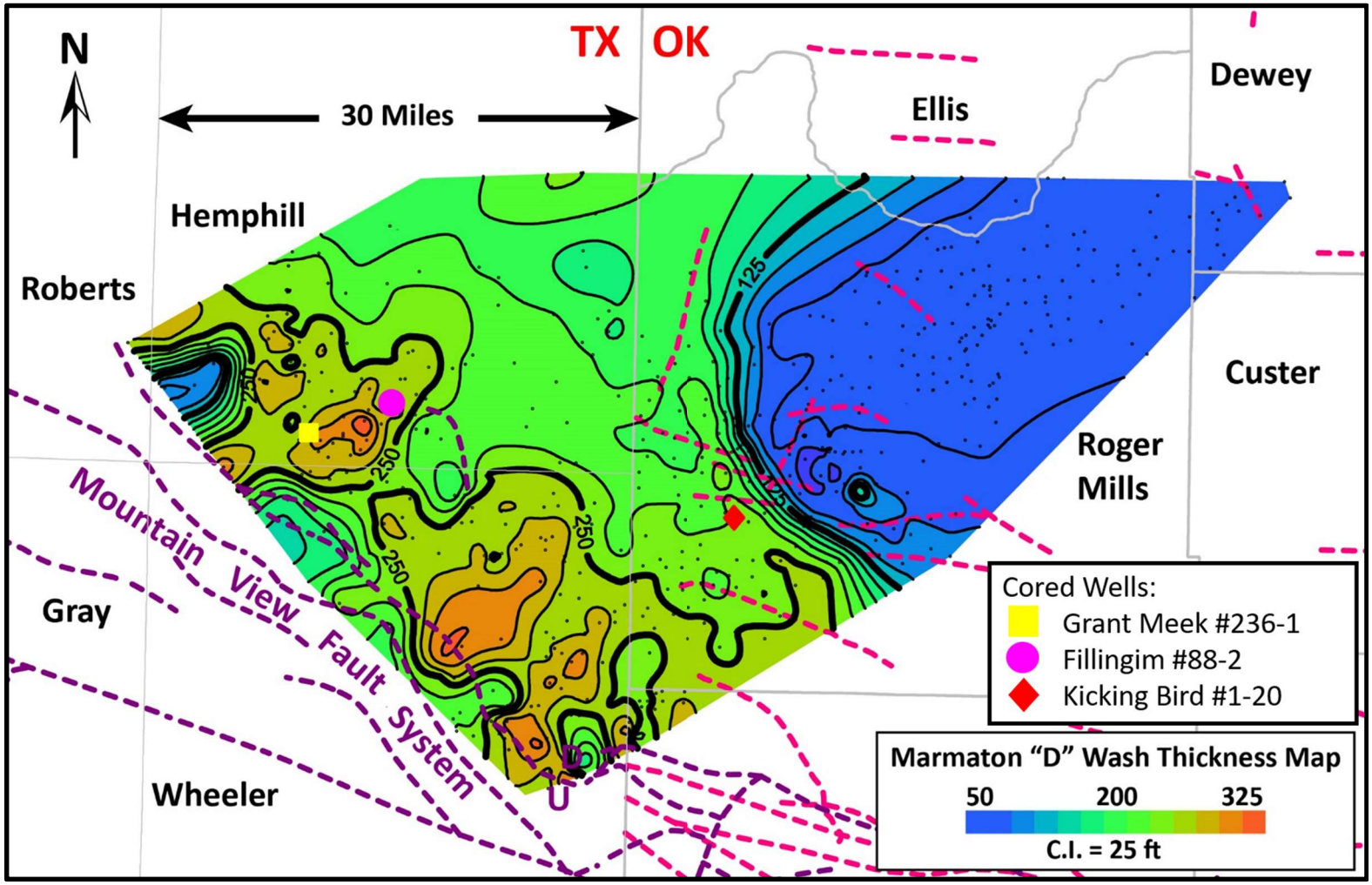

Figure 5.2: The general trend in thickness in the Marmaton "D" Wash suggests thinning to the northeast as thin areas adjacent to the uplift could be the result of syndepositional tectonics or post-depositional faulting that cut out section in wells. Contour interval is 25 feet. Pink fault lines are from Oklahoma Geological Survey (OGS) (Marsh and Holland, 2016) and purple fault lines are from the Bureau of Economic Geology (BEG) (Ewing, 1990).

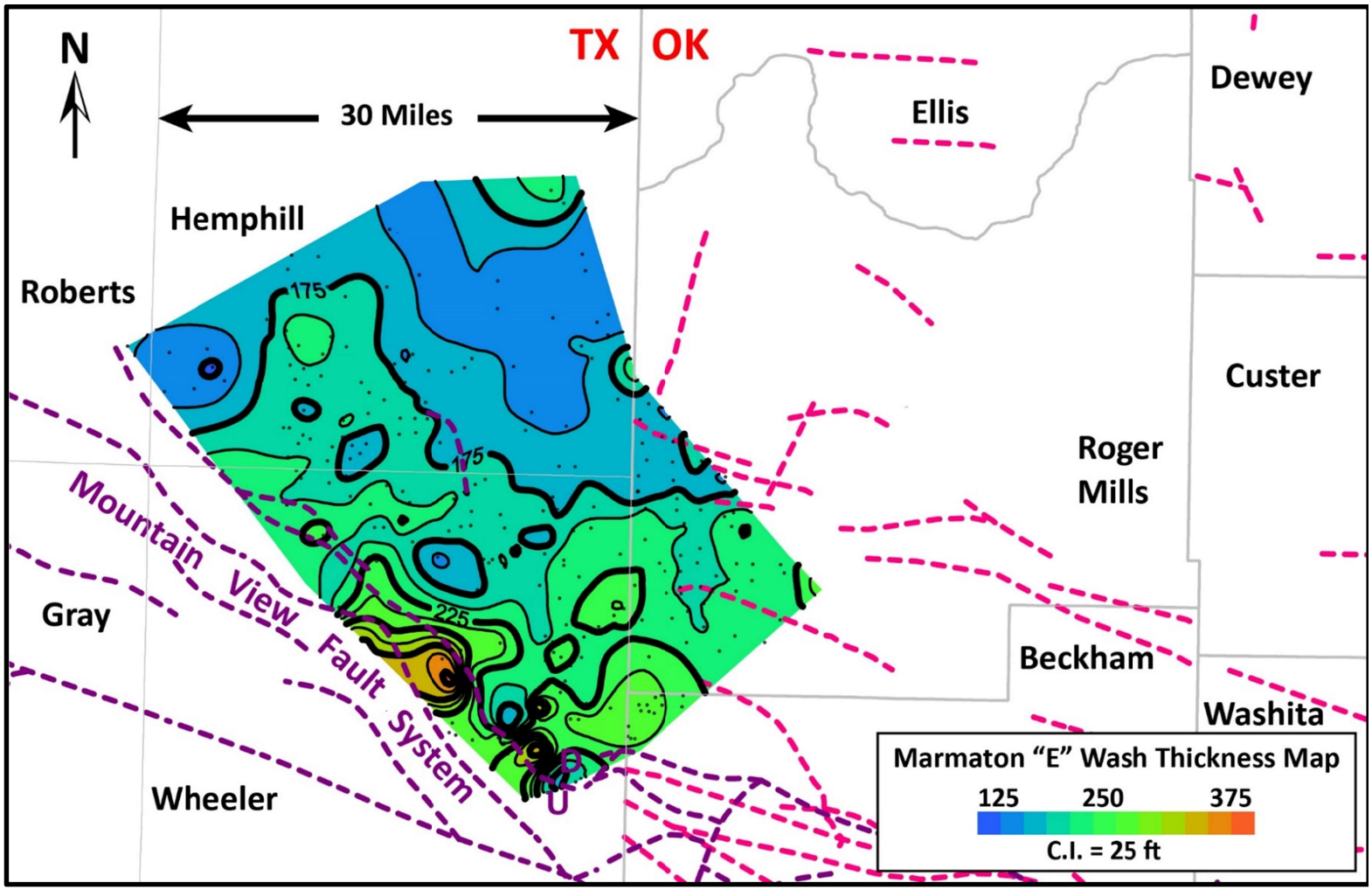

Figure 5.3: Thickness of the "E" wash interval suggest thinning to the northeast. Individual trends are less evident in the "E" interval. A narrow elongate trend occurs in northern Wheeler County, Texas. Contour interval is 25 feet. Pink fault lines are from Oklahoma Geological Survey (OGS) (Marsh and Holland, 2016) and purple fault lines are from the Bureau of Economic Geology (BEG) (Ewing, 1990).

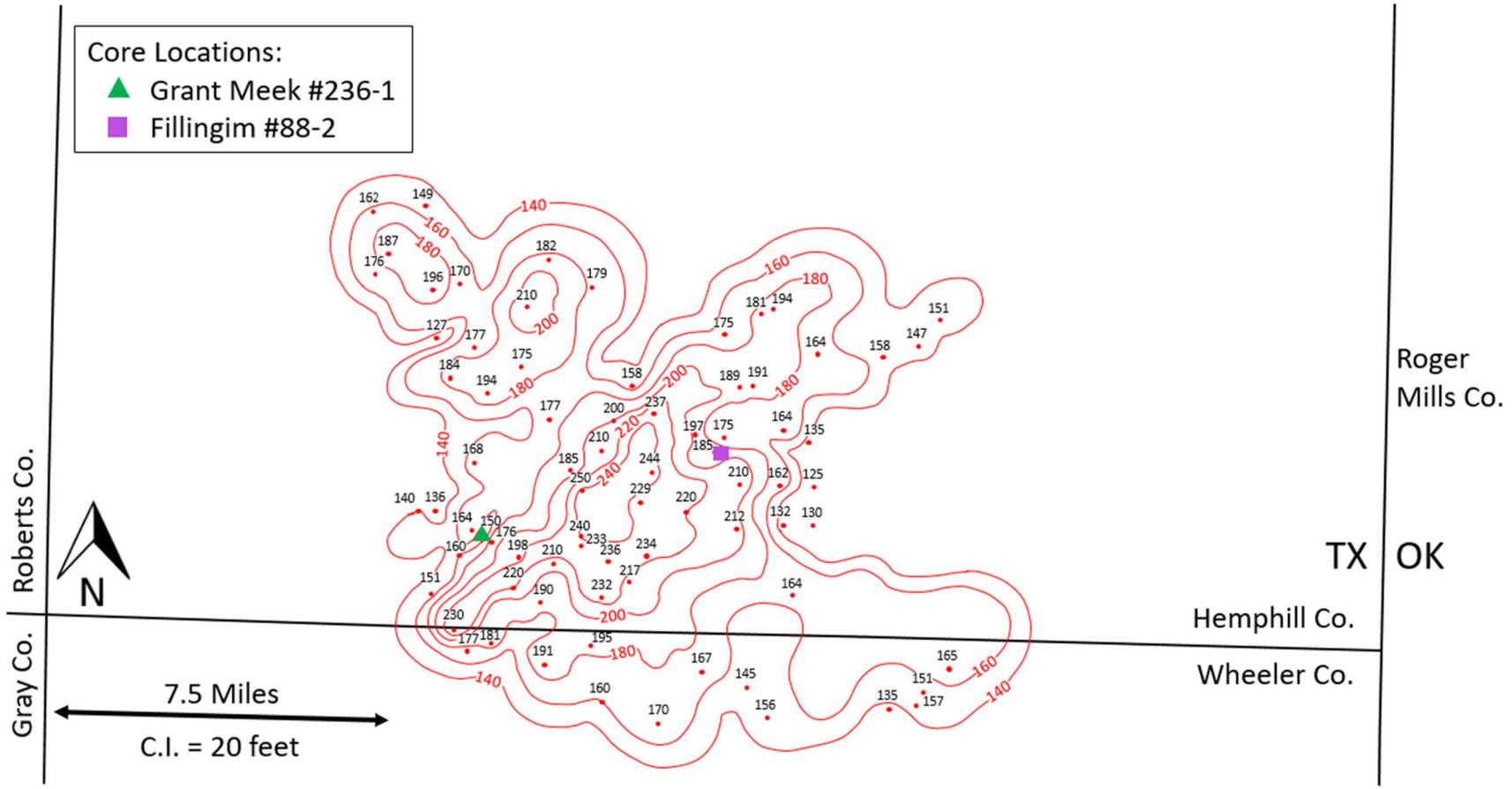

Figure 5.4: Net sandstone thickness map of Buffalo Wallow Field in Hemphill County, Texas and the surrounding area. Contour interval is 20 feet. All thicknesses are in feet.

CHAPTER VI

CORE ANALYSIS

6.1 Introduction to Core Analysis

This study utilized three conventional cores to examine and identify the lithology, texture, sedimentary structures, and depositional facies seen in the Marmaton Granite Wash in both proximal and distal environments. An understanding of the lateral variations in these sedimentological features ultimately allowed for a better understanding of the Marmaton Granite Wash depositional system as a whole. The cored intervals of all three wells are representative of the Marmaton "D" Wash interval of the Marmaton Granite Wash. This chapter focuses on the observations and results obtained from core analysis, while Section 9.1 includes an interpretation of the features seen in core and a discussion of the Marmaton Granite Wash depositional system.

The Kicking Bird #1-20 well is located at Sec. 20, T. 13 N., R. 25 W. (2,475' FNL, 1,650' FWL of S20) in Roger Mills County, Oklahoma. Both the Grant Meek #236-1 and the Fillingim #88-2 well are located in Buffalo Wallow Field in Texas Railroad Commission District 10, Hemphill County, Texas. The Grant Meek #236-1 is located on the western edge of Buffalo Wallow Field in the G&MMB&A Block C Survey, while the Fillingim #88-2 is more centrally located in Buffalo Wallow Field in the H&GN Block M1 Survey. The Buffalo Wallow wells are located approximately 30 miles to the west of the Kicking Bird #1-20 well and are more proximal to the Amarillo-Wichita Uplift source area. The locations of the three wells are shown on the Marmaton "D" Wash thickness map in **Figure 5.2**.

6.2 Kicking Bird #1-20 Core Features

The conventional core from the Kicking Bird #1-20 well consists of 54 feet of the Marmaton "D" Wash interval, covering a depth range from 12,760 to 12,814 feet. The core is slabbed, and conventional core analysis data was provided by Laredo Petroleum (**Table 6.1**). Gas porosimetry analysis was attempted on core samples for this study, but porosity values were too low to register on the teaching grade Core Lab PORG-200 helium gas porosimeter available at Oklahoma State University. For this reason, this study relies on the porosity data included in the core analysis provided by Laredo Petroleum. A detailed petrolog that documents the lithology, grain size, color, and sedimentary structures observed in the core is provided in Appendix B, while core photos are provided in Appendix A.

The Marmaton "D" Wash interval of the Kicking Bird core includes very fine- to medium-grain sandstones, mudstones, shales. Several characteristic profiles are exhibited in the core, including (1) interbedded sandstone and shale, (2) repeated fining-upward sequences, and (3) uniform sandstone packages with no discernible trend. While the sandstones reach a maximum grain size of medium sand at the base of a few individual fining upward sequences, the core is largely composed of very fine- to fine-grained sand. The sandstones are typically moderately well sorted. Sedimentary features observed include: massive bedding, wavy bedding, planar bedding, small-scale cross-bedding, sharp contacts, ripple laminations, bioturbation, burrows, mud rip-up clasts, convolute bedding, and soft sediment deformation.

Overall, the Kicking Bird core is characterized by repeated fining upward packages of interbedded very fine- to fine-grained sandstone and shale. Fining upward sequences range in vertical thickness from three inches to over four feet thick from base to top. Some fining upward packages consist of sediment that ranges from medium sand at the base to clay size at the top. Others appear to be "partial" sequences and depict a limited range in sediment size, but still

display a distinct gradational sequence from coarser grain at the base to finer grain at the top.

While some shale-sandstone contacts are gradual, the majority of bedding contacts are sharp (**Figure 6.1**). Low-flow regime planar laminated bedding is most common and is typical of contacts between the thicker fining upward sequences, but wavy bedding is also observed at the contacts of thinner fining upward packages. Bioturbation and burrowing are seen in shaley intervals (**Figure 6.1**). Convolute bedding and soft sediment deformation are commonly observed in the thicker sandstone units, depicting loose sediment packing and fluidized flow (**Figure 6.2**). Large mud rip-up clasts are commonly seen towards the top of fining upward sequences (**Figure 6.3**). The Kicking Bird is significantly finer-grained than the two Buffalo Wallow cores, which will each be discussed in the next two sections. It also contains more interbedded shale, and the vertical thickness of its fining upward sequences is thinner on average than in the Buffalo Wallow cores.

Table 6.1: Core analysis data for the Kicking Bird #1-20 core provided by Laredo Petroleum, including porosity, permeability, and grain density values.

Depth Below Surface	Porosity	Total Permeability	Grain Density
(ft)	(%)	(mD)	($g/cm^{3)}$
12761.7	1.3	<.0001	2.69
12763.7	1.0	<.0001	2.73
12764.9	1.2	<.0001	2.67
12766.3	1.4	0.013	2.66
12769.3	2.3	0.0001	2.65
12774.5	4.0	0.001	2.71
12775.6	3.6	0.0004	2.65
12776.3	4.2	0.001	2.59
12777.3	3.0	0.001	2.65
12778.7	4.7	0.001	2.67
12780.7	3.3	0.003	2.67
12781.8	3.2	0.001	2.71
12785.3	2.9	0.001	2.66
12786.7	7.3	0.002	2.65
12789.4	2.9	0.014	2.68
12790.2	2.5	0.0001	2.65
12797.7	2.5	<.0001	2.65
12798.8	1.3	<.0001	2.71
12802.7	3.5	<.0001	2.67
12803.7	2.9	<.0001	2.65
12804.4	1.4	<.0001	2.68
12804.8	1.0	<.0001	2.70
12805.3	3.2	<.0001	2.65
12806.4	2.9	0.001	2.65
12807.8	5.7	0.074	2.67
12808.8	3.3	<.0001	2.65
12809.6	3.2	0.001	2.65
12812.8	4.2	<.0001	2.66

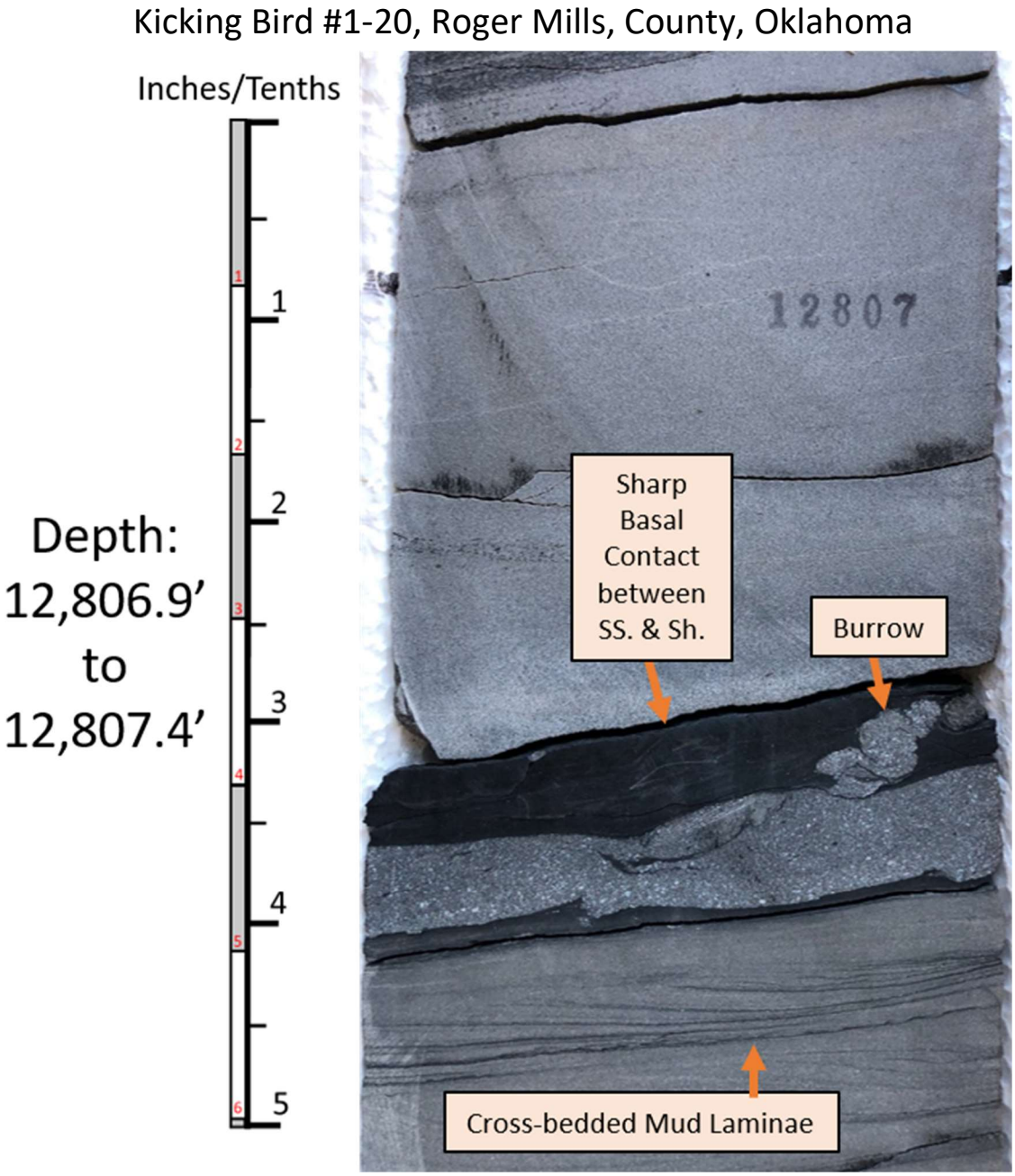

Figure 6.1: Sharp basal contact between sandstone and shale below, which contains an approximately 0.75-inch burrow. Kicking Bird #1-20 core. Depth: 12,806.9- 12,807.4 feet.

Kicking Bird #1-20, Roger Mills, County, Oklahoma

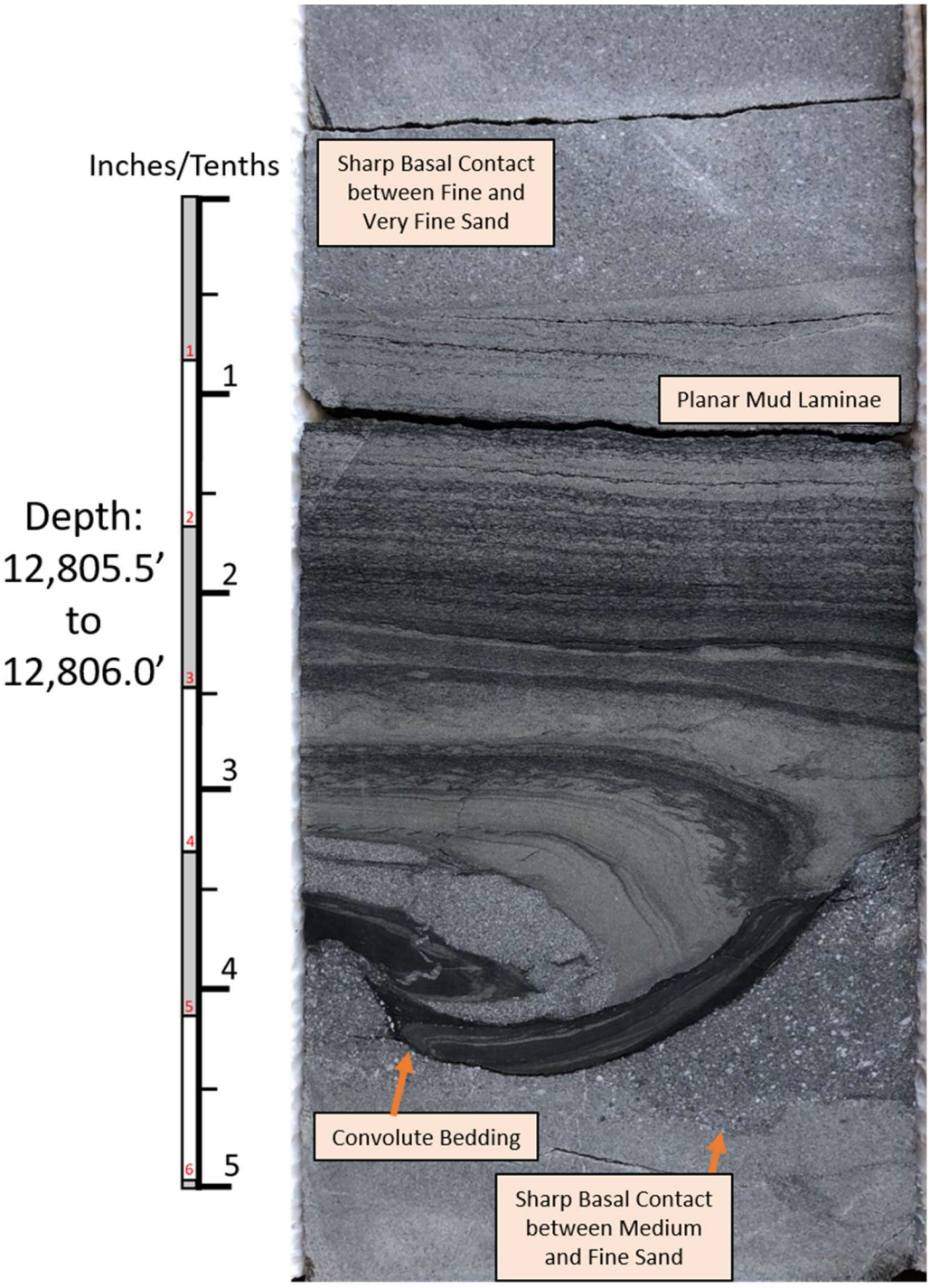

Figure 6.2: Convolute bedding, a form of soft sediment deformation and evidence of fluidized flow. Sharp basal contacts are seen between finer sand above and coarser sand below. Planar mud laminae are seen with increasing amounts of interbedded fine sand going up-section. Kicking Bird #1-20 core. Depth: 12,805.5- 12,806.0 feet.

Kicking Bird #1-20, Roger Mills, County, Oklahoma

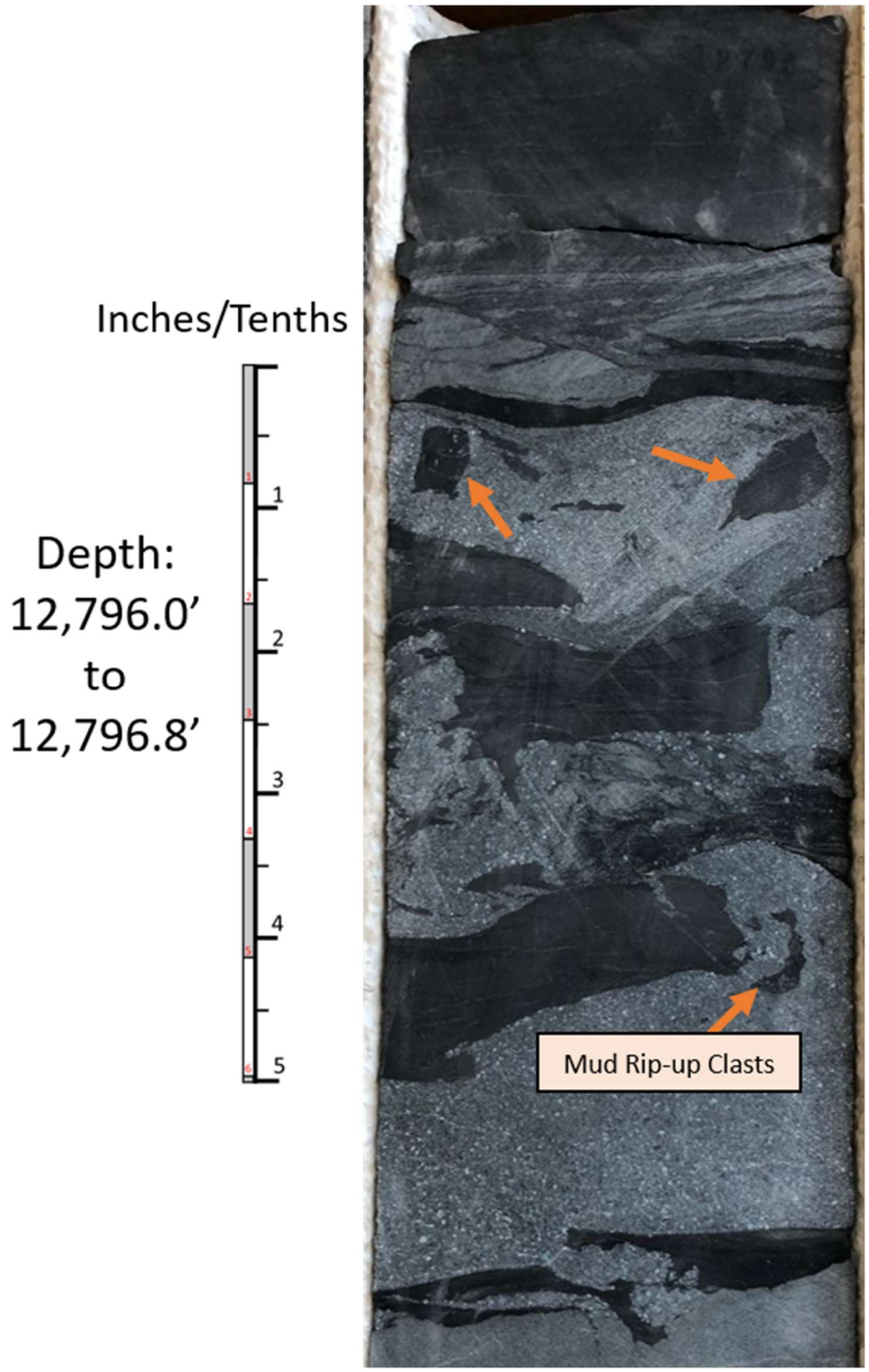

Figure 6.3: Abundant mud rip-up clasts. Kicking Bird #1-20 core. Depth: 12,796.0- 12,796.8 feet. Other features evident in the Kicking Bird core include chaotic intervals formed by mass wasting of sediment. An example would be at depth 12,798.0 feet, as shown in Appendix A.

6.3 Grant Meek #236-1 Core Features

The Grant Meek #236-1 conventional core contains a total of 89 feet of Marmaton "D" Wash at a depth interval of 11,333 to 11,422 feet. There are several sections of missing core: 11,339.0- 11,339.7 feet, 11,342.1- 11,342.3 feet, 11,367.9- 11,369.2 feet, 11,382.8- 11,383.4 feet, 11,385.0- 11,386.3 feet, 11,388.6- 11,389.3 feet, 11,391.0- 11,391.5 feet, and 11,393.0- 11,393.4 feet. The core is slabbed. A detailed petrolog is provided in Appendix D, and core photos are provided in Appendix C.

The Marmaton "D" Wash interval of the Grant Meek consists of shale, mudstone, very fine- to very coarse-grained sandstone, and pebble conglomerate. Like the Kicking Bird, the Grant Meek core interval is characterized by repeated fining upward sequences. Unlike the Kicking Bird, it consists almost entirely of sandstone and conglomerate, with shale and mudstone being only a minor constituent. Individual fining upward packages range in vertical thickness from around 3 inches to 4 feet from base to top. While sediments reach pebble size at the base and clay size at the top of multiple fining upward sequences, the entire cored interval largely falls in the range of medium to very coarse-grained sandstone. Sorting decreases with increasing grain size, with muds and very fine sands being well sorted and pebble conglomerates being poorly sorted. Pebble conglomerates and coarse sandstones most often appear matrix-supported. A few fining upward sequences range from pebble conglomerate at the base to shale at the top, but the majority are "partial" packages with a limited sediment size range. Most sequences have a sharp, erosional, planar contact at the base.

Sedimentary structures observed in the Grant Meek include planar bedding, massive bedding, bioturbation, planar mud laminae, and mud rip-up clasts as well as features that are indicative of dewatering and soft sediment deformation such as dish and pillar structures (**Figure 6.4**). A prominent, over two-inch-long pillar structure (sand dike) is shown in **Figure 6.5**. Dish

and pillar structures appear most frequently in sediments that are coarse sand or coarser.

The Grant Meek is the coarsest-grained of all three cores, but only marginally more so than the Fillingim core. It contains significantly less shale and mudstone than the Kicking Bird core. Mud rip-up clasts are less frequent in the Grant Meek than they are in the Kicking Bird.

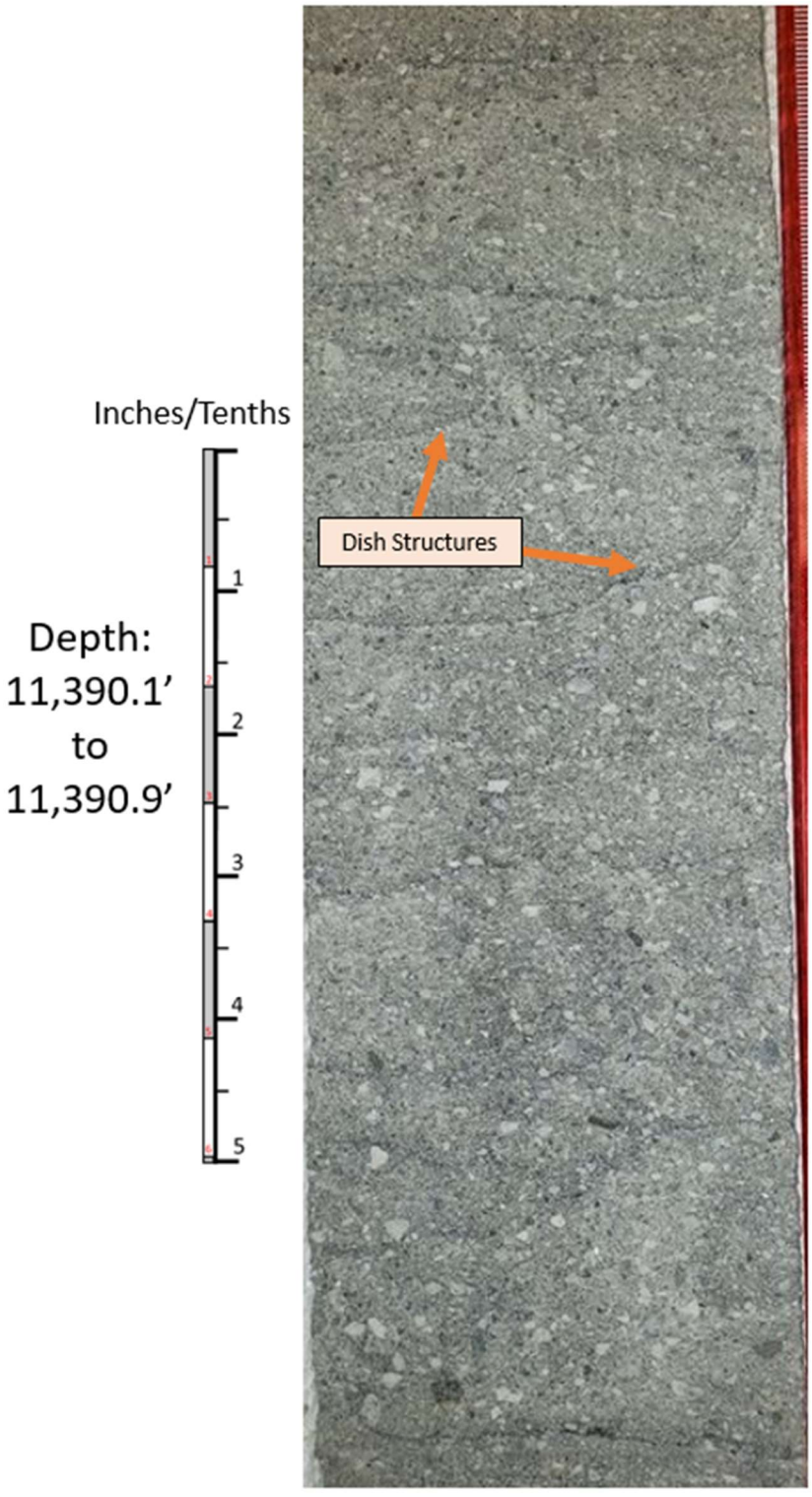

Figure 6.4: Dish structures indicative of rapid sedimentation. Grant Meek #236-1 core. Depth: 11,390.1 to 11,390.9 feet.

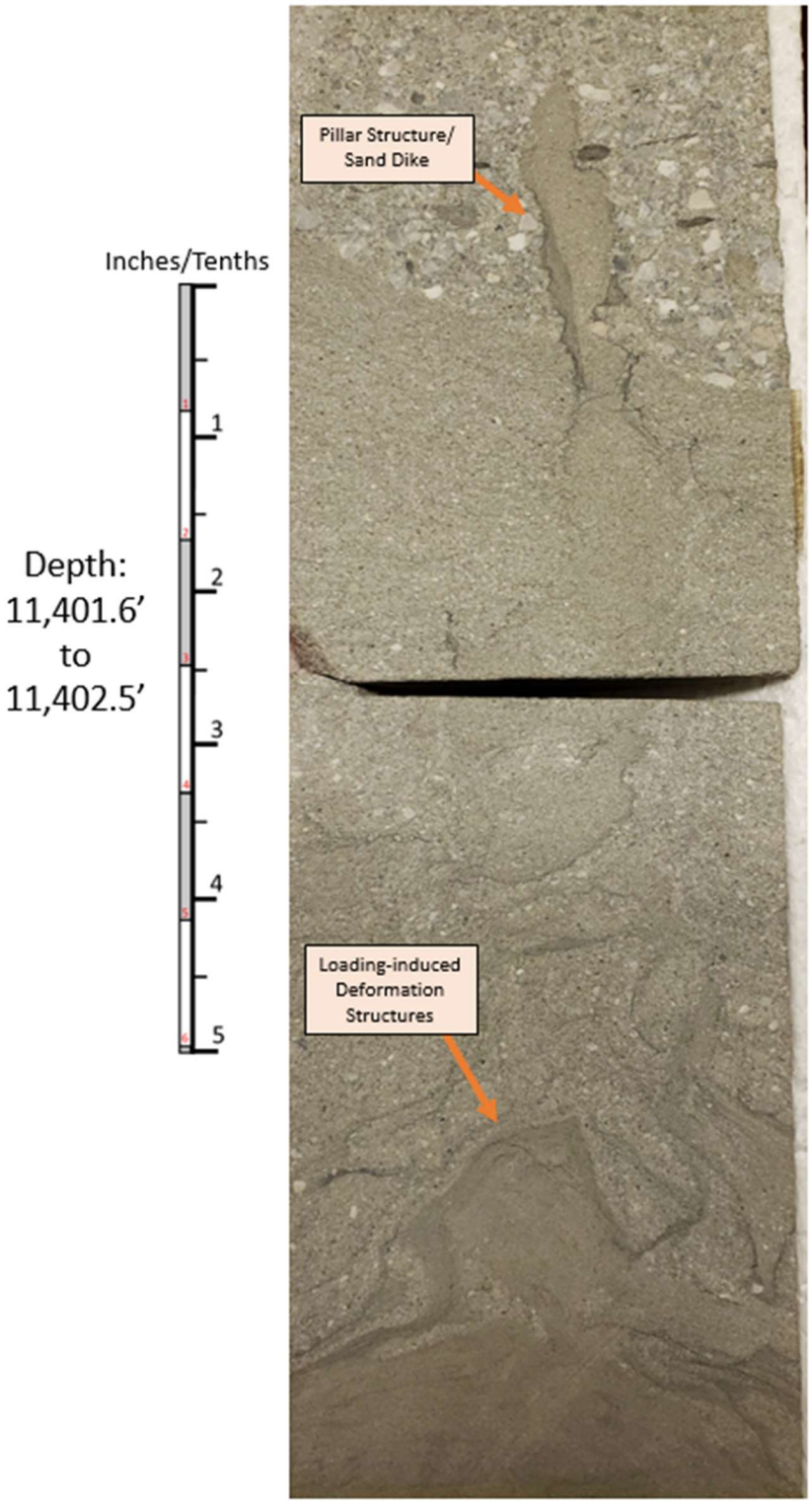

Figure 6.5: Pillar structure and loading-induced deformation structures. Grant Meek #236-1 core. Depth: 11,401.6 to 11,402.5 feet.

6.4 Fillingim #88-2 Core Features

The cored interval of the Fillingim #88-2 conventional core consists of a total of 62 feet of Marmaton "D" Wash. Core depth ranges from 11,402 to 11,462 feet. There are four sections of missing core, including one box that could not be located: 11,415.0- 11,417.8 feet, 11,428.0- 11429.0 feet, 11.439.5- 11,440.0 feet, and 11,458.0- 11,459.0 feet. Conventional core analysis data for the 2/3 butt core was acquired from Parks (2011; original data provided by Linn Energy) and is shown in **Table 6.2**. A detailed petrolog is provided in Appendix F, and core photos are provided in Appendix E.

Like the Grant Meek but unlike the Kicking Bird, the Fillingim core is composed of shale, mudstone, very fine- to very coarse-grained sandstone, and pebble conglomerate. As with the other two cores in this study, the Marmaton "D" Wash interval of the Fillingim core is characterized by repeated fining upward sequences. While some fining upward sequences are pebble size at the base and shale at the top, the dominant grain size across the entire cored interval is medium to coarse sand. Sorting decreases with increasing grain size, with the sandstones being largely moderately sorted. Individual fining upward packages vary in vertical thickness from around three inches to over four feet thick. Some packages display a complete fining upward sequence from pebble conglomerate to shale, while others are "partial" sequences that display a more limited range in sediment size. The fining upward sequences typically have sharp, planar, erosional contacts at the base. The pebble conglomerates and coarse sandstones appear to be matrix-supported. The Fillingim core is marginally finer-grained than the Grant Meek, but is significantly coarser-grained than the Kicking Bird. The Fillingim section contains much less shale than the Kicking Bird but a fairly equal amount to the Grant Meek.

Sedimentary structures observed in the Fillingim core include planar bedding, massive bedding, bioturbation, mud rip-up clasts, large rounded mud clasts, planar mud laminae, sand

lenses in shales, and structures that are indicative of dewatering and soft sediment deformation such as dish and pillar structures and flame structures (**Figure 6.6**). Large (three inches and greater in diameter) calcite concretions are also observed (**Figure 6.7**).

Table 6.2: Core analysis data for the Fillingim #88-2 core, including porosity, permeability, and grain density values (data from Parks, 2011).

Depth Below Surface	Porosity	Total Permeability	Grain Density
(ft)	(%)	(mD)	($g/cm^{3)}$
11404.0	4.60	0.2	2.63-2.66
11408.0	8.91	1.5	2.64-2.69
11414.7	7.84	0.5	2.64-2.69
11418.0	7.29	0.4	2.64-2.67
11419.0-A	7.23	0.5	2.65-2.68
11419.0-B	5.94	0.3	2.63-2.67
11230.0	3.30	0.3	2.62-2.67
11430.8	7.31	0.5	2.63-2.67
11433.0-A	7.52	0.4	2.63-2.67
11433.0-B	7.06	0.3	2.63-2.67
11433.0-C	7.48	0.3	2.63-2.71
11435.0	5.42	0.2	2.63-2.65
11441.0	2.45	0.2	2.62-2.67
11450.0	0.00	0.1	2.64-2.69
11454.0	4.20	0.3	2.64-2.66
11456.0	5.53	0.3	2.62-2.65
11460.0	5.29	0.3	2.64-2.67

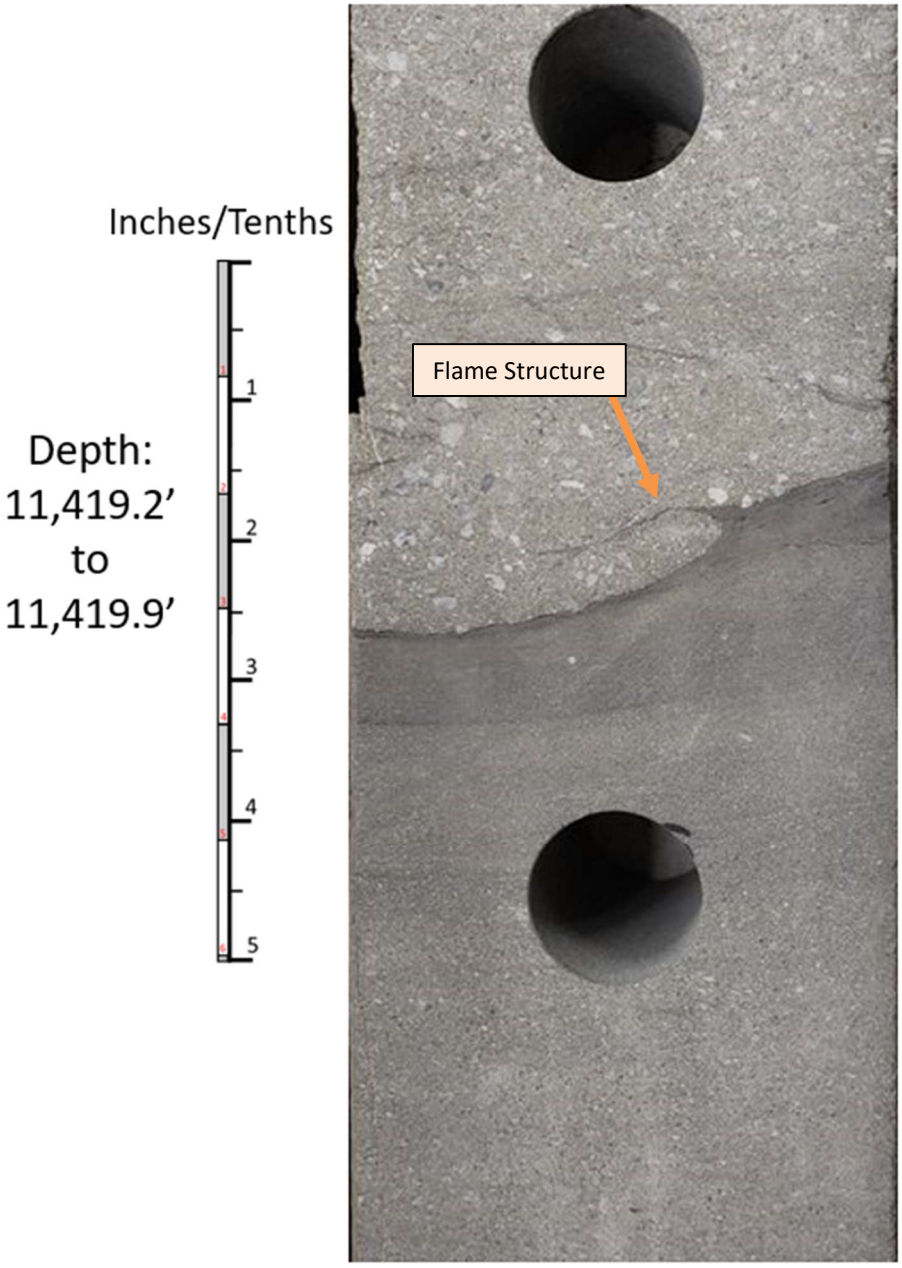

Figure 6.6: Flame structure at sharp contact between fine- and very coarse sand. Fillingim #88-2 core. Depth: 11,419.2 to 11,419.11 feet.

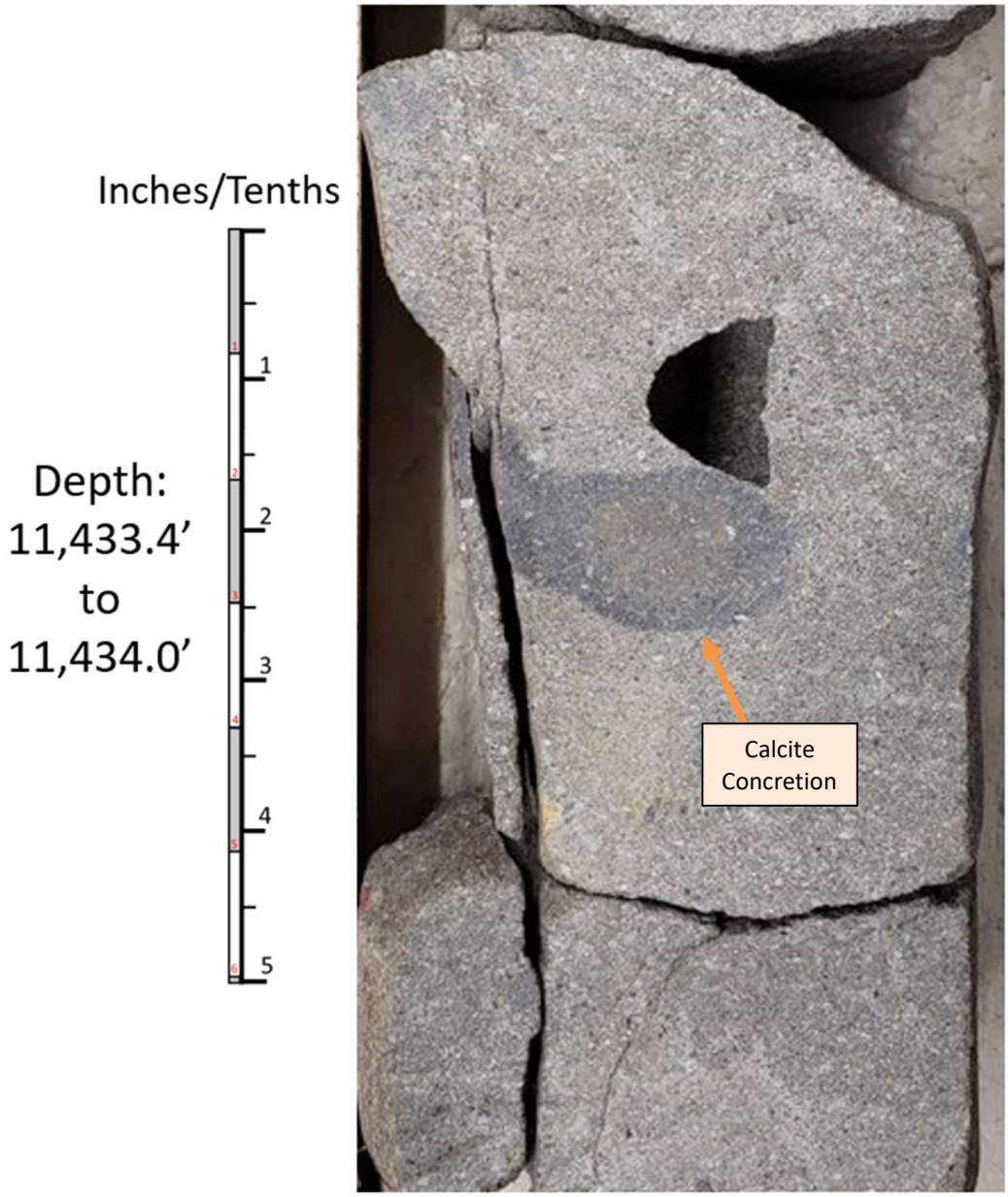

Figure 6.7: Large (1 to 2 inch) calcite concretion. Fillingim #88-2 core. Depth: 11,433.4 to 11,434.0 feet.

6.5 X-Ray Fluorescence (XRF) Analysis

Semi-qualitative energy-dispersive x-ray fluorescence (XRF) measurements were taken twice for every foot of the 54-foot-long Kicking Bird core in order to analyze the variations in elemental composition across the Marmaton "D" Wash interval. A plot depicting uranium (U) content versus lithology over depth was constructed in order to better understand the likely origin of the organic matter within the interbedded shales of the wash (**Figure 6.8**). Another plot depicting the variations in titanium (Ti), potassium (K), and aluminium (Al) content across depth was constructed to gain further insight into the nature of the interbedded shales (**Figure 6.9**) and was compared to the spectral gamma-ray log for the Kicking Bird core provided by Laredo Petroleum (**Figure 6.9**). As no core that included one of the surrounding hot shale markers (the Second or Third Marmaton Shale) was available, only interbedded shales within the wash interval were analyzed.

The plot of U content versus lithology depicts no clear trend. U content varied between 0 and 0.005 wt.% (percent by weight) and was highest within sandstones. However, the second highest percentages were just under 0.004 wt.% and were both in shale intervals. The majority of sample points within both sandstone and shale contained 0 wt.% U. When compared to the spectral gamma-ray log for the Kicking Bird core shown in **Figure 6.9**, the trend of U content across depth is similar. Further, it indicates that the ratio of thorium (Th) to U is less than three.

The Ti, K, and Al content versus depth plot depicts largely the same trend for all three elements across the cored interval, in that they varied simultaneously and were all highest within shalier intervals (**Figure 6.10**). Of the three elements, Al content was highest overall and reached almost 12 wt.%, followed by K that reached just over 4 wt.%, and lastly Ti with a maximum value of less than 1 wt. %. The trends of K and Th concentration versus depth are similar to the spectral gamma-ray curve in **Figure 6.9**, whereas the U content curve is much more homogenous and less similar to the other two curves. This establishes that K and Th are contributing much more to measured radioactivity in the Marmaton "D" Wash than U.

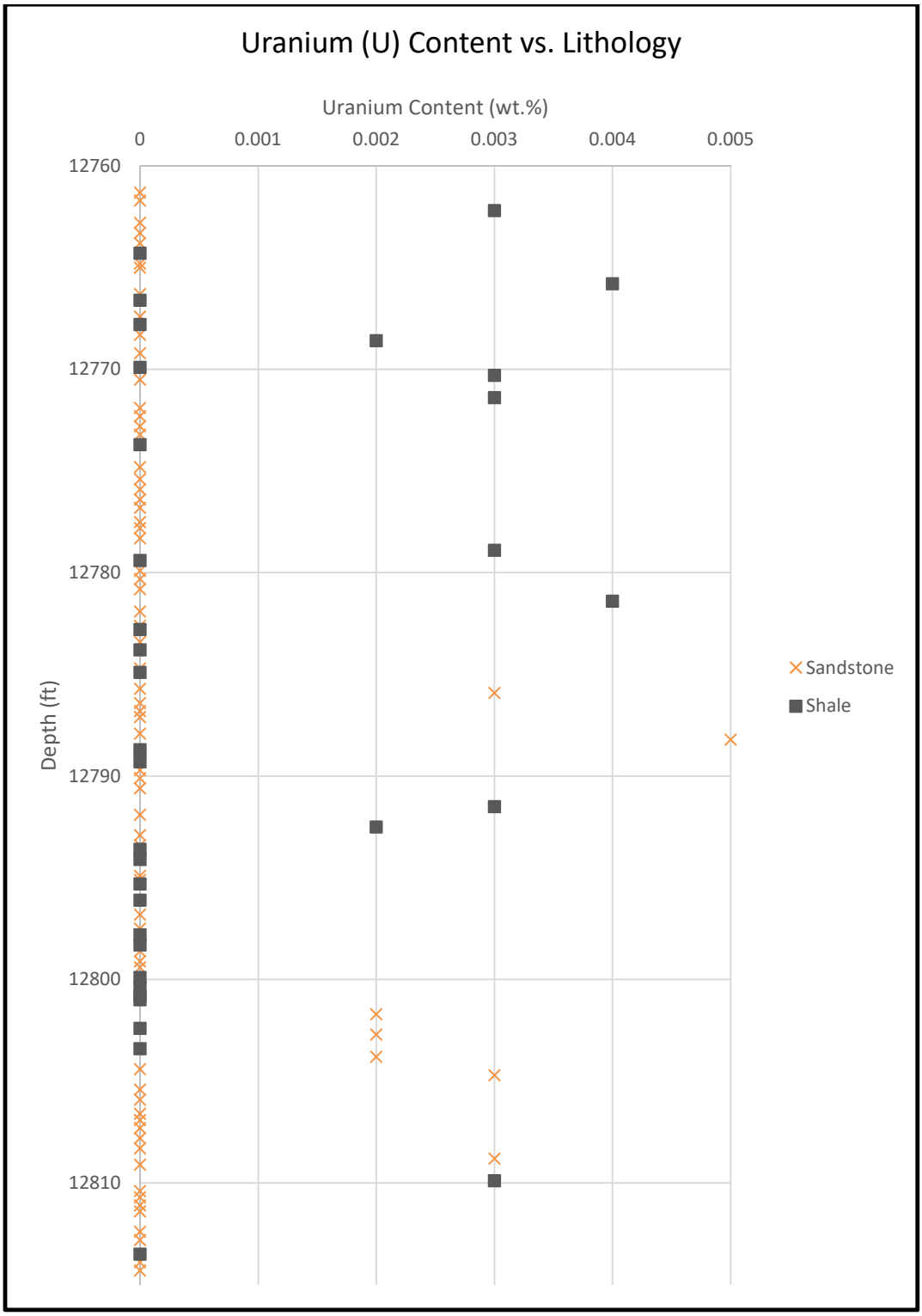

Figure 6.8: Plot of uranium (U) content versus lithology across the Kicking Bird #1-20 core. Elemental concentration acquired from x-ray fluorescence (XRF) analysis.

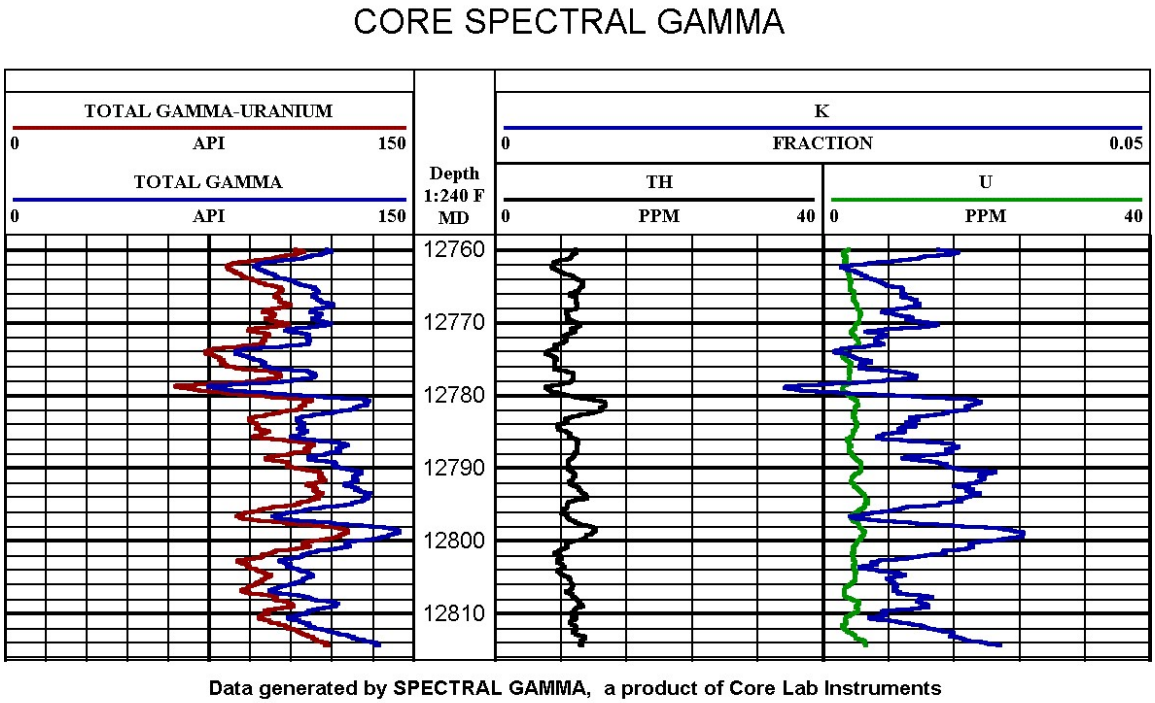

Figure 6.9: Core spectral gamma-ray log for the Kicking Bird #1-20 core showing high concentration of K around 0.03 to 0.04 wt % (300 to 400 ppm) compared to much lower concentration of Th (≈8 ppm or 0.0008 wt %) and U (≈3 ppm or 0.0003 wt %). Spectral gamma-ray provided by Laredo Petroleum.

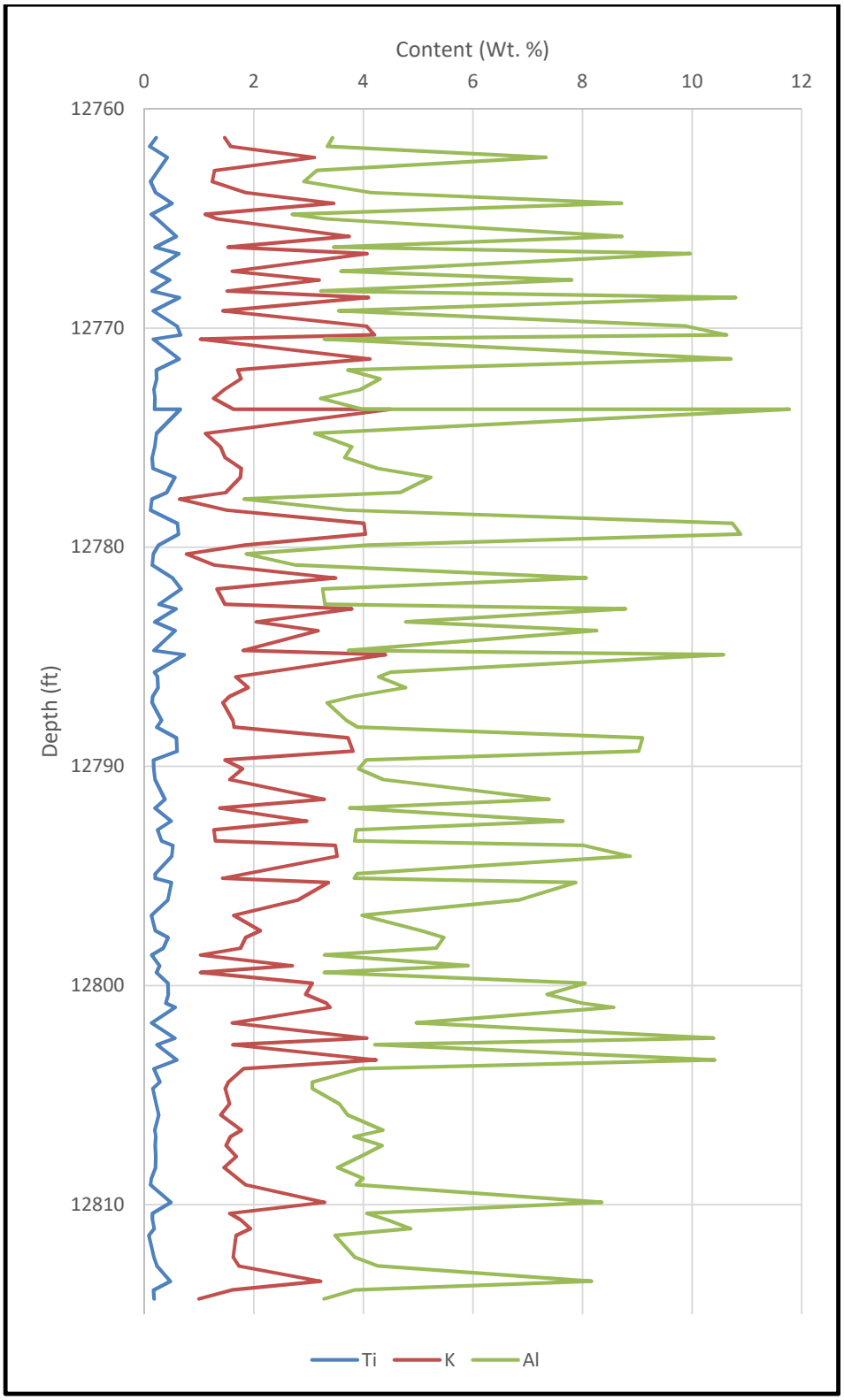

Figure 6.10: Plot of titanium (Ti) (blue), potassium (K) (red), and aluminum (Al) (green) across the Kicking Bird #1-20 core. Elemental concentrations acquired from x-ray fluorescence (XRF) analysis.

CHAPTER VII

WELL LOG ANALYSIS

7.1 Electrofacies of Cored Interval

Due to the high potassium feldspar content of the Marmaton Granite Wash, the gamma-ray log response can be a less reliable lithology indicator than it would be for a typical quartzose sandstone (for a detailed explanation of this phenomenon, see Section 2.1). However, a great deal of information regarding the depositional environment of the Marmaton Granite Wash can still be interpreted by examining the gamma-ray log signature and considering the log pattern across the interval. In general, variations in gamma-ray log character of siliciclastic sediments can be thought of as a vertical profile of grain size. Shales and clays most often contain naturally occurring radioactive elements (largely potassium, uranium, and thorium) read by the gamma-ray tool in much higher percentages than their coarser-grained, "clean" (containing little matrix material) sandstone counterparts. As such, the gamma -ray log can be viewed as a visual representation of changes in depositional energy: clean, coarse sandstones are representative of high energy environments, while clay-rich sandstones and shaley intervals reflect lower energy environments. For this reason, the character of the gamma-ray curve can be utilized as a basic, predictive tool for interpreting the depositional setting of sedimentary cycles. However, using log character to interpret depositional environment should be done with extreme caution: well log analysis is highly ambiguous in nature and must be supported with other evidence. Core data is

the ideal addition as it provides a direct sample of the formation and is much more precise in nature. This study analyzed Marmaton "D" Wash (of which the cored interval of all three wells utilized in this study belong) well log signatures to supplement conventional core analysis in the determination of Marmaton Granite Wash depositional processes.

The well log signature of the Marmaton "D" Wash interval of the more distal Kicking Bird well in Roger Mills County, Oklahoma depicts repeated coarsening upward packages of interbedded sandstone and shale. While it was stated in Sections 6.2, 6.3, and 6.4 that all three cores depict repeated fining upward packages at the core scale (each fining upward sequence ranging in vertical thickness from 3 inches to just over 4 feet), the gamma-ray log for the whole Marmaton Granite Wash section in the Kicking Bird depicts repeated coarsening upward packages on the log scale (**Figures 7.1, 7.2, and 7.3**) that average around 30 feet in vertical thickness (Figure 7.1). Each of these coarsening upwards packages seen on the log scale consists of the repeated fining upward sequences seen at the smaller core scale.

While the gamma-ray log for the Kicking Bird depicts many thin shales with a high gamma-ray reading interfingering with sandstone throughout the Marmaton Granite Wash section, the cored well that is most proximal to the source area, the Grant Meek in Hemphill County, Texas, appears to contain much fewer interbedded shales and displays a more "blocky" gamma-ray signature indicative of thick sandstone bodies with only minor amounts of interbedded shale (**Figure 7.2**). The gamma-ray signature of the Marmaton "D" Wash of the Fillingim well in Hemphill County, Texas is intermediate between them, showing more interbedded high gamma-ray shales than the Grant Meek but less than the Kicking Bird (**Figure 7.3**). Overall, the Grant Meek well has the "cleanest" (least amount of shale and lowest average gamma-ray) Marmaton "D" Wash interval, followed by the slightly more distal Fillingim. The gamma-ray log signature for the Marmaton Granite Wash section of the distal Kicking Bird well is interpreted to be composed entirely of coarsening upward sequences, while the most proximal

Grant Meek well consists largely of a “blocky” sandy interval around 150 feet thick between two coarsening upward packages that are around 25 and 50 feet thick. The Fillingim well in Hemphill County, Texas is slightly more distal than the Grant Meek well but not as distal as the Kicking Bird. It depicts two “blocky” sandy intervals (30 and 60 feet thick) with minor shales as well as multiple coarsening upward sequences that average around 30 feet thick.

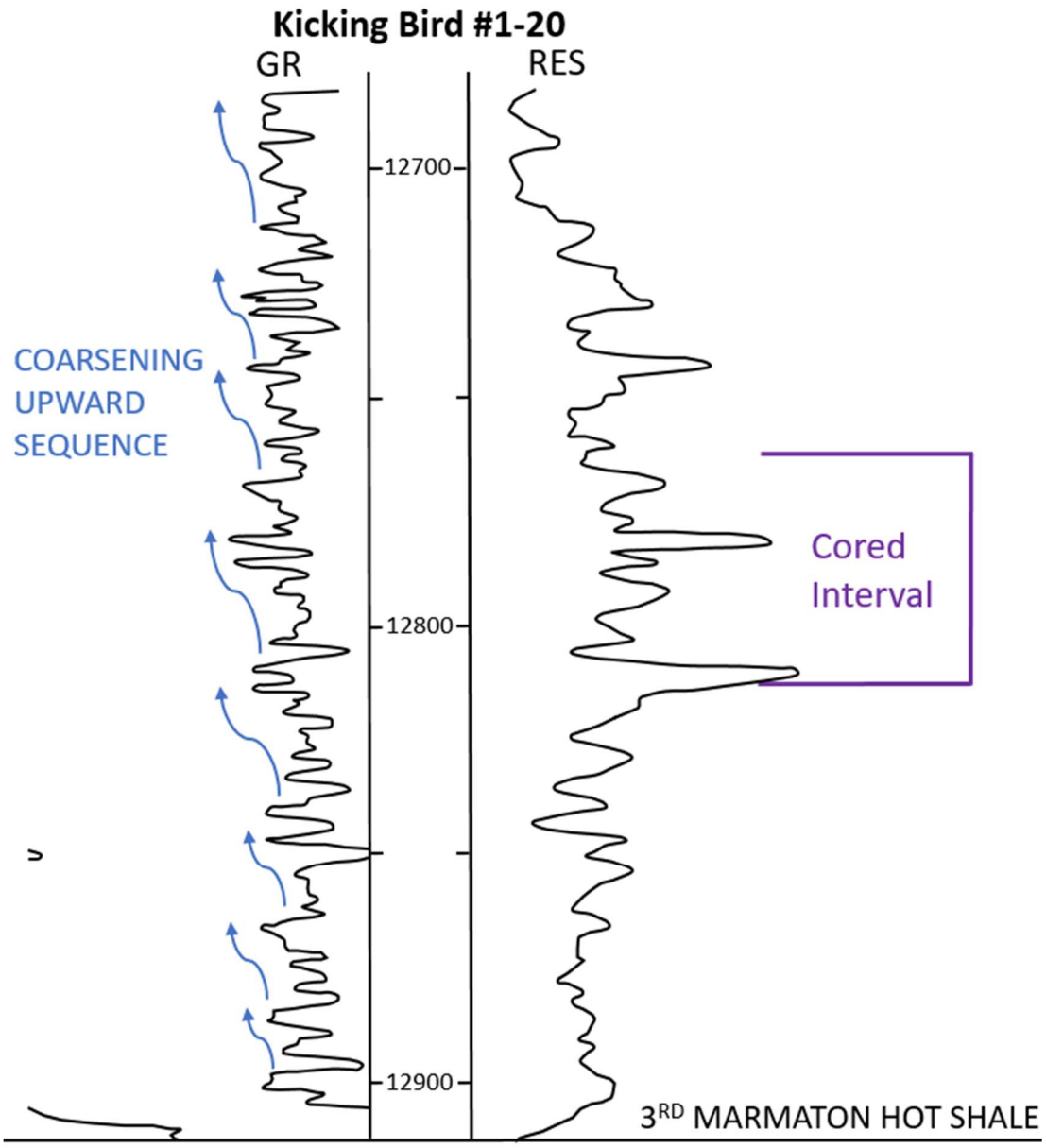

Figure 7.1: Well log signature for the Marmaton "D" Wash interval of the Kicking Bird #1-20 well in Roger Mills County, Oklahoma. The gamma-ray log depicts repeated coarsening upward sequences. These coarsening upward sequences at the log scale consist of the smaller, core-scale fining upward sequences seen in core.

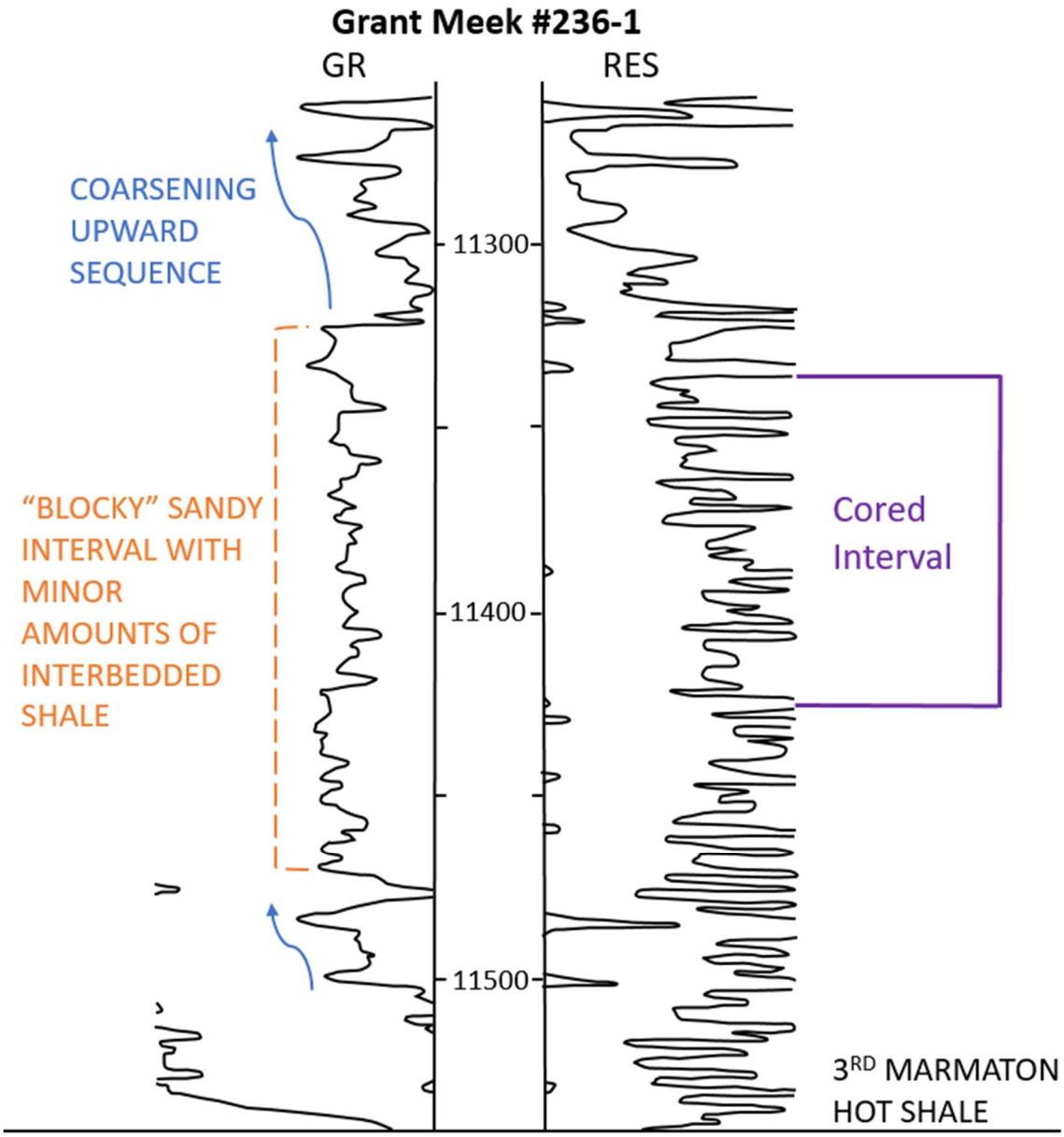

Figure 7.2: Well log signature for the Marmaton "D" Wash interval of the Grant Meek #236-1 well in Buffalo Wallow Field, Hemphill County, Texas. The gamma-ray log depicts coarsening upward packages like is seen in the Kicking Bird, but largely consists of a "blocky" sandy interval with minor amounts of interbedded shale that does not cause a major increase in gamma-ray value.

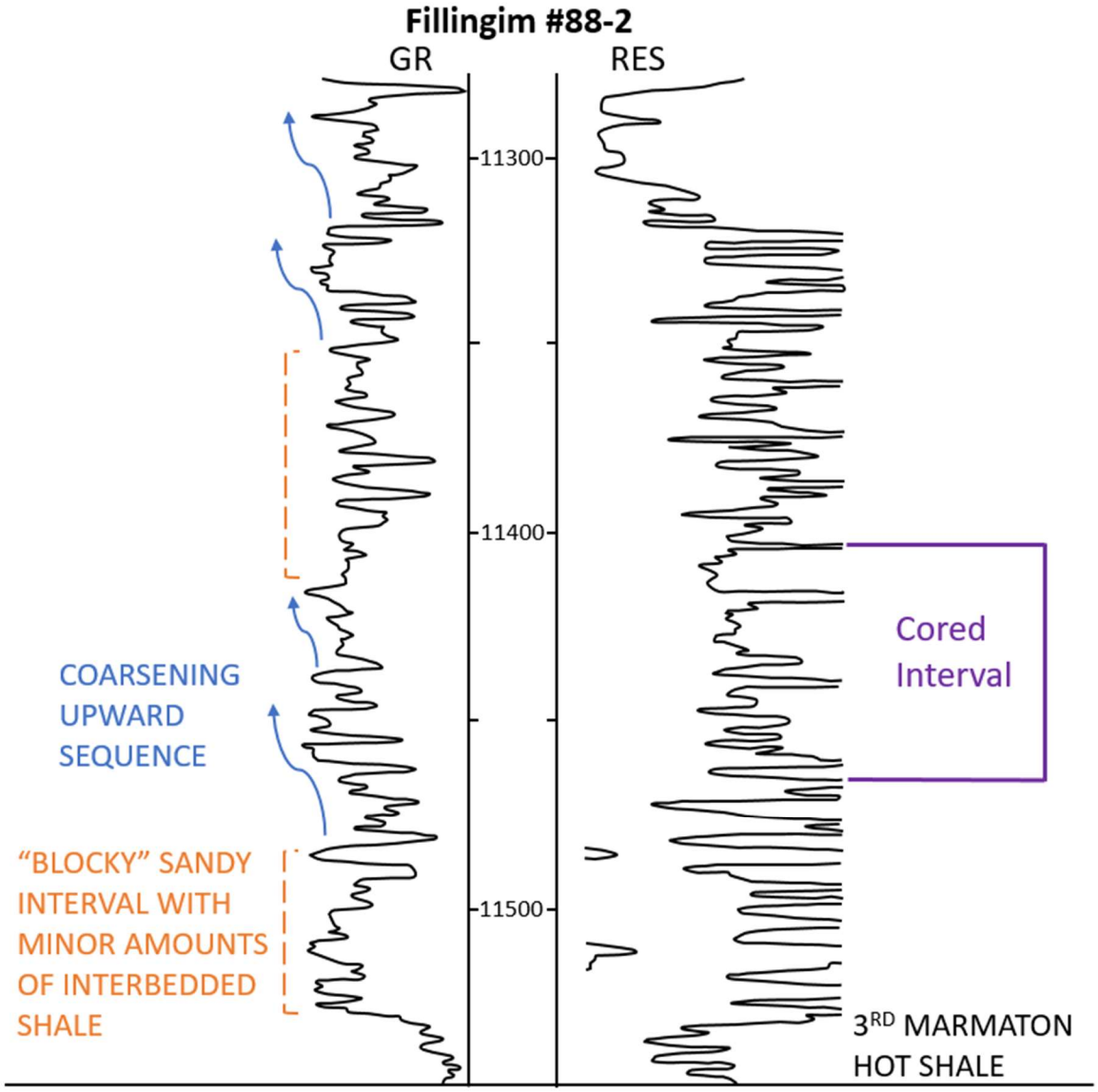

Figure 7.3: Well log signature for the Marmaton "D" Wash interval of the Fillingim #88-2 well in Buffalo Wallow Field, Hemphill County, Texas. The gamma-ray log depicts coarsening upward packages like is seen in the Kicking Bird, but has also has "Blocky" sandy intervals with minor amounts of interbedded low gamma-ray shale like the Grant Meek.

7.2 Gamma-ray Trends Across Study Area

The regional cross section shown in **Figure 4.2** extending from the Mountain View Fault System in Wheeler County, Texas in the southwest to the northeastern extent of the study area in Dewey County, Oklahoma not only depicts the structural trends of the various Marmaton Granite Wash intervals (as discussed in Chapter 4), but also illustrates the variations in gamma-ray log response across the study area. In the southwestern region of the study area adjacent to the Amarillo-Wichita Uplift, the four Marmaton Hot Shale markers are easily identifiable: the hot shales with a gamma-ray reading of over 150 API units are in stark contrast to the surrounding sandstones that average around 100 API units (keeping in mind that the arkosic, potassium-rich sandstones of the Marmaton Granite Wash have higher average gamma-ray values than typical quartzose sandstones, as discussed in Section 2.1). Here in the southwest, the gamma-ray signature of the entire Marmaton Granite Wash clearly depicts interbedded sandstone and shale. Going basinward to the northeast, the gamma-ray loses its hot shale spikes and increasingly resembles a homogenous interval with a relatively consistent API value, making it increasingly difficult to distinguish the hot shale markers from the surrounding sandstone wash. It is because of this homogenization that the most northeastern extent of the Fourth Marmaton Shale is reached in western Roger Mills County. The tops of the underlying Upper Skinner Wash, Lower Skinner Shale, and Lower Skinner Wash also reach their northeastern extent at this point. These extents coincide with the linear trend of rapid shallowing and increased thickness contour density seen in western Roger Mills County on the thickness maps of the various Marmaton Wash intervals described in Chapter 4 (**Figures 5.1, 5.2, and 5.3**). The regional cross section runs perpendicular to this linear shallowing feature, and hot shales are the hardest to discern along this feature. Stratigraphic markers are practically impossible to distinguish for the underlying Skinner intervals and the Fourth Marmaton Shale, but the younger units above are increasingly less affected going up-section.

Immediately to the northeast of this linear feature of rapid shallowing, the individual Marmaton Wash intervals are much thinner than they are on the southwestern side of the feature but keep a more constant thickness than they do to the southwest. Here, the gamma-ray log begins to appear less homogenous and depicts distinct shale markers once more, and the stratigraphic markers for the underlying Skinner intervals are picked up again. Across this area where the Marmaton Wash intervals are shallower and thinner, the First through Third Marmaton Shales begin to be more and more discernible towards the northeastern extent of the study area. The Fourth Marmaton Shale is likely also present in this shallow area to the northeast, but there are several shale markers that it could be and a correlation cannot be comfortably made after losing it along that linear shallowing feature.

7.3 Gamma-ray Trends Across an Individual Fan Lobe

The net sandstone thickness map of the Marmaton "D" Wash interval in Buffalo Wallow Field in Hemphill County, Texas and the surrounding area described in Section 5.3 provides a visual representation of the sandstone depositional trends at the individual fan lobe scale (**Figure 5.4).** Figure 7.4 expands on this visual representation by including the gamma-ray log signatures of three different wells in various lateral positions across the fan lobe. The well that displays a gamma-ray signature furthest to the northwest, the Mewbourne Oil Prater #1, has a Marmaton "D" Wash net sand thickness of 175 feet, and is located outside and to the northwest of the main lobe that runs through Buffalo Wallow Field. It clearly depicts interbedded sandstone and shale with alternating intervals of lower gamma-ray (sandstone) and higher gamma-ray (shale). The Unit Petroleum Teas 43 well is located near the center of the main fan lobe running through Buffalo Wallow Field and is about four miles southeast of the Prater #1. The Teas 43 well has a Marmaton "D" Wash net sandstone thickness of 244 feet, which is 69 feet more than the Prater #1 and is the second highest net sandstone thickness value on the map. The Marmaton "D" Wash gamma-ray signature of the Teas 43 is significantly more "blocky" and homogenous in nature

than the Prater #1, and it is difficult to distinguish shaley intervals from sandstone. About 3.5 miles southeast of the Teas 43 well, the Blackbeard Operating Hefley #1 well is located on the southeastern edge of the main fan lobe going through Buffalo Wallow Field. The Hefley #1 has a Marmaton "D" Wash net sandstone thickness of 132 feet, which is 112 feet less than the Teas 43 well that is only about 3.5 miles to the northwest. The Marmaton "D" Wash gamma-ray signature of the Hefley #1 closely resembles that of the Prater #1 (about 7.25 miles to the northwest) in that it clearly depicts interbedded sandstones and shales with alternating lower and higher gamma-ray values (respectively). Overall, the well located near the center of the main fan lobe through Buffalo Wallow Field displays not only a higher net sandstone thickness than wells on the lobe fringes, but also has a much more homogenous gamma-ray signature for the Marmaton "D" Wash that makes distinguishing shaley intervals from sandstone difficult.

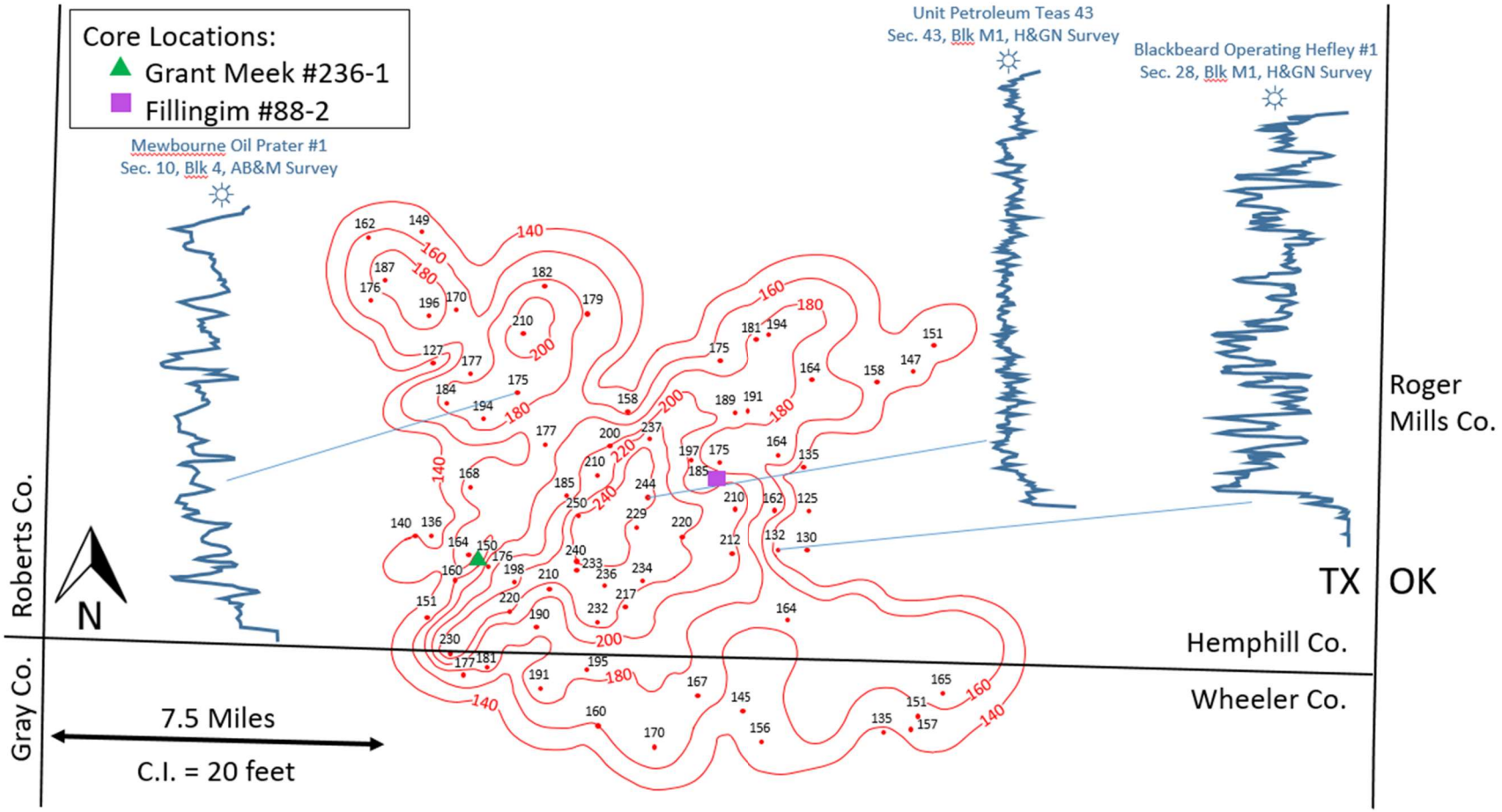

Figure 7.4: Net sandstone thickness map of Buffalo Wallow Field in Hemphill County, Texas and the surrounding area including gamma-ray signatures of wells in various lateral positions across the fan lobe. Note that the central well has the highest net sand value as well as the most homogenous well log signature, where it is difficult to distinguish shale interals from sandstone. Contour interval is 20 feet. All thicknesses are in feet.

7.4 Well Log Porosity Analysis

The Standard Resistivity Formation Density (RHOZ) log is a record of the formation's bulk density, or the overall density of the minerals forming the rock matrix as well as the density of the fluids within the pore spaces, recorded in g/cm^3. The main use of the bulk density log is to derive a value to calculate the total porosity of the formation, as density-derived porosity can be calculated using the equation:

$$\Phi_D = \frac{\rho_{ma} - \rho_b}{\rho_{ma} - \rho_f}$$

where:

- Φ_D = density-derived porosity
- ρ_{ma} = formation matrix density
- ρ_b = formation bulk density (log value)
- ρ_f = formation fluid density —usually mud filtrate (use 1.0 for freshwater and 1.1 for saltwater mud)

The formation bulk density is taken from the bulk density log, plugged into the equation above, and used to calculate porosity which will be shown on the Standard Resistivity Density Porosity (DPHZ) log. When calculating porosity from bulk density using this equation, the formation matrix density is determined by the lithology. For example, when assuming a formation is composed of sandstone, a density porosity log will be ran using a formation matrix density value of 2.65 g/cm^3.

The density porosity log for the Laredo Kicking Bird #1-20 well in Roger Mills County, Oklahoma was calculated using a formation matrix density value (ρ_{ma}) of 2.71 g/cm^3, which assumes a limestone lithology. The DPHZ log used this formation matrix density value, and showed an average density porosity (Φ_D) of 5.00% for the Marmaton Granite Wash. From both core analysis and thin section analysis, it was determined in this study that the main constituents

of the formation interval were quartz, potassium feldspar, and plagioclase, with minor amounts of calcite, clay minerals, and pyrite. This mineralogy resulted in an average grain density of 2.67 g/cm^3 in the core analysis data provided by Laredo Petroleum, which is significantly less than the 2.71 g/cm^3 a limestone lithology would render. For this reason, a true grain density recalculation was performed using 2.68 g/cm^3 as the formation matrix density value instead of the original 2.71 g/cm^3 value used to calculate density-derived porosity. A formation matrix density value of 2.68 g/cm^3 is commonly used for sandstone reservoirs in the Mid-Continent region, and is significantly closer to the calculated average grain density of 2.67 g/cm^3**.** The pore fluid density (ρ_{fl}) value was kept at 1.0 g/cm^3, and the average formation bulk density (ρ_z or ρ_b) value was found by taking an average value across the whole interval from the RHOZ log, which came out to 2.63%. Plugging these density values (ρ_{ma}, ρ_{fl}, and ρ_z or ρ_b) into the density-derived porosity equation yields a result of 3.2% porosity, which is much lower than the 5.00% porosity shown on the DPHZ log:

$$\Phi_D = \frac{\rho_{ma} - \rho_b}{\rho_{ma} - \rho_f} = \frac{2.68\ \text{g/cm}^3 - 2.63\ \text{g/cm}^3}{2.68\ \text{g/cm}^3 - 1.00\ \text{g/cm}^3} = \mathbf{3.2}\%$$

Parks (2011) recalculated density-derived porosity for the Fillingim #88-2 well of Buffalo Wallow Field in Hemphill County, Texas by performing a similar grain density calculation. Like the Kicking Bird, the DPHZ log for the Fillingim used a matrix density of 2.71 g/cm^3 and displayed an average density-derived porosity of 14.6% for the Marmaton Granite Wash interval. Using the same formula for density-derived porosity, a formation bulk density value derived from the RHOZ log of 2.46 g/cm^3, a matrix density value of 2.71 g/cm^3, a matrix value of 2.64 g/cm^3 as recorded by core plug measurements, and a fluid density of 1.00 g/cm^3, Parks (2011) calculated a porosity value of 10.97%, which is significantly lower than the average recorded log value of 14.6%:

$$\Phi_D = \frac{\rho_{ma} - \rho_b}{\rho_{ma} - \rho_f} = \frac{2.64\ \text{g/cm}^3 - 2.46\ \text{g/cm}^3}{2.64\ \text{g/cm}^3 - 1.00\ \text{g/cm}^3} = \mathbf{10.97}\%$$

CHAPTER VIII

PETROGRAPHY AND DIAGENESIS

8.1 Introduction to Petrography

Sandstone petrography and x-ray diffraction (XRD) analysis of the Marmaton "D" Wash interval was conducted on all three cores examined in this study in order to determine (1) mineralogy and texture and (2) to construct a paragenetic sequence of diagenetic events. Extensive point counting was performed using the Gazzi-Dickson method. The composition of the Marmaton Granite Wash in the Kicking Bird #1-20 core is summarized in **Table 8.1**. Petrographic data was acquired from Parks (2011) for the Marmaton "D" Wash interval in both the Grant Meek #236-1 and Fillingim #88-2 cores, and the composition of each is summarized in **Table 8.2**. XRD analysis was conducted on the Kicking Bird core (**Figure 8.1**), and mineralogy data determined by XRD for the Grant Meek (**Table 8.3**) and Fillingim (**Table 8.4**) cores was provided to Parks (2011) by Linn Energy and further utilized in this study. Scanning electron microscopy (SEM) was conducted on three samples each from the Marmaton "D" Wash interval of the Fillingim #88-2 and Kicking Bird #1-20 cores in order to evaluate and compare the porosity and pore structure at a micro- to nano-meter scale in wells proximal (Fillingim #88-2) and distal (Kicking Bird #1-20) to the Amarillo-Wichita Uplift source area. As the composition, texture, porosity, and pore structure of the two Buffalo Wallow cores (the Grant Meek #236-1

and the Fillingim #88-2) are similar, they will be discussed together and compared to the more distal Kicking Bird #1-20 core.

Table 8.1: Detrital constituents and porosity percentages derived from thin section point counting, Kicking Bird #1-20 core.

Thin Section (core depth in feet)	Porosity Average (%)	Quartz (%)	Plagioclase Feldspar (%)	Alkali Feldspar (%)	Rock Fragments (%)	Micas (%)	Calcite (%)	Clay/ Matrix (%)
12,761.7	0.00	35.56	4.17	2.50	32.22	1.39	5.55	18.61
12,763.7	0.00	27.22	1.39	1.11	45.00	0.00	3.61	21.67
12,766.3	0.00	40.00	7.33	0.00	16.33	1.00	2.67	32.67
12,774.5	0.00	34.72	0.83	4.17	36.12	2.22	2.22	19.72
12,776.5	0.00	39.17	3.33	1.11	34.72	1.39	0.56	19.72
12,785.3	0.00	38.61	2.78	1.67	25.83	0.56	2.22	28.33
12,781.8	0.00	33.89	0.00	0.55	37.50	1.39	2.50	24.17
12,778.7	0.00	26.38	0.00	0.56	47.78	0.00	5.00	20.28
12,780.7	0.00	36.11	1.11	1.39	30.28	2.78	2.22	26.11
12,804.4	0.00	38.06	0.83	0.00	37.78	1.11	2.50	19.72
12,804.8	0.00	28.89	3.89	0.00	37.5	0.00	3.05	26.67
12,805.3	0.00	38.61	1.11	0.00	41.39	0.00	1.67	17.22
12,806.4	0.00	51.39	2.22	1.67	23.61	1.11	0.56	19.44
12,809.6	0.00	35.00	0.83	4.72	36.11	2.50	4.45	16.39
12,812.8	0.00	42.22	3.06	3.06	24.72	1.11	0.00	25.83

Table 8.2: Detrital constituents and porosity percentages derived from thin section point counting, Grant Meek #236-1 and Fillingim #88-2 cores. "DF" denotes thin sections from the Fillingim, while "DGM" denotes those from the Grant Meek (Parks, 2011).

Thin Section	Porosity Average (%)	Quartz (%)	Plagioclase Feldspar (%)	Alkali Feldspar (%)	Micas (%)	Rock Fragments (%)	Clay/Matrix Material (%)
DF 11411	0.33	26	20	15	4	16	14
DF 11440	0	24	20	13	9	8	21
DF 11441	0.33	27	19	13	8	10	18
DF 11443	4.5	24	18	12	6	12	19
DF 11450	0.16	23	19	15	7	13	17
DF 11451.50	0.33	23	18	13	7	15	19
DF 11451.75	0	24	16	12	8	14	22
DGM 11352	1.16	28	17	14	9	13	13
DGM 11370	4.83	28	20	15	6	13	11
DGM 11388	6.5	29	16	16	5	15	9
DGM 11399	4.83	28	16	16	4	16	11
DGM 11405	3.3	27	13	16	4	19	13
DGM 11410	1.5	29	18	15	5	15	12
DGM 11411	1.8	28	18	15	6	16	12
DGM 11418	6.5	28	17	14	7	15	10
DGM 11419	0	25	18	15	5	14	20
DGM 11422	5	30	16	14	5	16	10

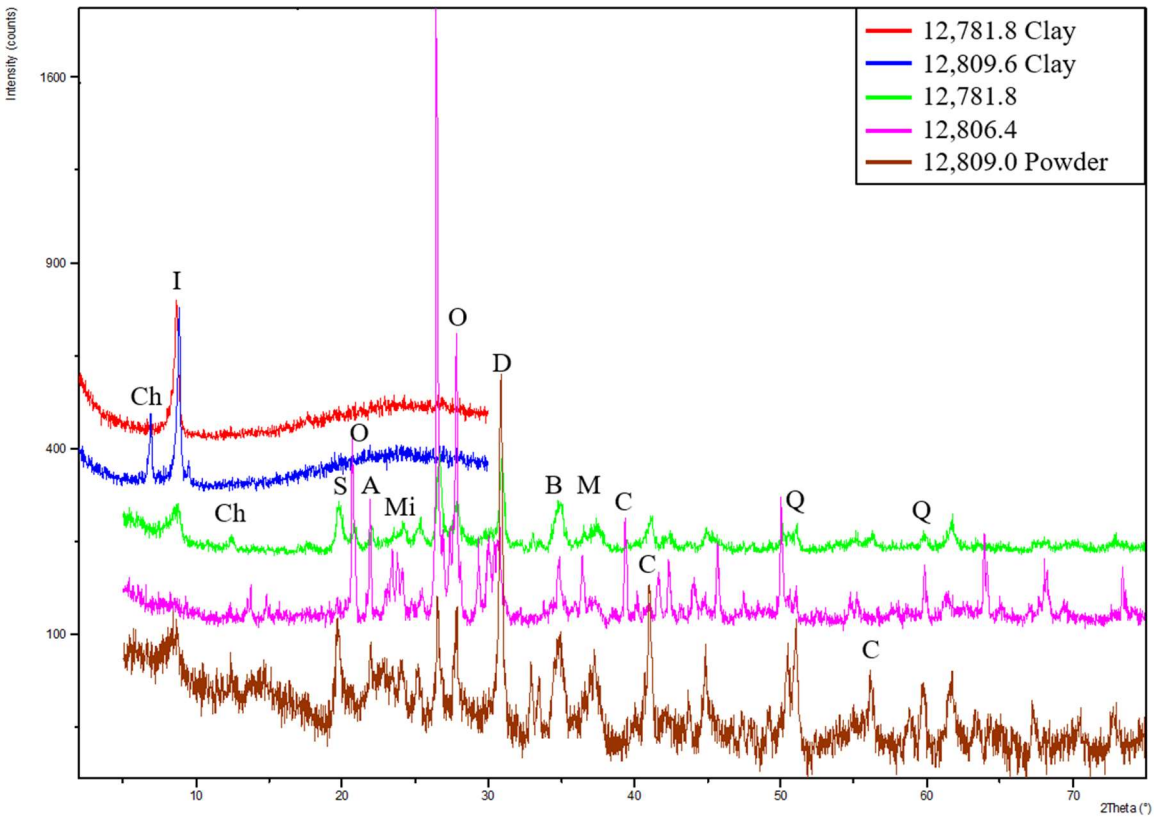

Figure 8.1: X-ray diffraction peaks revealing the detrital and authigenic components found within the Kicking Bird #1-20 core. Note the presence of authigenic clays illite (I), chlorite (Ch), and smectite (S). Other constituents include quartz (Q), orthoclase feldspar (O), albite/plagioclase feldspar (A), microcline/alkali feldspar (Mi), dolomite (D), muscovite (M), biotite (B), and calcite (C).

Table 8.3: Mineralogical data for the Grant Meek #236-1 core, determined by x-ray diffraction (XRD) (Parks, 2011, originally provided by Linn Energy).

	Whole Rock Mineralogy (Weight %)					Relative Clay Abundance (Normalized to 100%)	
Depth	Quartz	K-Feldspar	Plagioclase	Calcite	Total Clay	Illite & Mica	Chlorite
11342.9	31.6	23.6	30.4	3.2	11.2	12.1	87.9
11346.2	32.8	20.6	28.3	0.6	17.7	14.5	85.5
11351.5	19	19.8	26.8	2.6	31.8	8.9	91.1
11353.5	32.9	18.7	33.9	1.7	12.7	7.3	92.7
11357.5	31.5	19.7	29.1	1.2	18.6	6.9	93.1
11364.5	33.5	21.0	31.9	1.7	11.9	5.9	94.1
11368.5	30.3	19.3	29.0	1.1	20.3	4.2	95.8
11393.5	29.2	22.4	29.5	0.6	18.4	9.9	90.1
11407.5	30.3	21.4	27.9	0.5	19.8	8.5	91.5
11411.5	26.4	17.2	32.3	14.9	9.2	13.2	86.8
Min	19.0	17.2	26.8	0.5	9.2	4.2	85.5
Max	33.5	23.6	33.9	14.9	31.8	14.5	95.8
Average	29.8	20.4	29.9	2.8	17.2	9.1	90.9

	Whole Rock Mineralogy (Volume %)					
Depth	Quartz	K-Feldspar	Plagioclase	Calcite	Illite & Mica	Chlorite
11342.9	31.8	24.2	30.8	3.2	1.4	8.7
11346.2	33.2	21.3	28.9	0.6	2.6	13.5
11351.5	19.6	20.9	27.8	2.6	2.9	26.2
11353.5	33.2	19.2	34.5	1.7	0.9	10.4
11357.5	32.0	20.4	29.7	1.2	1.3	15.4
11364.5	33.8	21.5	32.4	1.7	0.7	9.9
11368.5	30.9	20.1	29.7	1.1	0.9	17.3
11393.5	29.6	23.2	30.1	0.6	1.8	14.7
11407.5	30.8	22.2	28.6	0.5	1.7	16.2
11411.5	26.6	17.6	32.8	14.7	1.2	7.1
Min	19.6	17.6	27.8	0.5	0.7	7.1
Max	33.8	24.2	34.5	14.7	2.9	26.2
Average	30.2	21.1	30.5	2.8	1.5	13.9

Table 8.4: Mineralogical data for the Fillingim #88-2 core, determined by x-ray diffraction (XRD) (Parks, 2011, originally provided by Linn Energy).

	Whole Rock Mineralogy (Weight %)						Relative Clay Abundance (Normalized to 100%)	
Depth	Quartz	K-Feldspar	Plagioclase	Calcite	Pyrite	Total Clay	Illite & Mica	Chlorite
11407.5	31.1	20.9	33.8	2.6	0.0	11.6	7.6	92.4
11417.5	35.2	21.1	31	0.8	0.0	11.9	7.2	92.8
11432.5	33.7	19.8	30.8	6.5	0.4	8.8	7.9	92.1
11440.5	24.3	16.1	30.2	0.6	1.3	27.4	7.3	92.7
11447.5	33.6	14.7	29.5	4.3	0.8	17.1	8.7	91.3
11461.5	32.4	20.1	32.6	1.3	1.7	11.9	12.5	87.5
Min	24.3	14.7	29.5	0.6	0.0	8.8	7.2	87.5
Max	35.2	21.1	33.8	6.5	1.7	27.4	12.5	92.8
Average	31.7	18.8	31.3	2.7	0.7	14.8	8.5	91.5

	Whole Rock Mineralogy (Volume %)						
Depth	Quartz	K-Feldspar	Plagioclase	Calcite	Pyrite	Illite & Mica	Chlorite
11407.5	31.4	21.5	34.3	2.5	0.0	0.9	9.5
11417.5	35.4	21.6	31.5	0.8	0.0	0.9	9.8
11432.5	33.9	20.4	31.3	6.4	0.2	0.7	7.2
11440.5	25.2	17.0	31.5	0.6	0.7	2.1	23.0
11447.5	34.2	15.3	30.3	4.3	0.4	1.5	14.0
11461.5	32.9	20.8	33.3	1.3	0.9	1.5	9.3
Min	25.2	15.3	30.3	0.6	0.0	0.7	7.2
Max	35.4	21.6	34.3	6.4	0.9	2.1	23.0
Average	32.2	19.4	32.0	2.7	0.4	1.3	12.1

8.2 Detrital Constituents and Texture

The provenance for Granite Wash detritus was the granitic basement of the Amarillo-Wichita Uplift, located immediately to the south-southwest of the deep Anadarko Basin. These Precambrian to Cambrian source rocks are largely composed of granite (56%) with lesser amounts of diabase (14%), granodiorite (12%), quartz diorite (7%), gabbro (7%), diorite (2%), and rhyolite porphyry (2%), as determined by analysis of basement exposures in the Wichita Mountains (Flawn, 1956; Dutton and Land, 1985). Sandstones in the Kicking Bird #1-20 core (more distal from the source area) are primarily very fine to fine-grained, while the more proximal Buffalo Wallow cores exhibit coarse sand to pebble-conglomerate grain sizes.

The primary detrital constituent of the Marmaton "D" Wash in both the Kicking Bird #1-20 and the Buffalo Wallow cores is quartz, averaging 35.4% (ranging between 26.4 and 51.4%) in the Kicking Bird and 26.5% (ranging between 23 and 30%) across the two Buffalo Wallow cores (**Tables 8.1** and **8.2**). Monocrystalline quartz is the most common form of quartz in all three cores, but trace amounts of polycrystalline quartz are also recognized. Quartz grains in all cores are sub-angular to angular.

The source rock composition reported by Flawn (1956) and Dutton and Land (1985) is strongly reflected in the Marmaton "D" Wash sandstones of all three cores, as quartz, feldspar, and granitic rock fragments (particularly microperthite and granophyre) constitute the framework grains (**Figures 8.2** and **8.3**). However, lithic fragments make up over twice as many of the grains seen in the more distal Kicking Bird than in the more proximal Buffalo Wallow samples, while the Buffalo Wallow cores display over eight times as many detrital feldspar grains as the Kicking Bird. Lithic fragments average 33.8% of grains observed in the Kicking Bird but only 14.1% in the Buffalo Wallow. Feldspar averages only 3.7% of grains in the Kicking Bird, but 31.9% in the Buffalo Wallow. Micrographic texture is common throughout all three cores, with quartz intergrowths being observed within the plutonic rock fragments. Volcanic rock fragments are identified by randomly-oriented microcrystals in an aphanitic groundmass. Chert is also a common lithic grain, and the visible sponge spicules of spicular chert are documented in several samples from the Kicking Bird core. Plagioclase is the most abundant feldspar seen in all three cores, but is just slightly more common than alkali feldspars. Lithic rock fragments as well as the feldspar grains range from sub-rounded to angular in every core, but sub-rounded feldspar grains are more prevalent in the Kicking Bird. Dissolution of feldspar grains is much more common in the Buffalo Wallow (**Figures 8.3** and **8.7**), while feldspar grains shown in SEM of the Kicking Bird appear generally unaltered by dissolution (**Figure 8.4**).

Biotite and muscovite mica are seen in most samples but are significantly more common in the Buffalo Wallow cores, averaging 6.2% (and reaching as high as 9% in some samples) as opposed to 1.1% in the Kicking Bird. Glauconite is observed in all three cores. Ductile mica grains such as biotite and glauconite have been deformed to form pseudomatrix. Dark-brown organic matter can be seen between the framework grains in all samples, but is especially prevalent in the Kicking Bird. Detrital clay matrix is abundant is the Kicking Bird and can readily be seen filling the intergranular pore space between the framework grains (**Figure 8.2** and **8.7**). This detrital clay is The Buffalo Wallow cores are much cleaner in regards to detrital clay matrix. While the Kicking Bird samples display 22.4% clay matrix material on average, the Buffalo Wallow cores average only 14.8% (**Tables 8.1** and **8.2**).

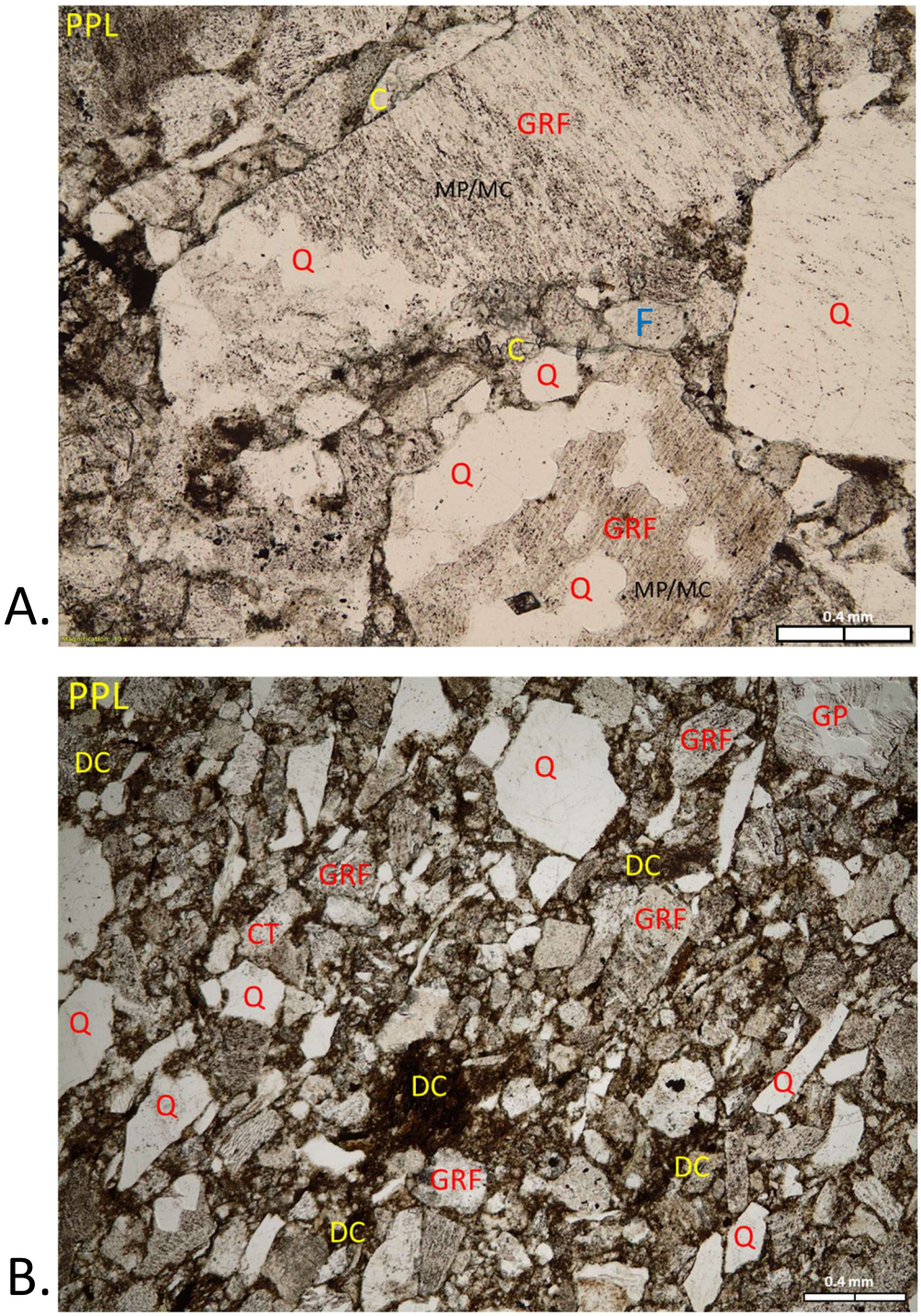

Figure 8.2: Photomicrographs from the Kicking Bird #1-20 well displaying constituents of Marmaton Granite Wash detritus: quartz (Q), granitic rock fragments (GRF) particularly microperthite (MP) and granophere (GP), feldspar (F) particularly microcline (MC), chert (CT), and calcite (C). A. Calcite replaces feldspar within granitic rock fragments and matrix material at 12,806.4 feet, 10x magnification. B. Note the high amount of detrital clay (DC) between framework grains at 12,812.8 feet, 5x magnification. Both images are plane-polarized light (PPL).

A.

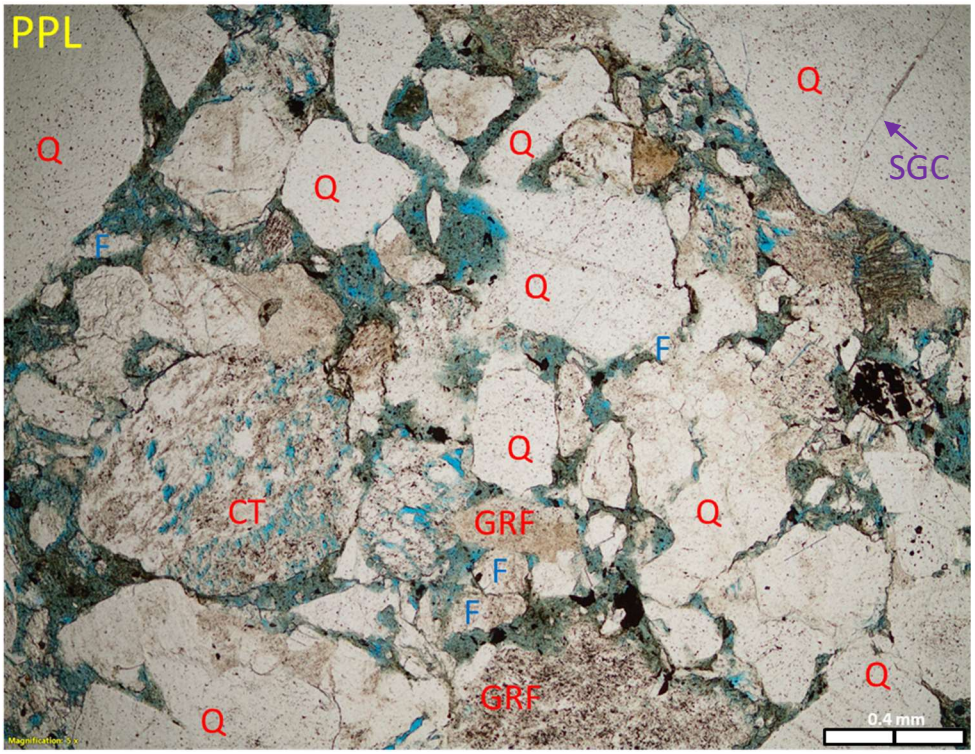

B.

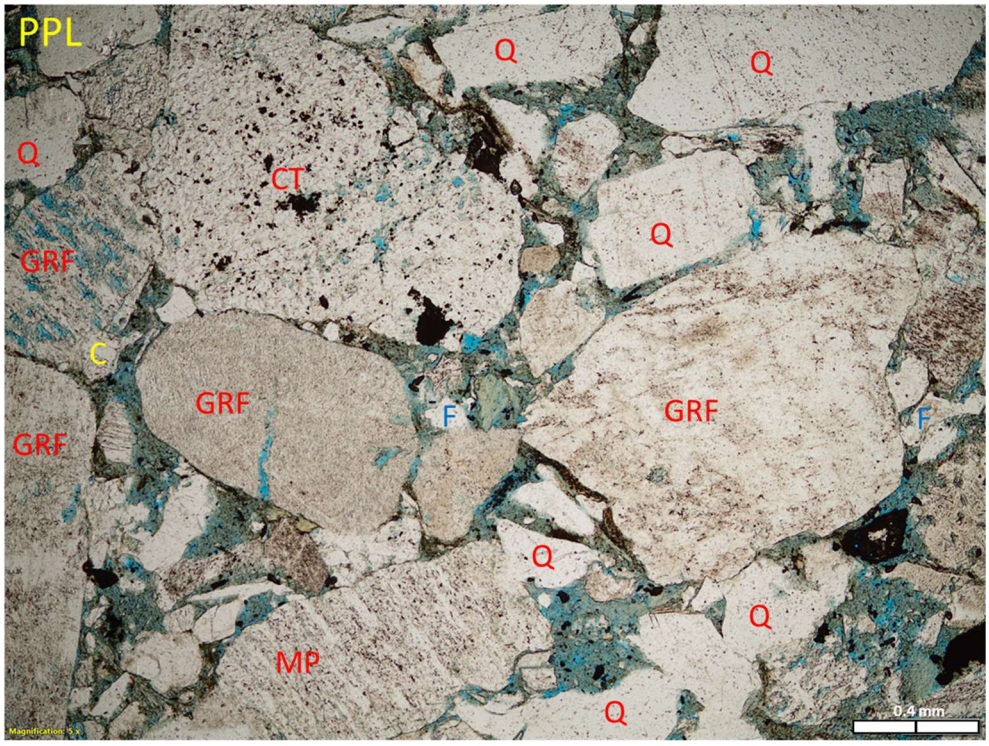

Figure 8.3: Photomicrographs from the Grant Meek #236-1 well in Buffalo Wallow Field at 11,411.0 feet displaying constituents of Marmaton Granite Wash detritus: quartz (Q), granitic rock fragments (GRF) particularly microperthite (MP), feldspar (F), chert (CT), and calcite (C). A. Sutured grain contacts (SGC) between quartz grains indicates pressure dissolution. B. Note calcite replacing feldspar in granitic rock fragment, center left. Both images PPL, 5x magnification.

A.

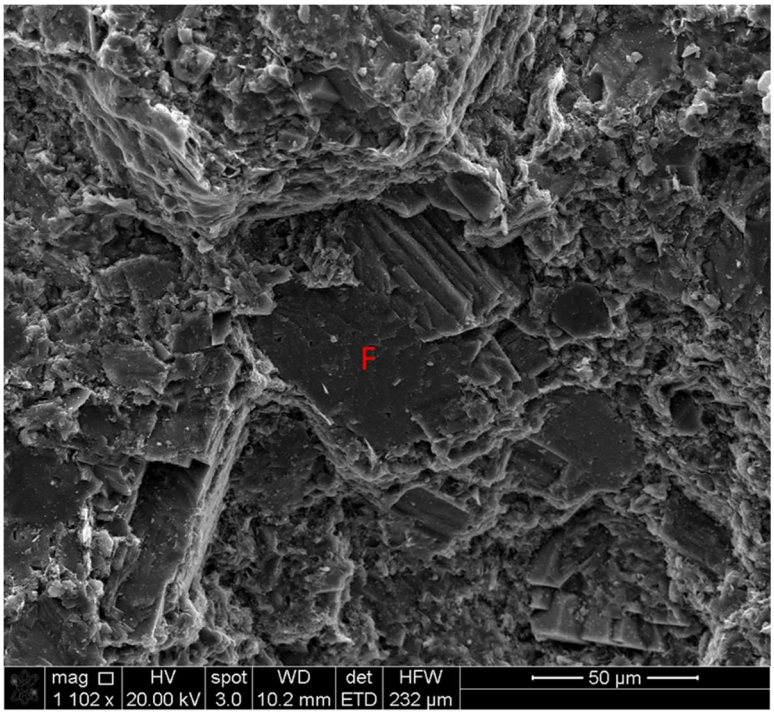

B.

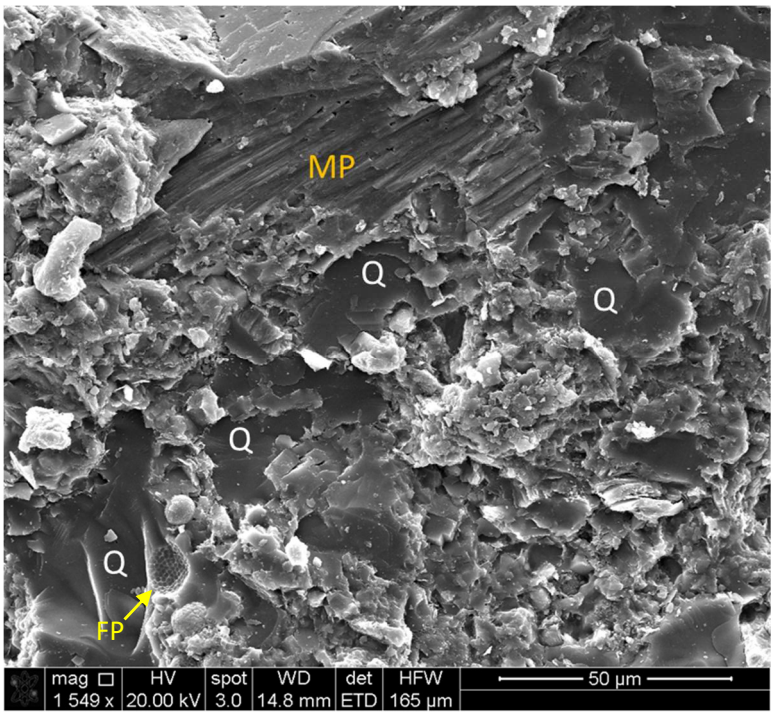

Figure 8.4: Scanning electron microscope (SEM) images from the Kicking Bird #1-20 core showing some detrital constituents. (A) At 1,102 x magnification (scale bar is 50 µm), cleavage of the tetrahedral silicate structure of feldspar (F) and lack of dissolution are apparent. Depth: 12,807.6 feet. (B) At 1,549 x magnification, a flat, planar mineral is likely an igneous rock fragment, particularly microperthite (MP), which is characteristic of Amarillo-Wichita uplift granitic rocks. Quartz (Q) is abundant. The spherical aggregate structure in the bottom left appears to be framboidal pyrite (FP). Depth: 12,786.7 feet.

8.3 Diagenetic Features

Diagenetic constituents documented in the Marmaton "D" Wash interval include silica, feldspar, calcite, chlorite, and illite. Authigenic silica is rare in all cores. Quartz overgrowths with dust rims are scarce in all samples, but occasional quartz grains have a planar margin that could be interpreted as a euhedral quartz overgrowth. Feldspar overgrowths are even more rare and were not identified in this study, but were reported by Dutton and Land (1985) to occur in the Missourian (Middle to Late Pennsylvanian) Granite Wash sandstones of Mobeetie Field (northwestern Wheeler County, Texas, about 10 miles north of the Amarillo-Wichita Uplift) at a volume of less than 0.5%. Calcite cement is rare across all samples, but is more commonly seen in the Kicking Bird, where it is observed filling fractures and replacing both plagioclase and potassium feldspar in the dissolution voids of detrital feldspar grains (**Figures 8.2** and **8.3**).

Dissolution features are only minor in the Kicking Bird, but are significantly more prevalent in the Buffalo Wallow samples. The dissolution of detrital granitic rock fragments, chert, quartz, feldspar, and matrix are all extensive in the Buffalo Wallow. **Figures 8.3** and **8.7** illustrate the prevalent dissolution of framework grains, generating intragranular porosity. Note the "honeycomb" texture of the altered granite rock fragments, as the feldspar within the grain is being preferentially dissolved before the quartz. The dissolution of quartz grains is also present in the Buffalo Wallow, but is much less common or extensive as feldspar dissolution. When quartz grains do depict evidence of dissolution, it is most commonly along corroded margins or fractures that have subsequently been filled in with calcite. Matrix dissolution is common in the Buffalo Wallow but rare in the Kicking Bird where dissolution of any kind is minimal and both the detrital grains and the matrix appear largely unaltered (**Figures 8.2** and **8.4**).

In petrographic studies, authigenic clays can be difficult to distinguish from those that are detrital in nature. Detrital clays are fine-grained material that are syndepositional to the framework grains, and are most easily recognized by their bimodal deposition (a fine matrix deposited

alongside framework detrital grains) and their intergranular position. Authigenic clays, on the other hand, can be found in sandstones as pore linings, pore and fracture fillings, and pseudomorphous replacements (Wilson and Pittman, 1977). Wilson and Pittman (1977) describe the most reliable criteria for identifying authigenic clays: (1) delicacy of clay morphology, which would have been destroyed in sediment transport, (2) occurrence of clay as pore linings that are missing only at grain contacts, and (3) composition that is greatly different from associated detrital clays. These criteria were used in this study to distinguish authigenic clays from their detrital counterparts and from each other in SEM.

Authigenic illite is present in both the Kicking Bird and the Fillingim of Buffalo Wallow Field as cement, and displays both platy and pore-lining morphologies. Authigenic chlorite is present as a cement in both but is significantly more prevalent in the Buffalo Wallow, with pore-occluding psuedohexagonal flakes forming a diagnostic "house of cards" arrangement (**Figure 8.6**). The presence of authigenic illite and chlorite was confirmed in both the Kicking Bird (**Figure 8.1**) and the Buffalo Wallow (**Tables 8.3** and **8.4**) through x-ray diffraction analysis (XRD). Chlorite is seen both as a grain coat and as pore-fill in both the Kicking Bird and Fillingim (**Figure 8.6**). While the Kicking Bird appears to be more rich in detrital clay matrix, the Buffalo Wallow samples display more authigenic clays, which is evident in SEM.

Fracturing resulting from compaction is evident in all cores through the observation of deformed micas that have formed pseudomatrix, microfractures in detrital grains, pressure solution features, and the offset twinning of feldspar grains. Sutured quartz grain contacts representing pressure solution due to compaction are identified in both the Kicking Bird and the Buffalo Wallow (**Figure 8.23**). Framboidal pyrite, seemingly forming in clusters, can be seen in samples of the Kicking Bird core in SEM (**Figure 8.4**).

A.

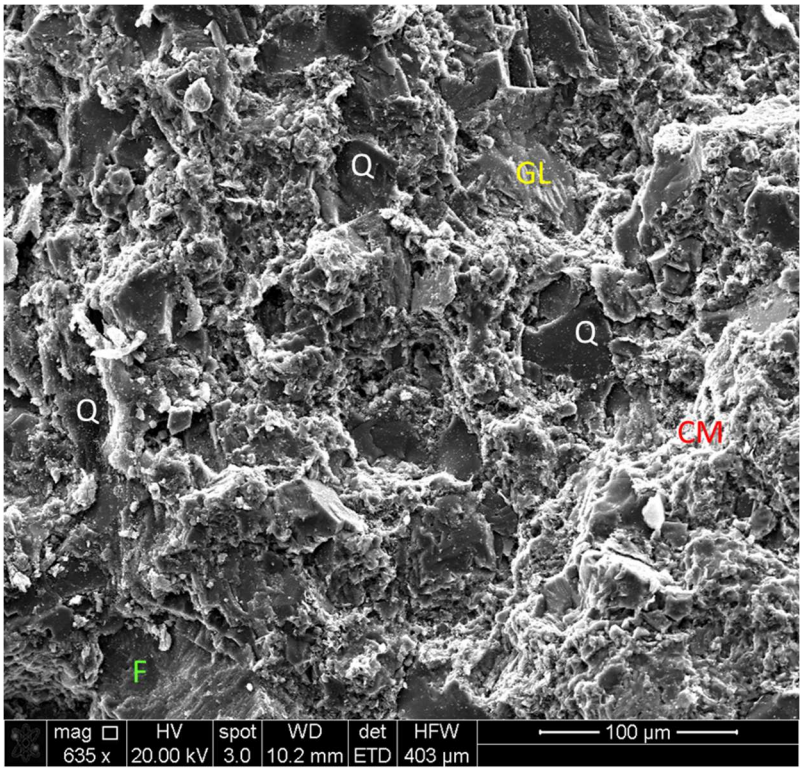

B.

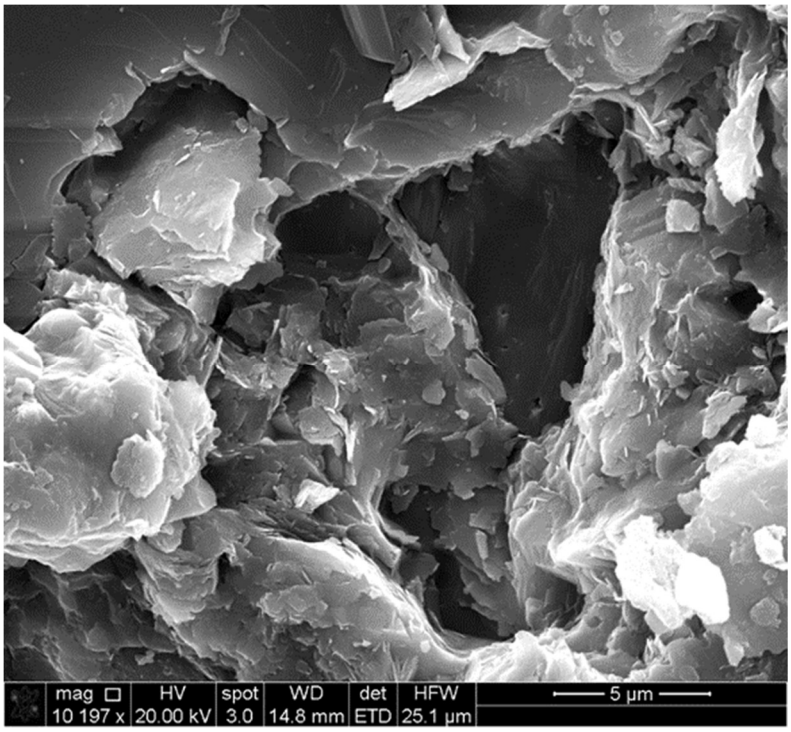

Figure 8.5: Scanning electron microscope (SEM) images from the Kicking Bird #1-20 core at a depth of 12,807.6 feet. (A) General grain fabric is visualized at a magnification of 635x with quartz (Q), granitic lithics (GL) and feldspars (F) as the dominant minerals. Clay minerals (CM) coat detrital grains. Scale bar is 100 µm. (B) At 10,197x magnification, pore space that is imperceptible in thin section is seen. Scale bar is 5 µm.

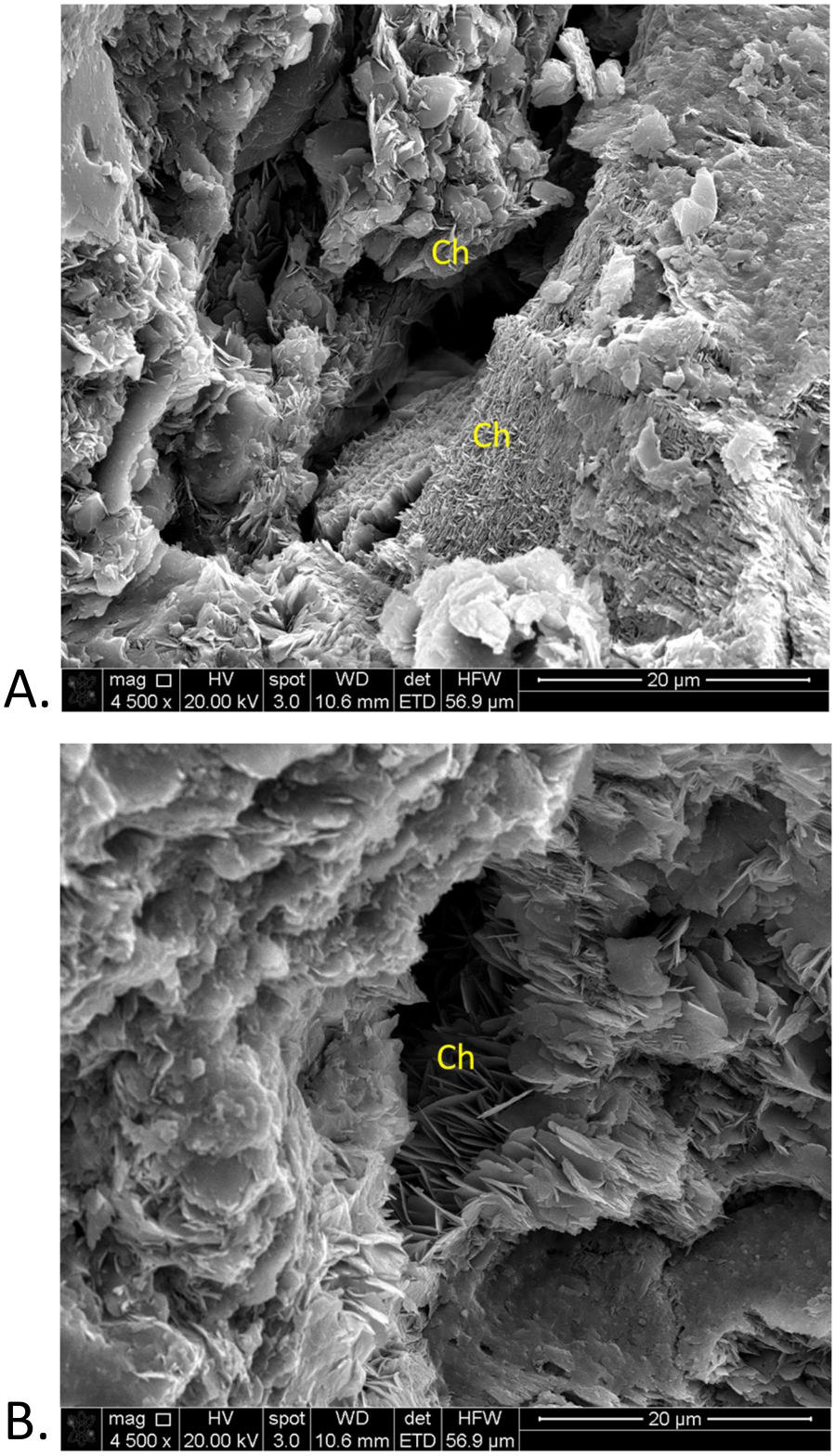

Figure 8.6: Scanning electron microscope (SEM) images from the Fillingim #88-2 core of Buffalo Wallow Field depicting widespread partially pore-filling chlorite, identified by its psuedohexagonal flake morphology. Pore spaces exceed 30 µm. Both images at 11,442.5 feet, 4500x magnification. Scale bar is 20 µm.

8.4 Porosity

No porosity of any kind is evident in thin sections of the Marmaton "D" Wash interval of the Kicking Bird core. As is the case in many other tight gas sandstone reservoirs, a good sense of the porosity present in the Kicking Bird is practically impossible to grasp using transmitted light thin section microscopy alone. Further, pore sizes were too minute to register accurately on the teaching-grade Core Lab PORG-200 helium gas porosimeter available for this study. In the core analysis data provided by Laredo Petroleum, porosity averaged 3.0% across the Kicking Bird core, reaching a high of 7.3% but commonly was less than 1.5% (**Table 6.1**). SEM analysis was necessary to visualize and understand the volume and type of porosity present in the Kicking Bird core. Higher recorded porosity values as reported in the core analysis data were sampled for SEM analysis.

SEM revealed that there is a volume of porosity in the Kicking Bird that cannot be seen in thin section, but this volume is so minute that it cannot be seen until a magnification of around 1,500x (**Figure 8.5**). Porosity is largely intergranular. Secondary dissolution is scarce, and clay minerals appear to partially obstruct intergranular pores. Pore diameters are most often less than 10-15 μm, and commonly even less than 5 μm.

The Buffalo Wallow samples display significantly higher amounts of porosity than those from the Kicking Bird core, and include multiple porosity types: (1) primary intergranular porosity, (2) secondary intragranular porosity, and (3) microporosity. Secondary porosity is more common than primary porosity within the Buffalo Wallow samples, but they still display significantly more primary porosity than samples from the Kicking Bird core. Porosity values for the Buffalo Wallow core derived from conventional core plug analysis of the Fillingim #88-2 core performed by Parks (2011) averages arouund 5.7% and reached a maximum of 8.9% across the Marmaton "D" Wash interval (**Figure 6.2**).

Primary intergranular porosity is seen preserved in the Buffalo Wallow samples as preserved pore space. It can be identified by the planar surfaces generated by euhedral faces of quartz overgrowths. This primary intergranular porosity aided in the development of secondary porosity by providing pathways for corrosive fluids to come into contact with metastable framework grains.

Secondary intragranular porosity, the dominant porosity type in the Buffalo Wallow wash, resulted from the dissolution of rock constituents including feldspar, granitic rock fragments, chert, quartz, and pseudomatrix (**Figures 8.3** and **8.7**). Natural fractures in detrital grains are another source of secondary porosity. Secondary porosity appears to be higher in samples with larger grain sizes, indicating that coarser-grained sandstones may have had more preserved primary porosity that allowed fluids to contact grains and generate greater amounts of secondary porosity than in finer-grained sandstones (**Figure 8.3**).

Microporosity, as defined by Pittman (1979), includes all pores with pore-aperture radii less than 0.5 μm. This not only includes the microscopic pores present within authigenic clays and partially leached feldspar grains, but the porosity associated with surface roughness as well. Being that the Buffalo Wallow contains more authigenic clays and has more prevalent dissolution of framework grains such as feldspar and granitic rock fragments than the Kicking Bird wash, it is likely that the Buffalo Wallow contains higher microporosity.

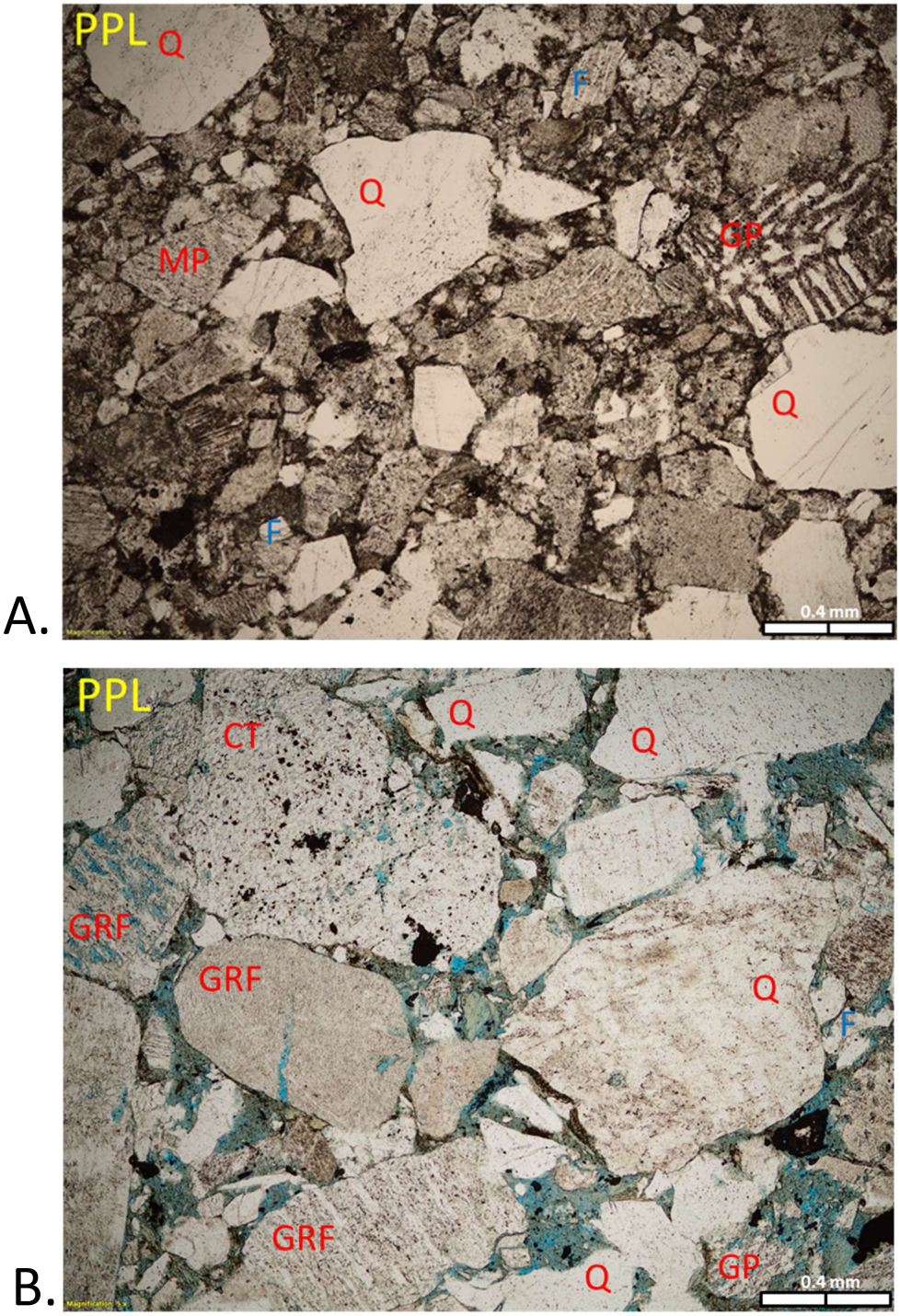

Figure 8.7: Photomicrographs comparing the Kicking Bird #1-20 in Roger Mills County, Oklahoma to the Grant Meek #236-1 in Buffalo Wallow Field, Hemphill County, Texas. A. Kicking Bird #1-20 at a depth of 12,806.4 feet with a 5x magnification. B. Grant Meek #236-1 at a depth of 11,418 feet with a 5x magnification, highlighting the higher amount of secondary dissolution porosity (blue) present in the Grant Meek thin section than in the Laredo Kicking Bird thin section. Dissolution of feldspar grains and rock fragments is significantly more prevalent in the Grant Meek #236-1. Both images PPL.

8.5 Paragenesis

The diagenetic history of the Marmaton "D" Wash interval was evaluated petrographically based on textural relationships within the Kicking Bird core and is summarized graphically in **Figure 8.8**. Clay-rich detrital matrix and organic matter are syndepositional, having been emplaced between the framework grains at the time of deposition. Upon burial, the Granite Wash sediments underwent differential compaction, resulting in the deformation of mica grains and their subsequent formation as pseudomatrix. This pseudomatrix likely formed early in the diagenetic history of the formation, as the neighboring quartz grains appear to have maintained their original morphology.

As compaction increased as a factor of increasing depth and increasing overburden pressure, pressure dissolution along quartz grain contacts moved silica into solution. This silica was then precipitated as syntaxial overgrowths on the surface of detrital quartz grains. The formation of silica cement in the form of syntaxial quartz overgrowths commonly occurs during mesogenesis (the diagenetic domain between the end of surficial influence and exposure), usually at temperatures around 60-80° C (Ulmer-Scholle et al., 2014).

Next, a period of acidic conditions prevailed, resulting in dissolution of matrix and feldspar by organic acids that migrated in through preserved primary porosity. Feldspar dissolution is evident by the prevalence of dissolved lithic fragments. However, the negligible amount of secondary porosity seen in thin sections of the Kicking Bird core indicates that the framework grains were likely coated with detrital clay prior to this stage of dissolution, preventing significant secondary porosity formation.

A short time after the dissolution of matrix and feldspar, illite formed through the compaction and dewatering of smectite. This illite likely coated the detrital grains as well, providing further protection from secondary porosity formation. During this time, organic acids

likely migrated out of the system along with the water derived from the dewatering of smectite. This lowered the acidity of the system and raised the pH.

As the system turned basic after the expulsion of organic acids, the formation of authigenic calcite, which favors higher pH conditions, occurred as intergranular calcite cement and replacement of feldspar. This late-stage calcite formation is highlighted by the jagged shape of the calcite grains and calcite's tendency to replace feldspar both in feldspar grains and within lithic rock fragments, indicating that it formed contemporaneously with or shortly after the dissolution of feldspar (**Figures 8.2 and 8.3**). Finally, hydrocarbon migration occurred during the late stage of mesogenesis, after most of the organic acids had been expelled from the system.

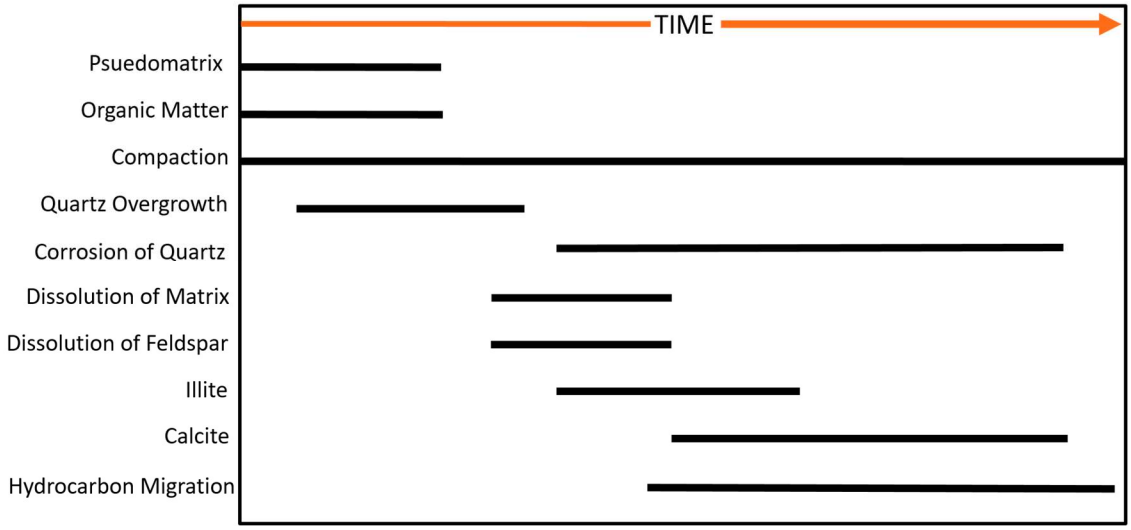

Figure 8.8: Paragenetic sequence of diagenetic events for the Marmaton "D" Wash interval of the Kicking Bird #1-20 core.

CHAPTER IX

DISCUSSION

9.1 Depositional Setting

Data from multiple sources including core, well logs, structure and thickness maps, and previous literature were integrated to better understand the Marmaton Granite Wash depositional system. In particular, analysis of three cores from the Marmaton "D" Wash interval across the study area allowed for inference regarding the environment of deposition, sediment transport processes, and detrital mineralogy of the Marmaton Granite Wash. The Marmaton "D" Wash interval in all three cores is characterized by repeated fining upward packages of interbedded sandstone and shale. The vertical thickness of the individual fining upward sequences are variable within each core, which indicates that the depositional pulses of Marmaton "D" Wash detritus being shed off the uplift are not uniform in magnitude. Some pulses were stronger than others, causing variable amounts of sediment to be deposited into the basin. Given the humid climate of the region, this thickness variability could likely be a function of precipitation in the source area and/or drainage basin. The high moisture regime of the region due to its equatorial location as well as the fact that the Amarillo-Wichita Uplift was likely around its peak rate of uplift during Marmaton Granite Wash deposition likely facilitated rapid erosion and deposition. As the plentiful feldspars within the granitic detritus are relatively unstable at normal surface conditions when compared to more quartz-rich sands, the largely unweathered nature of the detrital feldspar

and granitic rock fragments seen in thin section in all three cores indicates that transport to the depocenter was short and occurred before the grains could be significantly altered. Sometimes, due to climate cyclicity and variations in tectonic activity, erosion rates would be so low that little to no coarse-grained siliciclastic material would be carried into basin. These periods of low sedimentation rates and decreased tectonic activity fostered lower flow regimes in the basin that allowed suspension settling and shale deposition to dominate.

The repeated fining upward sequences as well as several other sedimentary features observed in the three Marmaton "D" Wash cores suggest sediment gravity flows are the primary means of sediment deposition. Many of the individual sequences of upward-fining grain size (normal grading) display at least a portion of the Bouma Sequence, the standard vertical sequence of sedimentary structures used to identify turbidites (Bouma, 1962). A graphical representation of the Bouma Sequence (also called the turbidite facies model) is shown in **Figure 9.1A**. A turbidite is the lithified product of a turbidity current, a sediment gravity flow with Newtonian rheology in which sediment in turbulent suspension is carried swiftly down a subaqueous slope due to the density differential between the sediment-laden water and the surrounding water (Shanmugam, 2021). Turbidites are differentiated from the deposits of other types of sediment gravity flows (debris flow, fluidized flow, or grain flow) in core by the recognition of (1) whole or partial Bouma Sequences that depict a characteristic upward decrease in grain size, and (2) parallel bedding with regular alterations between sandstone and shale (Walker, 1978). Both of these criteria are readily observed in the more distal Kicking Bird core, with most fining upward sequences having a shale at the top that has a sharp, planar bedding contact with the sandstone above (**Figure 6.1**). Turbidites compose major portions of submarine fans and can occur as channel-fill, lobes, or sheet sands (Shanmugam and Moiola, 1988).

Turbidity flows begin with slope failure in soft sediment, which may be triggered by a number of different processes that include (but are not limited to) earthquakes, slope instability,

oversupply of sediment, tsunamis, or even meteorite impacts (Shanmugam, 2021). The basal division of a turbidite, T_a, represents the initial deposition of the coarsest sediment out of the turbidity flow followed by increasingly finer-grained sediment as the depositional energy slows (Bouma, 1962). The resultant graded sandstone interval is observed within the cores at the base of the fining upward sequences. The next Bouma division up, T_b, forms as the sediment concentration decreases, hydraulic sorting decreases, and the sediment depicts upper planar laminar of the upper flow regime as the flow is still moving with a high velocity. This division is represented in the cores as planar laminations. Small-scale cross bedding and ripple laminations occurring in the upper sections of thicker fining upward sequences of the Kicking Bird were attributed to division T_c of the Bouma sequence, which forms as deposition from a turbidity current begins to slow from the upper flow regime and the finer sediment that is left in suspension begins to form ripples. Following this, the turbidity current slows even more to the point that bedload transport stops and deposition consists mostly of the settling of silt and then clay, which forms the parallel laminae of Bouma division T_d and T_e, respectively.

Soft sediment deformation, particularly convolute bedding, is observed in all three cores (**Figure 6.2**). Convolute bedding results from the deformation of liquefied sediment, is commonly seen in turbidite sandstones, and is considered evidence of rapid deposition (Collinson, Mountney, and Thompson, 2006). Flame structures, another indicator of soft sediment deformation, result when sediment is rapidly deposited on a layer of unlithified mud, which causes the sand to sink and form wavy tongues of mud that resemble flames (Collinson, Mountney, and Thompson, 2006). Flame structures are observed in both the Grant Meek and Fillingim cores (**Figure 6.6**). Dish and pillar structures are known to form as a result of the compaction of rapidly deposited, unconsolidated sands and are commonly seen in the Grant Meek core, particularly in sediments that are coarse sand or coarser (**Figures 6.4** and **6.5**). As the unconsolidated sediment was gradually compacted and dewatered, semi-permeable laminations

(usually finer sand or mud) acted as a barrier to the upward movement of fluidized sediment, causing it move horizontally until vertical fluid escape was possible (Lowe and LoPiccolo, 1974). The resultant concave-up, bowl-like shapes (dish structures) and vertical water-escape channels (pillar structures or sand dikes) are typical sedimentary structures formed by fluidized flows (Lowe and LoPiccolo, 1974; Shanmugam, 2021). Fluidized flows (also called liquefied flows) are sediment gravity flows in which sediment is kept in suspension by the upward-moving intergranular flow of fluid (Shanmugam, 2021). Some turbidity currents rapidly evolve from fluidized flows and start to form Bouma Sequence structures indicative of turbidity flows, because fluid turbulence results as soon as the fluidized flow begins to move (Lowe, 1976). Dish and Pillar structures, flame structures, and convolute bedding are often found in submarine fan environments where sediment gravity flows such as high velocity turbidity currents and fluidized flows cause rapid deposition. Mud rip-up clasts of various size and shape are commonly seen within vertically thicker fining upward sequences in all three cores (**Figure 6.3**). These clasts became entrained within the sand during local erosion of preexisting mud on the seafloor during rapid sedimentation. While the Kicking Bird core consists almost entirely of sedimentary structures indicative of turbidity flows, the Grant Meek and Fillingim cores depict structures typical of a fluidized sediment flow (which could rapidly develop turbidity currents) as well. Structures indicative of grain flows, a sediment gravity flow in which sediment is supported by grain-to-grain interactions, are not observed in any core, which is expected as they require a steeper slope of 18 to 37° to generate and are thus not a common type of sediment gravity flow responsible for sediment deposition within submarine fan environments (Middleton and Hampton, 1973; Shanmugam and Moiola, 1988).

The Kicking Bird core has a shale at the top of many of its numerous repeating fining upward packages that grade upwards from medium-grained sand at the coarsest, while the Grant Meek and Fillingim cores are almost entirely comprised of medium- to very-coarse-grained

sandstone and conglomerate with only minor amounts of shale. The observations that the more distal Kicking Bird core has a much lower sand-to-shale ratio than the Buffalo Wallow cores and that an overall decrease in grain size is observed going from the proximal wells to the more distal one is representative of the Kicking Bird's greater distance away from the Amarillo-Wichita Uplift source area. As sediment was transported away from the uplift, coarser material was deposited in proximal environments while increasingly finer sediment was carried out further into the basin and was deposited in more distal environments.

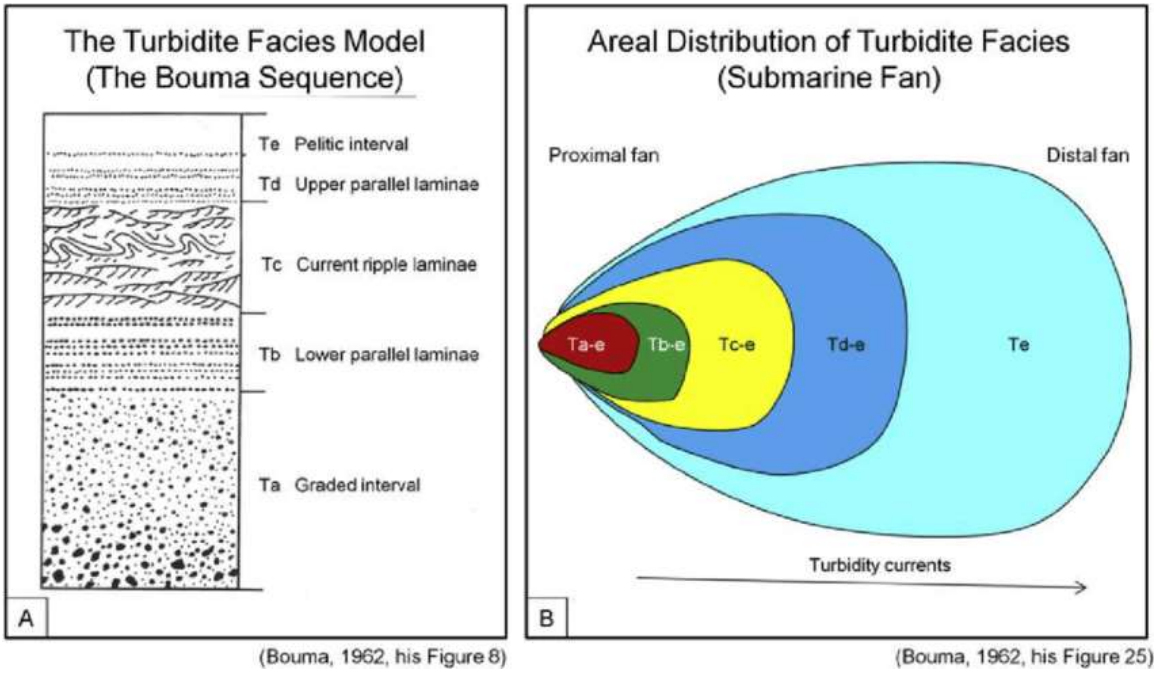

Figure 9.1: A. The turbidite facies model- known as the "Bouma Sequence"- with five internal divisions (Ta, Tb, Tc, Td, and Te); B. Areal distribution of turbidite facies in a submarine fan. (Shanmugam, 2016, after Bouma, 1962).

This system in which all three cores consist of repeated fining upward packages, both the sand-to-shale ratio and general grain size decrease downdip into the basin away from the source, and the cores depict sedimentary structures suggestive of deposition through sediment gravity flows is consistent with that of a sand-rich submarine fan (sometimes called a "turbidite system"), as classified by Bouma (2000) (**Figure 9.2**). While there are no unique sedimentary structures or lithofacies relations that are restricted to a submarine fan setting, the combination of these

characteristic features observed in core are convincing evidence when considered together. Sand-rich submarine fans represent the deposition of sand-rich sediment by sediment gravity flows into a basin and are characterized by sandy channels and fan lobes (Bouma, 2000). The areal distribution of turbidite facies within a submarine fan setting is summarized graphically in **Figure 9.1B**, which depicts the decrease in both velocity and grain size in the direction of the current as depositional energy is lost away from the source (Bouma, 1962; Shanmugam, 2016). New turbidity currents continue to deposit sand-rich sediment in prograding fans, developing a system of overlapping fan lobes. Such sand-rich submarine fan complexes are common along active margins such as this one and are characterized by the short continental transport of sediment across a narrow shelf before sediment is carried over the continental shelf break by sediment gravity flows, developing a series of prograding fans (Bouma, 2000). This short continental transport is exemplified by the lack of significant weathering of detrital feldspar and the high angularity of grains seen in all cores, but particularly the Grant Meek and Fillingim of Buffalo Wallow Field. Bioturbation and glauconite are both observed in all three cores, signifying that the sediment was deposited in marine oxic to suboxic conditions. Glauconite is an iron-rich clay mineral that is indicative of outer marine shelf or upper slope deposits, but can also be found in deeper water up to 2,000 m deep (Hesse and Schacht, 2011). Suboxic conditions are necessary for the later stages of glauconite formation when divalent iron is incorporated, as the divalent iron comes from the reduction of Fe-oxyhydroxides under suboxic conditions (Hesse and Schacht, 2011).

Further indicating that the Marmaton “D” Wash interval in all three cored wells was deposited in a submarine fan environment is their gamma-ray log signature across the Marmaton Granite Wash section. While the Marmaton “D” Wash interval consists of repeated fining upward packages of interbedded sandstone and shale at the core scale, all three cored wells contain coarsening upward packages within the Marmaton Granite Wash section on gamma-ray logs

(**Figures 7.1**, **7.2**, and **7.3**). The Marmaton Granite Wash of the most distal Kicking Bird consists almost entirely of these coarsening upward sequences, while the most proximal Grant Meek is largely composed of a "blocky" sandy interval with only minor amounts of shale. The Fillingim well that is at an intermediate location between them has more "blocky" sandy intervals than the Kicking Bird but more coarsening upward sequences than the Grant Meek. These coarsening-upward sequences that consist largely of turbidite sandstones are likely caused by the progradation of the submarine fan system into the basin, in a manner similar to that of a delta. This fan progradation and resultant vertical coarsening upward trend can be interpreted in terms of temporal and spatial variations in energy regime, as the vertical increase in grain size implies that there was an increase in depositional energy given that coarser grains require more energy to be carried out into the basin than finer grains do. The increase in depositional energy can likely be attributed to an increasingly wet climate, heightened basin-margin relief due to increased tectonic activity, or a combination of both. At the base of each coarsening-upward package is a shale with a relatively high gamma-ray reading, indicative of an interval where suspension settling dominated that marks the start of a new progradational sequence. The "blocky" sandy intervals seen in the Grant Meek and Fillingim wells consist of coarser material than the sediment seen in the Kicking Bird, and could likely be channel fill sandstone bodies or channelized turbidites.

Models of ancient submarine fan systems are typically divided into inner-, middle-, and lower fan facies, each of which display their own characteristic sand-body geometries, grain size distributions, and lithology assemblages. The classic model of an ancient submarine fan system developed by Mutti and Ricci Lucchi (1972) provides an easily understood framework for submarine fan deposition and is shown in **Figure 9.3**. The model divides a submarine fan into submarine canyon, inner-, middle-, and outer-fan facies that pass distally into basin-plain strata (Mutti and Ricci Lucchi, 1972). The inner fan is characterized by massive deposits of conglomerate and coarse sandstone within a major feeder canyon, the middle fan is represented

by a network of coalescing channelized sandstone bodies (and their associated overbank deposits) that form thinning and finning upward sequences, the outer fan begins beyond the limits of distributary channels and is recognized by sheet sands or prograding fan lobes that result in thickening and coarsening upward sequences, and the basin plain is typified by laterally extensive hemipelagic and pelagic mudstones (Mutti and Ricci Lucchi, 1972; Howell and Normark, 1982).

Based on the grain size variation, sedimentary structures, and well log signatures described in this section as well as the fan facies associations of the ancient submarine fan model developed by Mutti and Ricci Lucchi (1972), the Marmaton Granite Wash interval in the Kicking Bird well was determined to have been deposited in an outer submarine fan environment while the Grant Meek and Fillingim wells were likely deposited in a middle submarine fan environment. All core locations were interpreted to have been deposited in a deep marine setting, below wave base. The complete and partial Bouma Sequences that comprise the Marmaton "D" Wash interval in the Kicking Bird core, low sand-to-shale ratio, grain size that does not exceed medium-grained sand, and gamma-ray well log signature across the entire Marmaton Granite Wash section that depicts repeated coarsening upward packages at the log scale are all indicative of the progradational fan lobes that characterize the outer submarine fan environment (**Figure 9.3**). The conglomerate and coarse-grained sand, higher sand-to-shale ratio, and sedimentary structures indicative of both turbidity flows and fluidized flows seen in the Grant Meek and Fillingim Marmaton "D" Wash cores demonstrate that the wash represented in these cores were likely deposited in a middle submarine fan environment. Further, the "blocky" sandy intervals seen on the Grant Meek and Fillingim gamma-ray logs for the whole Marmaton Granite Wash section are likely sandy distributary channels found in a middle submarine fan environment.

All three Marmaton Granite Wash interval thickness maps (Marmaton "C", "D", and "E" Wash) created in this study clearly depict lobate, fan-shaped deposits across the western study area that abut the Amarillo-Wichita Uplift and trend northeast (**Figures 5.1**, **5.2**, and **5.3**).

Thickness values are highest along the central axes of these lobate fan bodies which run perpendicular to the uplift, demonstrating that the uplift to the southwest is the primary source of sediment. Immediately adjacent to the uplift, the lobate fan bodies are distinctly separated from each other by interlobe areas (where the sediment is much thinner) and appear to increasingly coalesce to the northeast in the lower fan areas. This increase in overlap of multiple different fan lobes away from the source indicates a point-source submarine fan system with multiple point sources within the uplift that channeled detritus through submarine canyons and distributary channels across a narrow shelf and into the basin.

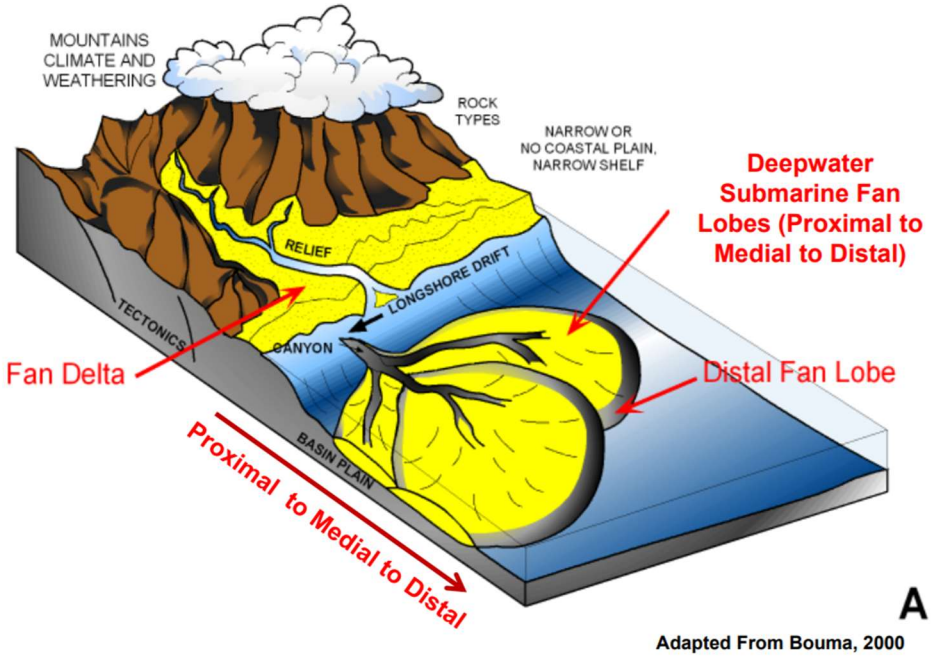

Figure 9.2: Schematic depositional model for a coarse-grained, sand-rich submarine fan system (Mitchell, 2011, after Bouma, 2000).

The thickness of all three wash intervals generally decreases away from the uplift, indicating a decrease in depositional energy as sediment is carried across the study area. This thickening towards the uplift in the south and southwest is likely reflective of rapid subsidence and/or increased uplift during this time. A sudden increase in thickness contour density indicative of a narrow shelf break is evident in western Roger Mills County, Oklahoma on the Marmaton

"C" (**Figure 5.1**) and Marmaton "D" Wash intervals thickness maps (**Figure 5.2**). The Marmaton "E" Wash thickness map does not extend this far northeast (**Figure 5.3**). The wash intervals thin rapidly along this shelf break and then remain fairly consistent in thickness off to the northeastern extent of the study area. It is probable that this narrow shelf break formed as a result of both the rapid subsidence of the deep Anadarko Basin to the southwest and the deposition of sediment coming from the greater Appalachian orogen to the east and northeast, which has recently been shown through detrital zircon geochronology to have been the primary sediment source for the Anadarko Basin during the Middle Pennsylvanian (Tunin, 2020; Kushner et al., 2022).

In addition to the multiple point sources with various canyons and channels that cyclically transported and deposited overlapping fans of sediment onto the slope or ocean floor, preexisting topographic variations contributed to the convoluted pattern of avulsing washes in the Marmaton Granite Wash submarine fan complex. As sediment was carried into the basin, topographically low areas became local depocenters with thicker wash accumulations as the sediment filled in these low spots first. Following the infill of low areas, sediment accumulation became more widespread and topographic highs became areas of thinner wash accumulation. Depositional trends of sediment transport away from the sediment sources in the uplift source area for each mapped interval are shown in **Figures 9.4**, **9.5**, and **9.6**. The depositional trends are fairly consistent temporally from the oldest Marmaton "E" Wash to the youngest Marmaton "C" Wash. The net sandstone depositional trends within Buffalo Wallow Field in Hemphill County, Texas and the surrounding area are shown in **Figure 9.7**, which depict a single sediment source for the local area to the southwest, consistent with the sediment being sourced by the Amarillo-Wichita Uplift. These depositional trends indicate sediment was carried along a central trend going to the northeast before branching off to the northwest and southeast, likely due to depositionally-induced topography on the basin floor. Net sandstone thickness decreases along

these depositional trends away from the sediment source in the southwest due to the loss in depositional energy as sediment was carried away from the source.

The submarine fan depositional environment described here for the Marmaton Granite Wash and the fan deltas that are often considered to be the depositional setting of the Early Pennsylvanian washes of the Anadarko Basin are similar in source area and morphology, but are very different in regards to length of sediment transport and depositional features. Submarine fan deposits are considered to have been deposited by sediment gravity flows in the deep marine environment beyond the continental shelf (Shanmugam and Moiola, 1988). Fan deltas, on the other hand, are considered to be alluvial fans that prograde into a body of water from an adjacent uplift and develop in shallow water environments, such as on the continental shelf (Alberta, 1987; McPherson, Shanmugam, and Moiola, 1987; Shanmugam and Moiloa, 1988). The Marmaton Granite Wash of the Middle Pennsylvanian was deposited during a period of marine transgression and continued basin subsidence, so it is logical that the same area that saw Early Pennsylvanian fan delta deposition would be marked by submarine fan deposition later on in the Middle Pennsylvanian.

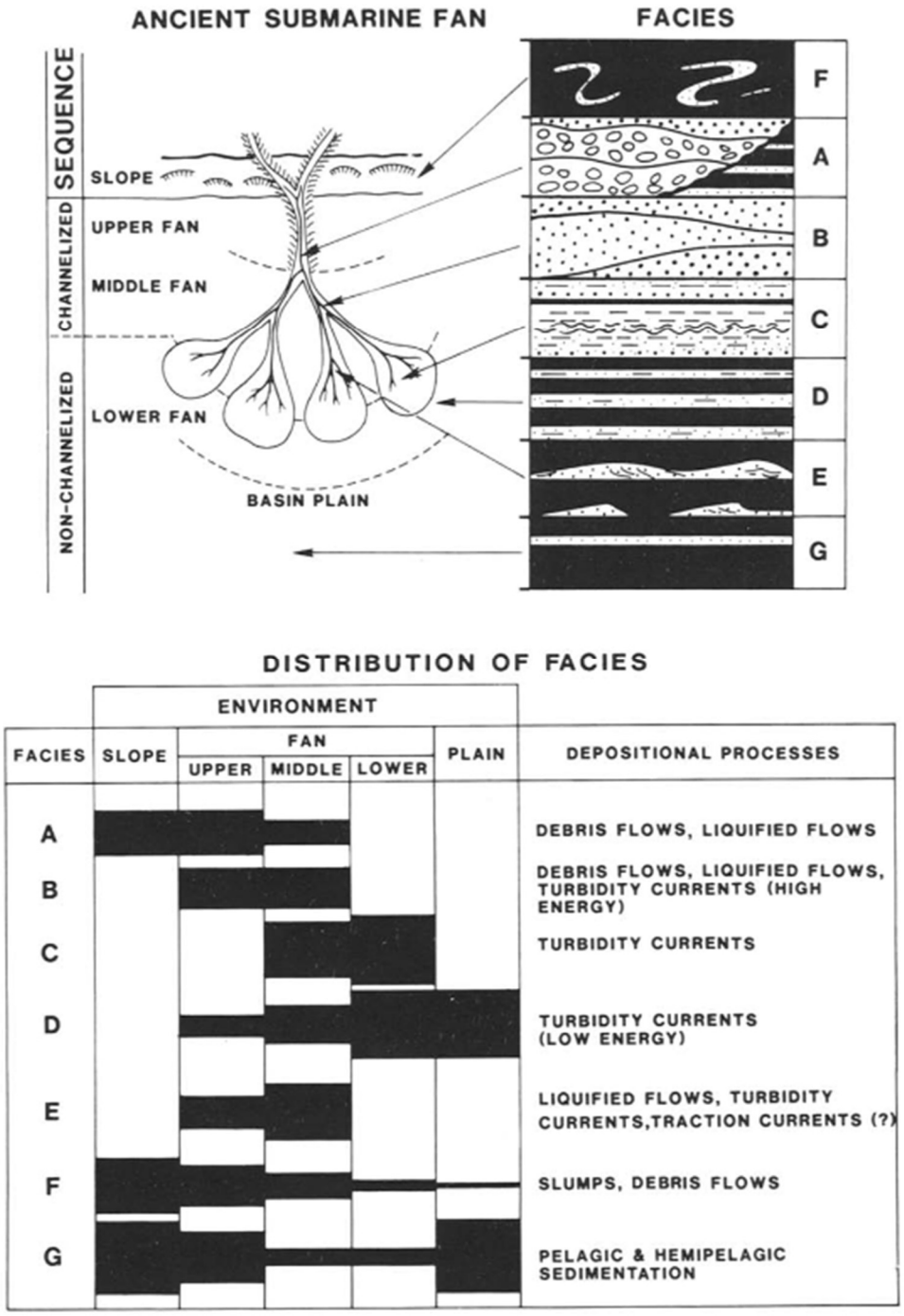

Figure 9.3: Ancient submarine fan components and the corresponding distribution of characteristic facies observed in each part of the fan. A major submarine canyon is seen in the upper fan, distributary channels are seen in the middle fan, and non-channelized lobes are seen in the lower fan (Shanmugam and Moiola, 1988).

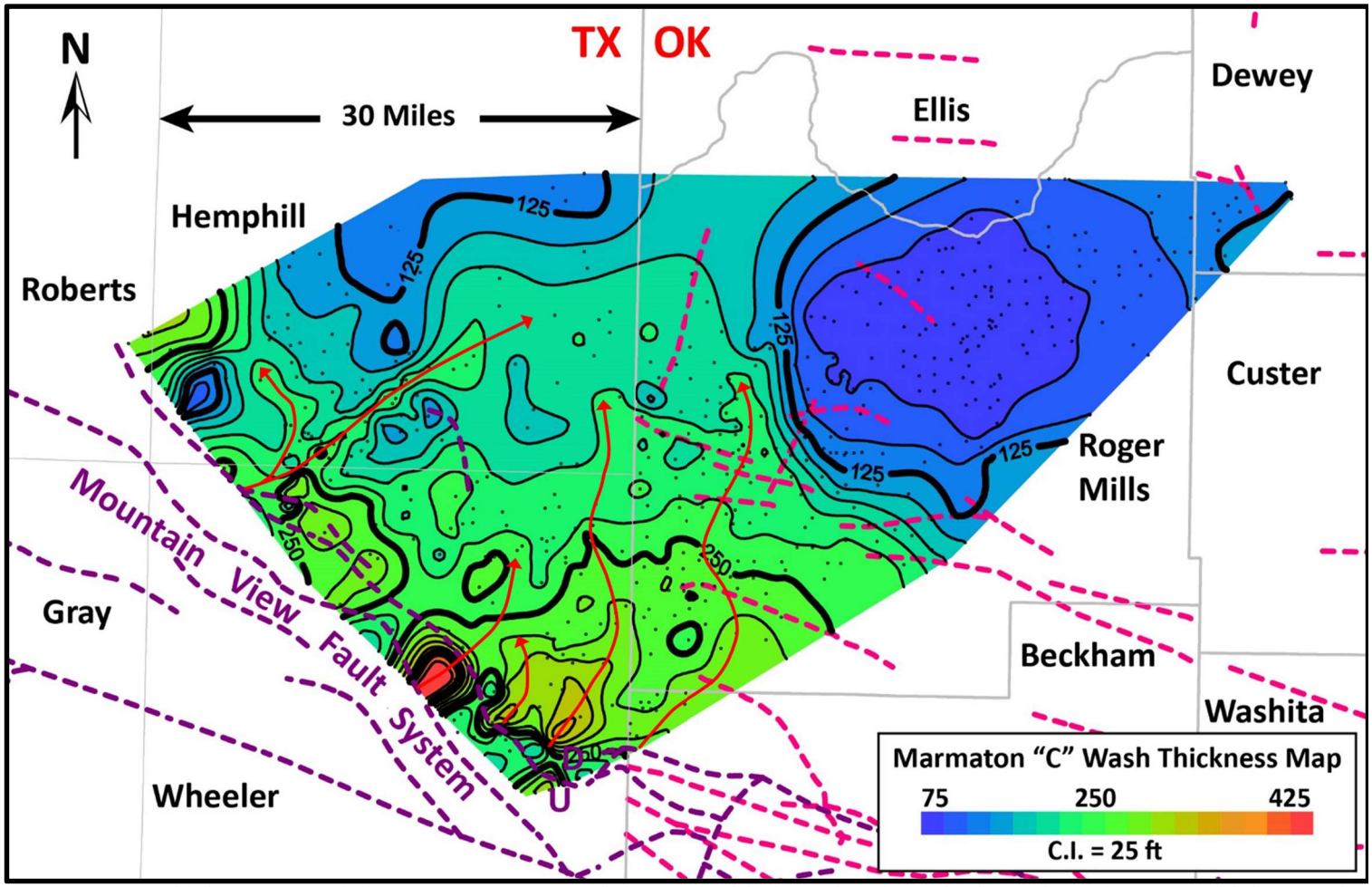

Figure 9.4: Thickness map of the Marmaton "C" Wash interval with depostional trends shown by red arrows. Thicker trends are oriented southwest to northeast and north-northeast supporting interpretation of expected southerly source area. Region of increased thickness contour density and rapid thinning is interpreted as the shelf to basin break. Contour interval is 25 feet. Thickness values are in feet. Pink fault lines are from Oklahoma Geological Survey (OGS) (Marsh and Holland, 2016) and purple fault lines are from the Bureau of Economic Geology (BEG) (Ewing, 1990).

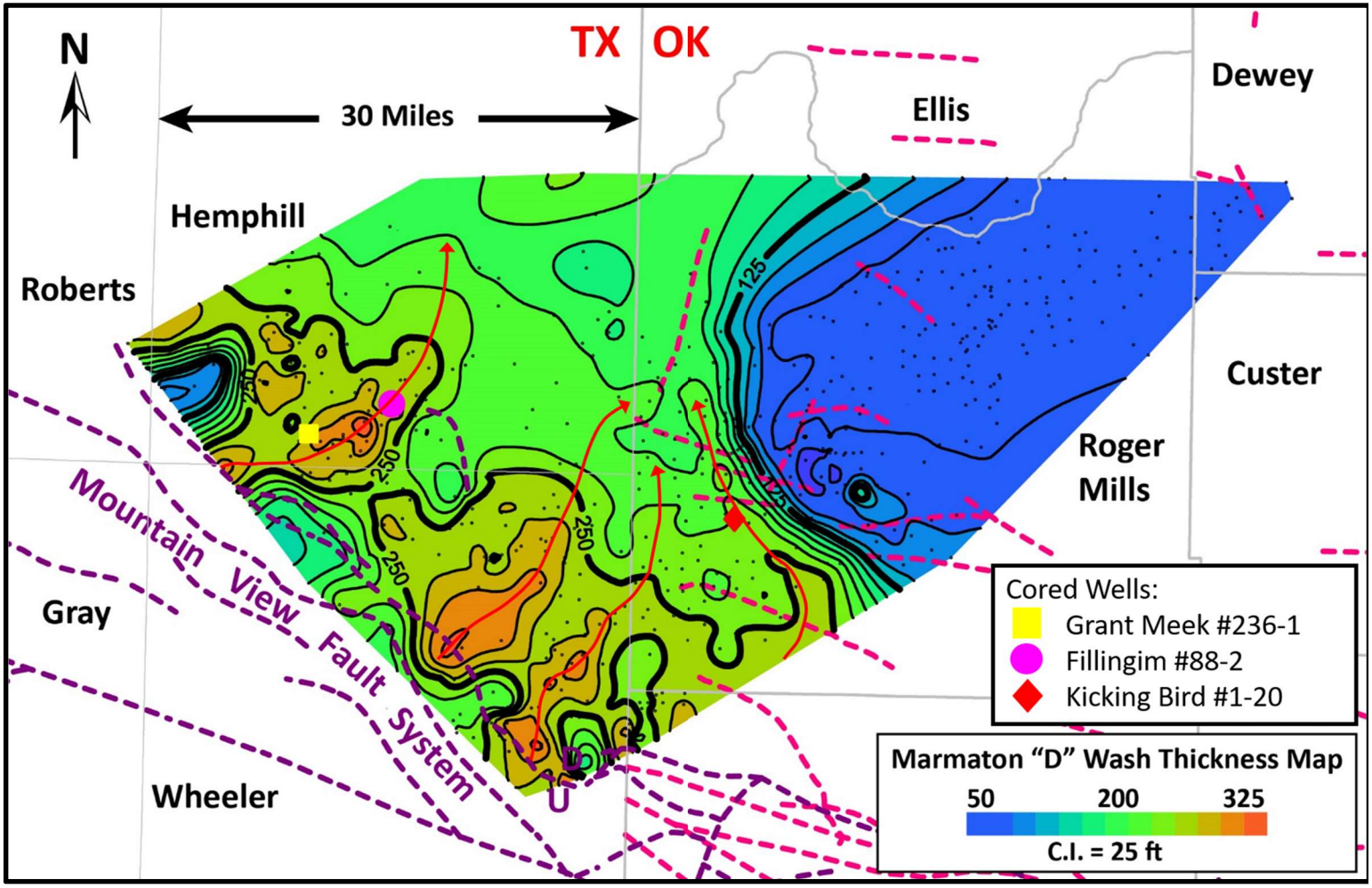

Figure 9.5: Thickness map of the Marmaton "D" Wash interval with depostional trends shown by red arrows. Thicker trends are oriented southwest to northeast. Region of increased thinning is interpreted as the shelf to basin break. Contour interval is 25 feet. Thickness values are in feet. Pink fault lines are from Oklahoma Geological Survey (OGS) (Marsh and Holland, 2016) and purple fault lines are from the Bureau of Economic Geology (BEG) (Ewing, 1990).

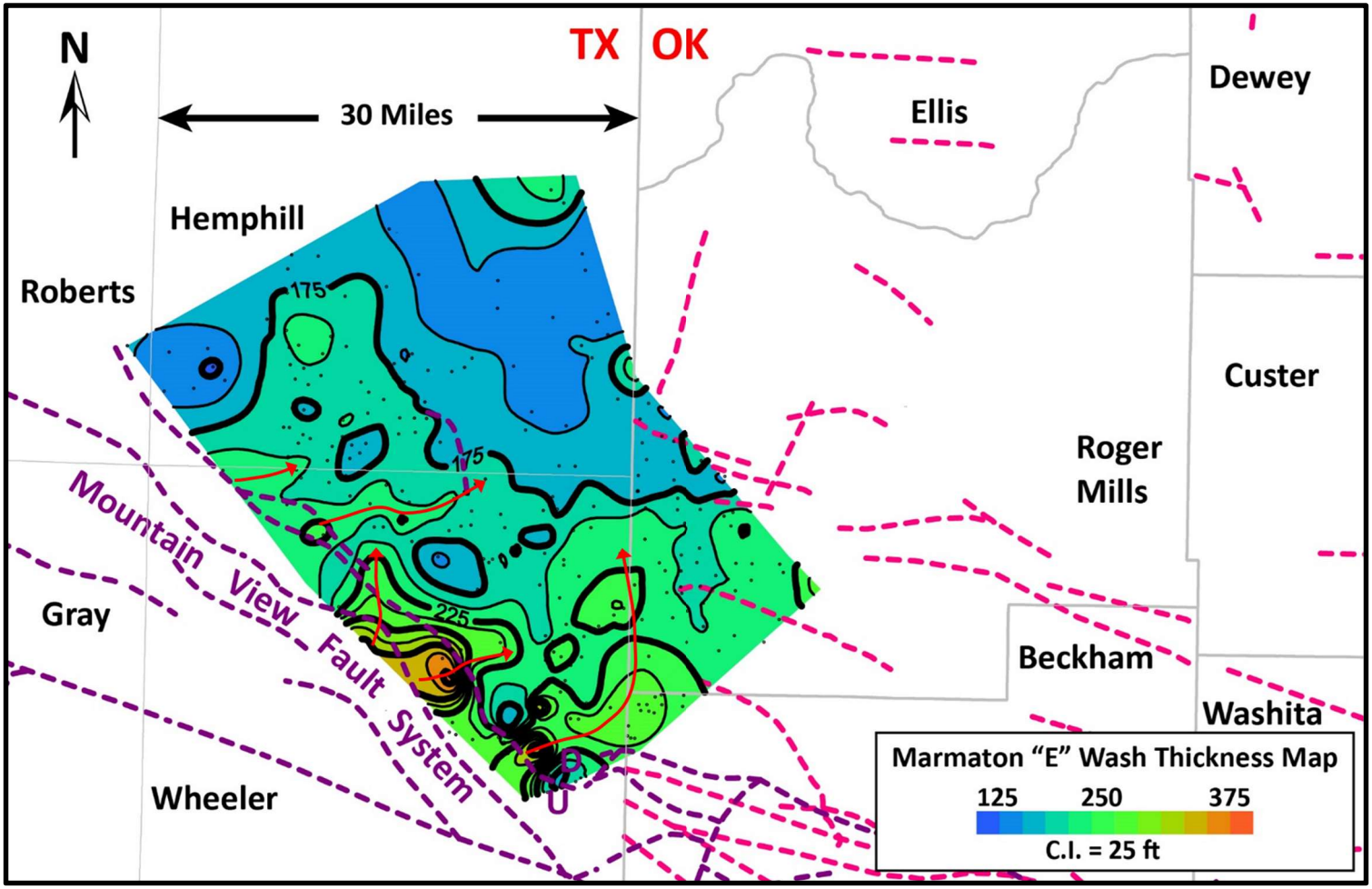

Figure 9.6: Thickness map of the Marmaton "E" Wash interval with depostional trends shown by red arrows. Thicker trends are oriented west-southwest to east-northeast, supporting interpretation of expected southerly source area. Northeastern map extent limited by mappable extent of Fourth Marmaton Shale. Contour interval is 25 feet. Thickness values are in feet. Pink fault lines are from Oklahoma Geological Survey (OGS) (Marsh and Holland, 2016) and purple fault lines are from the Bureau of Economic Geology (BEG) (Ewing, 1990).

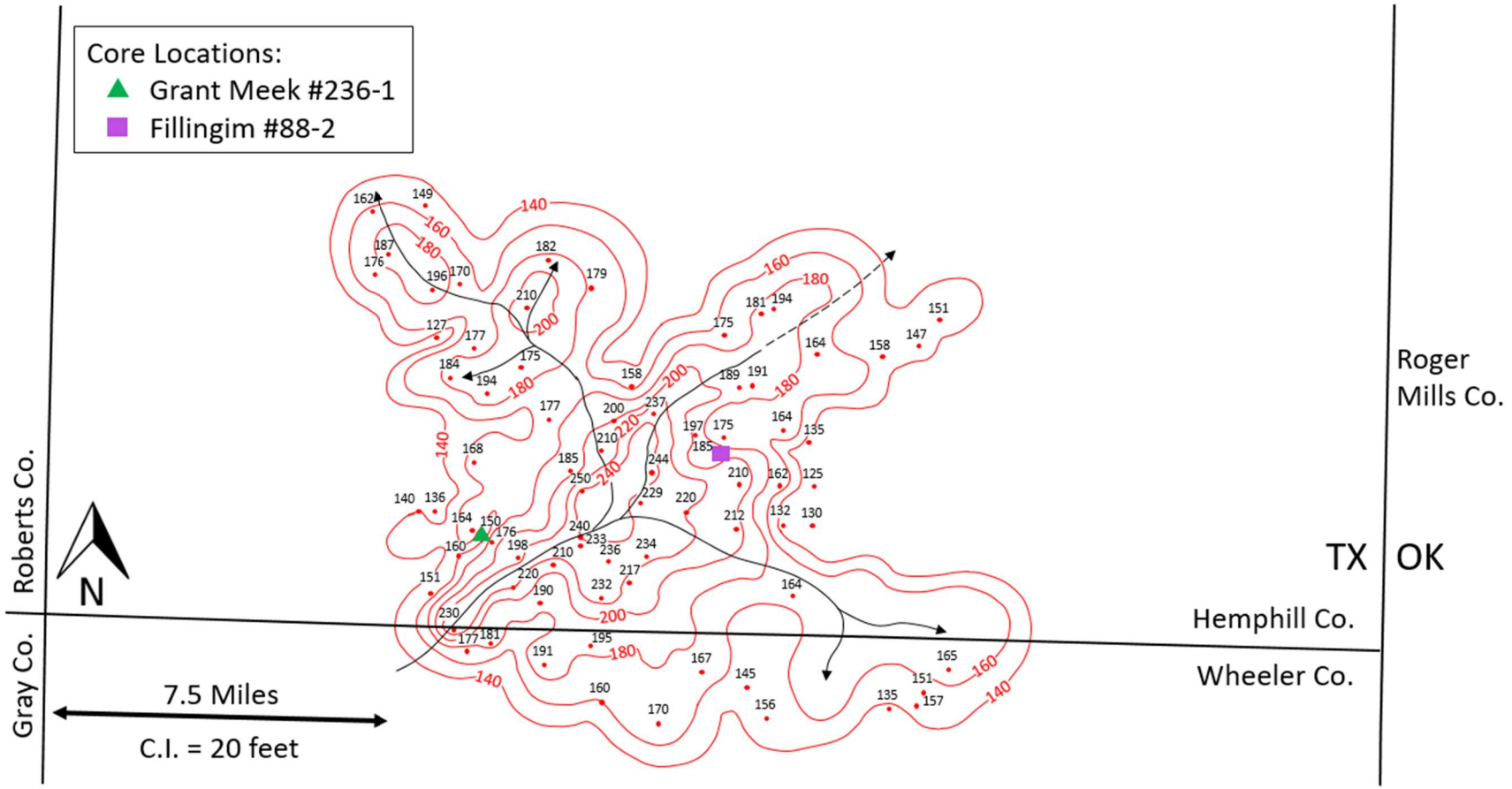

Figure 9.7: Net sandstone thickness map of Buffalo Wallow Field in Hemphill County, Texas and the surrounding area. Depositional trends are shown with black arrows. Contour interval is 20 feet. All thicknesses are in feet.

9.2 Depositional Model

Potassium (K), Thorium (Th), and uranium (U) are the main isotopes responsible for the natural radiation of shales, and are therefore primary influencers on the spectral gamma-ray log shown in **Figure 6.9**. K is found in silicate minerals (namely K-feldspars), clay minerals, and salts, while Th is commonly adsorbed onto clays. Both K and Th are common in terrestrial sediments. U, on the other hand, is not typically associated with clay minerals but is instead associated with the organic matter that it commonly binds to in marine settings. As the spectral gamma-ray log for the Marmaton "D" Wash interval of the Kicking Bird core is extremely consistent with both the K and Th concentration curves (and fairly consistent with Al and Ti, other indicators of detrital input) but only marginally consistent with the U concentration curve, it can be concluded that aluminosilicate clays and the potassium-rich granitic wash detritus are the greatest contributors to formation radioactivity. Further, the lack of a clear trend between U content and lithology within the Marmaton "D" Wash interval of the Kicking Bird core illustrates that the U within the interbedded shales are of similar origin to the sandstone wash material, which have been shown to consist primarily of detritus shed from the Amarillo-Wichita Uplift (**Figure 6.8**). Lastly, the Th/U ratio, which is commonly used to discriminate between terrestrial and marine settings, is less than three across the Kicking Bird Marmaton "D" Wash (**Figure 6.9**). A Th/U ratio in sedimentary rocks less than seven is often considered to indicate oxidized continental deposits rather than marine deposits (Adams and Weaver, 1958). All of this evidence, when examined together, indicates that the uranium-poor, potassium-rich interbedded shales within the Marmaton "D" Wash most likely consists of terrestrially-sourced organic matter.

The Marmaton hot shales (>150 API) that divide the individual Marmaton wash packages, however, are widely extensive across the basin and have been considered to represent marine flooding surfaces and periods of widespread transgression and inundation (Mitchell, 2011; Parks, 2011). The Late Paleozoic paleoclimate was dominated by glaciation in Gondwana, and

these hot, transgressive shales can likely be tied to the periodic melting of Gondwanan ice sheets causing eustatic sea level to rise (Montañez and Poulsen, 2013). A spectral gamma-ray log or XRF data for a Marmaton hot shale would be ideal to fully analyze the composition and thus origin of the hot shales, but no such core was available for this study. In cross section, the Marmaton hot shale markers are easily distinguished from the sandstone wash intervals adjacent to the mountain front in the southwest study area (central Wheeler County, Texas), but the stratigraphically lowest (oldest) hot shale markers (the Fourth Marmaton Shale and the underlying Upper Skinner Shale of the Skinner Group below) become difficult to identify in southwestern Roger Mills County, Oklahoma where the Marmaton section is the deepest (**Figure 4.2** and **4.7**). Along the interpreted narrow shelf break in western Roger Mills County, the wash intervals thin rapidly and the well log signatures become so homogenous that it is practically impossible to distinguish them from the surrounding sandstone wash material, as illustrated by the northwestern extent of the Fourth Marmaton Shale in **Figure 4.2**. Just to the northeast of this shelf break, the structure becomes less steep and the hot shales become easily distinguishable again.

Several factors could contribute to the seemingly "disappearing" hot shales and the homogenization of the well log signature in the deeper part of the study area, which is especially severe along the narrow shelf break. The hot shales are likely less developed in this deeper area of the basin due to lesser amounts of organic matter preservation when compared to the shallower area in the southwest that is adjacent to the rising Amarillo-Wichita Uplift and the shallow shelf area to the northeast (**Figure 4.2** and **4.4**). While the exact nature of the variations in organic matter preservation across the study area is beyond the scope of this study, multiple working hypotheses regarding controls on shale development are proposed here and summarized graphically in **Figure 9.8**. As the hot shales formed during transgressive periods, the shallow areas to the far southwest and northeast were likely inundated, creating shallow seas with

stratified water and poor circulation of bottom waters. Circulation would have likely been greater in the deeper part of the basin in southwestern Roger Mills County, where density-driven deep water currents would have prevented the preservation of organic matter. These deep water currents would have caused upwelling of nutrient-rich waters to the shallower areas, creating an oxygen minimum zone (OMZ) on both the southwestern shallow area adjacent to the uplift and the narrow shelf to the northeast that would have been ideal for organic matter preservation. Along the narrow shelf break to the northeast where shale development was the worst, it is possible that currents such as contour currents, eddies, or even turbidity currents created even better circulation than in the deep basin, generating an environment with sufficient oxygen to be unfavorable for organic matter preservation. This same oxygenated environment would be unfavorable for the accumulation of U in bottom water and adjacent sediments.

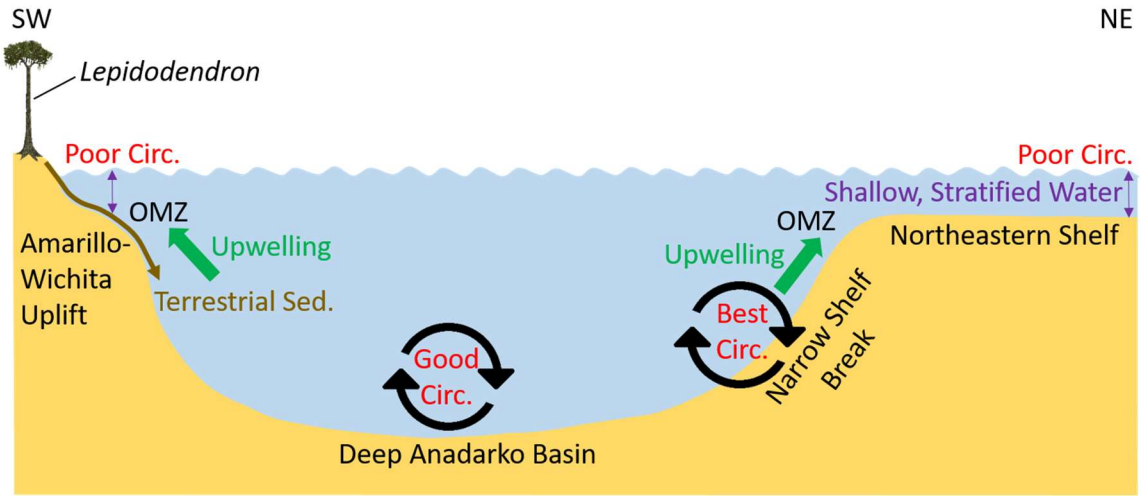

Figure 9.8: Schematic depositional model for the Marmaton hot shales, depicting hypothesized controls on organic matter preservation and subsequent shale formation. Circulation is greatest along the narrow shelf break, likely due to increased water depth and greater current activity. Oxygen minimum zones (OMZ) are created as a result of density-driven deep water currents bringing nutrient-rich water to shallower portions of the basin. Density flows or mass wasting events could have obliterated the hot shale physically and/or caused currents that prevented stratification. Lepidodendron, a primitive vascular plant common to the region throughout the Carboniferous, is shown to represent terrestrial sediment source.

9.3 Variations in Porosity Controls from Proximal to Distal Fan Environments

Thin section samples from the Marmaton "D" Wash interval of the two wells in Buffalo Wallow Field in Hemphill County, Texas appear to contain the same dominant detrital grains as those from the same interval in the Kicking Bird well of Roger Mills County, Oklahoma: quartz, plagioclase, potassium feldspar, and lithic rock fragments with minor amounts of calcite, pyrite, and clay minerals. This coordinating detrital grain composition substantiates that the samples are all of the same granitic provenance. While all three cored intervals display the same framework grain composition, samples from the Buffalo Wallow wells have a higher combined percentage of quartz and feldspars on average (**Tables 8.1** and **8.2**). This observation, along with the larger grain size and higher angularity of Buffalo Wallow samples observed in thin section, points to the Buffalo Wallow being in a more proximal environment than the Kicking Bird. As the Buffalo Wallow samples display more large, discrete grains of quartz and feldspar, it can be hypothesized that these samples were weathered from coarser grained granite than the Kicking Bird samples, where many grains are likely weathered from microperthite and granophyre.

Thin sections from both Buffalo Wallow wells appear to be much cleaner in regards to detrital clay matrix than those from the Kicking Bird (**Figure 8.7**). This is consistent with the Kicking Bird being more distal from the Amarillo-Wichita Uplift source area than the Buffalo Wallow Field wells, as this finer-grained detrital material was carried to the more distal lower fan environments before dropping out of suspension. As the detrital matrix is composed largely of illite and other metastable clays, the matrix in the Buffalo Wallow dissolved at a higher rate relative to the framework grains and is largely dissolved in many areas. Detrital clay matrix is so prevalent in the Kicking Bird, however, that it likely blocked pore throats and coated the framework grains, destroying intergranular primary porosity and severely hindering fluid movement. It is for this reason that framework grains in the Kicking Bird samples appear largely unaltered. In contrast, partially dissolved lithic rock fragments are prevalent in the Buffalo

Wallow samples, apparently by selective dissolution of alkali feldspar and other metastable rock constituents. This dissolution is likely caused by the preserved interganular primary porosity (due to lack of detrital clay matrix) allowing corrosive fluids to come into contact with and corrode the grains through the dissolution of metastable rock constituents. Al-Shaieb and Walker (1986) determined that the development of secondary porosity in the Early Pennsylvanian Morrow sandstones of the Anadarko Basin was largely dependent on the hydrogen (H^+) ions available for reaction within leaching fluids produced from the maturation of organic matter in Morrow shales. Al-Shaieb and Walker (1986) found that these H^+ ions may be sourced by organic acids, carbonic acid (a result of decarboxylation of organic acids), and/or hydrogen sulfide (H_2S, formed by the decomposition of sulfur-bearing organic matter at relatively high temperatures) (Al-Shaieb and Walker, 1986). As the early Pennsylvanian Morrow sandstones were deposited in fan deltas after being eroded off of the Amarillo-Wichita Uplift in a similar manner to the Marmaton Granite Wash during an earlier period of Anadarko Basin subsidence, it's probable that these controls on secondary porosity evolution outlined by Al-Shaieb and Walker (1986) are also applicable to the Marmaton washes.

The preserved primarily porosity in the Buffalo Wallow samples allowed for better permeability and fluid flow which resulted in precipitation of more authigenic clays in pores. As a result, more authigenic clay is observed in SEM images from the Buffalo Wallow samples compared to those from the Kicking Bird core. Authigenic quartz overgrowths are not common in any sample from any core, but this is expected as Dutton and Land (1985) report in their study of Pennsylvanian arkosic washes in Mobeetie Field (northwestern Wheeler County, Texas) that an abundance of preexisting chlorite and/or calcite cement coat the detrital grains and cover the nucleation sites, significantly limiting the precipitation of authigenic quartz in Granite Wash sandstones. Calcite cement is more readily seen in thin section in the Kicking Bird filling fractures, as the high volume of detrital matrix and low permeability caused authigenic calcite to

be concentrated along fractures. For a detailed explanation of the diagenetic history of the Marmaton Granite Wash and a visual representation of the paragenetic sequence of diagenetic events, see Section 8.5 and **Figure 8.8**, respectively.

9.4 Porosity Interpretation

Porosity in the Marmaton "D" Wash interval of the Kicking Bird core was too low to register on the teaching grade Core Lab PORG-200 helium gas porosimeter available for this study, and averaged 3.0% but commonly did not exceed 1.5% porosity in the core analysis data provided by Laredo Petroleum. The Fillingim core, which is located approximately 30 miles to the west of the Kicking Bird and more proximal to the Amarillo-Wichita Uplift source area, averaged 5.73% porosity across the cored Marmaton "D" Wash interval in the core plug analysis performed by Parks (2011) (**Table 6.2**). In thin section, no porosity was evident in the Kicking Bird core, but point counts for the Fillingim and Grant Meek averaged 0.81% and 3.54% porosity, respectively (**Table 8.1** and **Table 8.2**). From this core analysis and thin section point count data, it is inferred that porosity in the Buffalo Wallow cores is at least 1.5 times greater than that of the Kicking Bird, but is more likely 2 to more than 3 times greater. This poor porosity in the more distal Kicking Bird core can largely be attributed to the high volume of detrital clay matrix destroying primary intergranular porosity that coated the framework grains and prevented corrosive fluids from contacting them and generating secondary porosity.

Through well log analysis, it was determined that the whole Marmaton Granite Wash interval in the Kicking Bird has a true average density-derived porosity of 3.2%, while the Fillingim averaged 10.97% (see Section 7.4 for a detailed explanation of the well log porosity analysis performed in this study). From this, it can be concluded that the density porosity logs, when calibrated with a formation matrix density that is representative of lithology, show that the Marmaton Granite Wash interval of the Fillingim in Buffalo Wallow Field in Hemphill County,

Texas has a density-derived porosity value 3.43 times that of the Kicking Bird in Roger Mills County, Oklahoma. The grain density calculations performed on both the Kicking Bird and the Fillingim determined lower porosity values than were shown on the density porosity logs. This demonstrates that the logs as received (A.R.) are optimistic and that the true porosity is much lower, likely indicating that the reservoir quality is poorer than is indicated on the logs. This illustrates that the choice of matrix values greatly affects the calculated porosity value, and can result in overly optimistic evaluations of production potential. Identifying lithology is essential for choosing matrix values or reading porosity on logs as corrections may be needed. Besides detrital grain mineralogy, the presence of carbonate cements, heavy minerals like pyrite, and clay minerals can cause the average matrix density to vary and impact calculated porosity values.

CHAPTER X

CONCLUSIONS

This study examined the Marmaton Granite Wash in the Anadarko Basin to determine controls on porosity evolution. Based on the integration of petrologic, core, mapping, and wireline-log derived data, the following conclusions are proposed:

1. Sedimentary and biogenic features in core, characteristics of rock fabric including variations in grain size and composition in thin section, and wireline well log signatures of the three Marmaton "D" Wash interval in the cored wells provide evidence supporting the interpretation that the wash was deposited below wave base in a marine, sand-rich submarine fan depositional environment. Coarser-grained (primarily coarse-grained sandstone to pebble-conglomerate) wash in the Grant Meek and Fillingim wells of Buffalo Wallow Field in Hemphill County, Texas are characterized by fining-upward sequences and abundant fluidized flow features that are indicative of a middle submarine fan environment with sandy distributary channels. This interpretation is further justified by the "blocky" sandy intervals seen on gamma-ray logs. The finer-grained (medium-grained sand at largest) Kicking Bird well in Roger Mills County, Oklahoma is interpreted to have been deposited in an outer submarine fan environment where turbidity flows dominate sediment deposition, beyond the extent of distributary channels and where prograding fan lobes and sheet sands dominate.

2. The detrital framework grains of the Marmaton Granite Wash are primarily quartz, feldspar, and granitic rock fragments microperthite and granophyre, which is consistent with a granitic basement source on the Amarillo-Wichita Uplift. The Marmaton "D" Wash in the more proximal Grant Meek and Fillingim wells in the Buffalo Wallow Field in Hemphill County, Texas is coarser-grained than the more distal wash in the Kicking Bird well in Roger Mills County, Oklahoma. This more distal depositional environment in the Kicking Bird well is further indicated by the prevalence of detrital clay-matrix-rich sandstone and abundant interbedded shale.

3. Depositional patterns established by mapping the thickness of the Marmaton Granite Wash packages depict lobate, fan-shaped deposits that prograded northward away from the Amarillo-Wichita Uplift. Fan lobes are separated from one another closer to the uplift, but coalesce to the northeast, indicating a point-source submarine fan system with multiple separate point source areas along the uplift. These sources fed distributary channel-submarine canyon systems that carried detritus across a narrow shelf and into the basin.

4. The Marmaton Granite Wash can be divided into distinct, mappable wash intervals and correlated across the southwestern Anadarko Basin using cyclic radioactive (hot) shale markers associated with periods of rapid transgression and flooding. Regional correlation demonstrates that the four Marmaton-age hot shales of the deep Anadarko Basin are correlative to black shales of the Marmaton and Cabaniss (Upper "Cherokee") Group on the Anadarko Shelf to the northeast. These hot shales are not evident along the shelf break in southwestern Roger Mills County, Oklahoma, where it is proposed that increased water depth and ocean circulation/currents hindered preservation of organic matter and uranium.

5. Porosity in the Marmaton "D" Wash interval of the Buffalo Wallow wells is mostly secondary and formed by the dissolution of metastable minerals, primarily detrital grains of potassium feldspar and the potassium feldspar within granitic rock fragments. No porosity is

visible in thin sections of wash from the Kicking Bird, but isolated intergranular pores less than 10 μm and commonly less than 5 μm were visible in SEM at high magnification. Authigenic clay minerals appear to partially obstruct intergranular pores, with pore-lining and pore-bridging illite common in both Buffalo Wallow cores and the Kicking Bird wash. However, abundant detrital clay deposited simultaneously with sand in the Kicking Bird wash protected the detrital framework grains from dissolution, thus preventing the generation of secondary porosity essential to reservoir development and economic production of oil and gas from the Granite Wash in the deep Anadarko Basin.

6. The location of the Laredo Kicking Bird well in Roger Mills County, Oklahoma is too distal from the Amarillo-Wichita source area to possess ideal reservoir properties. Porosity in the samples from wells in Buffalo Wallow Field in Hemphill County, Texas is at a minimum 1.5 times, and likely 2 to 3 times higher than porosity in samples from the Laredo Kicking Bird well in Roger Mills County, Oklahoma. Wireline log density porosity is optimistic for the Marmaton "D" Wash in both Buffalo Wallow Field and the Kicking Bird area and should be corrected for the proper grain density to properly assess porosity in wells without core.

REFERENCES

Adams, J. A. S. and C. E. Weaver, 1958, Thorium-to-uranium ratios as indications of sedimentary processes: example of concept of geochemical facies: American Association of Petroleum Geologists Bulletin, v. 42, no. 2, p. 387-430.

Asquith, G. B., C. R. Gibson, D. Krygowski, S. Henderson, and N. F. Hurley, 2004, Basic well log analysis: American Association of Petroleum Geologists, 244 p.

Alberta, P. L., 1987, Depositional facies analysis and porosity development of the (Pennsylvanian) Upper Morrow chert conglomerate "Puryear" member, Roger Mills and Beckham Counties, Oklahoma: Master's thesis, Oklahoma State University, Stillwater, Oklahoma, 135 p.

Al-Shaieb, Z., and P. Walker, 1986, Evolution of secondary porosity in Pennsylvanian Morrow sandstones, Anadarko Basin, Oklahoma, *in* Spencer, C.W., and R.F. Mast, eds., Geology of tight gas reservoirs: American Association of Petroleum Geologists Studies in Geology, no. 24, p. 45-67.

Anderson, C. J., 1992, Distribution of submarine fan facies of the Upper Red Fork interval in the Anadarko Basin, Western Oklahoma: Master's thesis, Oklahoma State University, Stillwater, Oklahoma, 301 p.

Bahadori, A., 2014, Natural gas processing: technology and engineering design: Gulf Professional Publishing, 896 p.

Ball, M. M., M. E. Henry, and S. E. Frezon, 1991, Petroleum geology of the Anadarko Basin region, province (115), Kansas, Oklahoma, and Texas: U.S. Geological Survey Open File Report 88-450W, 36 p.

Bouma, A. H., 1962, Sedimentology of some flysch deposits: a graphical approach to facies interpretation: Elsevier Publishing, p. 168.

Bouma, A. H., 2000, Fine-grained, mud-rich turbidite systems: model and comparison with coarse-grained, sand-rich systems, *in* A.H. Bouma and C.G. Stone, eds., Fine-grained turbidite systems, American Association of Petroleum Geologists Memoir 72/SEPM Special Publication 68, p. 9–20.

Boyd, D. T., 2008, Stratigraphic guide to Oklahoma oil and gas reservoirs: Oklahoma Geological Survey Special Publication 2008-1, 1 p.

Brown Jr., L. F., 1979, Deltaic sandstone facies of the Mid-Continent, *in* Hyne, N. J., ed., Pennsylvanian sandstones of the Mid-Continent: Tulsa, Oklahoma, Tulsa Geological Society, vol. 1, p. 35-63.

Brueseke, M. E., C. L. Bulen, and S. A. Mertzman, 2014, Major- and trace-element constraints on cambrian basalt volcanics in the Southern Oklahoma Aulacogen from well cuttings in the Arbuckle Mountains region, Oklahoma (U.S.A.), *in* Suneson, N. H., ed., Igneous and tectonic history of the Southern Oklahoma Aulacogen, Oklahoma Geological Survey Guidebook 38, p. 95–104.

Candelaria, M. P., and C. R. Handford, 1995, Sequence stratigraphic model for Simpson Group of the southern mid-continent, *in* Hyne, N. J., ed., Sequence stratigraphy of the mid-continent: Tulsa Geological Society Special Publication, no. 4, p. 319-332.

Carter, L. S., S. A. Kelley, D. D. Blackwell, and N. D. Naeser, 1998, Heat flow and thermal history of the Anadarko Basin, Oklahoma: American Association of Petroleum Geologist Bulletin, v. 82, no. 2, p. 291-316.

Collinson, J. D., N. P. Mountney, and D. B. Thompson, 2006, Sedimentary structures: Terra Publishing, Harpenden, England, 292 p.

Dutton, S.P., 1982, Pennsylvanian fan-delta and carbonate deposition, Mobeetie Field, Texas Panhandle: American Association of Petroleum Geologists Bulletin, v. 66, no. 4, p. 389-407.

Dutton, S. P., 1984, Fan-delta Granite Wash of the Texas Panhandle: Oklahoma City Geological Society Short Course, p. 1–44.

Dutton, S. P., and L. S. Land, 1985, Meteoric burial diagenesis of Pennsylvanian arkosic sandstones, southwestern Anadarko Basin, Texas: American Association of Petroleum Geologists Bulletin, v. 69, p. 22-38.

Edwards, A. R., 1958, Facies changes in Pennsylvanian rocks along the north flank of the Wichita Mountains: The Panhandle Geonews, v. 6, no. 2, p. 5-18.

Evans, J. L., 1979, Major structural features of the Anadarko Basin, *in* Hyne, N. J., ed., Pennsylvanian sandstones of the mid-continent: Tulsa Geological Society Special Publication, no. 1, p. 97-113.

Ewing, T. E., 1990, Tectonic map of Texas: Bureau of Economic Geology, The University of Texas at Austin, Austin, Texas.

Feinstein, S., 1981, Subsidence and thermal history of Southern Oklahoma Aulacogen: implications for petroleum exploration: American Association of Petroleum Geologists Bulletin, v. 65, no. 12, p. 2521-2533.

Flawn, P. T., 1956, Basement rocks of Texas and southeast New Mexico: University of Texas Bureau of Economic Geology Publication 5605, 211 p.

Gaswirth, S. B. and D. K. Higley, 2014, Geologic assessment of undiscovered oil and gas resources in the Cambrian– Devonian stratigraphy of the Anadarko Basin, Oklahoma, Kansas, Texas, and Colorado, *in* D. K. Higley, ed., Petroleum systems and assessment of undiscovered oil and gas in the Anadarko Basin province, Colorado, Kansas, Oklahoma, and Texas—USGS Province 58: U.S. Geological Survey Digital Data Series DDS–69–EE, 42 p.

Hanson, R. E., R. E. Puckett, G. R. Keller, M. E. Brueseke, C. L. Bulen, S. A. Mertzman, S. A. Finegan, and D. A. McCleery, 2013, Intraplate magmatism related to opening of the southern Iapetus Ocean: Cambrian Wichita Igneous Province in the Southern Oklahoma rift zone: Lithos, v. 174, p. 57–70.

Hendrickson, W. J., P. W. Smith, and R.J. Woods, 2001, Regional correlation of mountain-front "washes" and relationship to marine sediments of Anadarko Basin and shelf, *in* K. S. Johnson, ed., Pennsylvanian and Permian geology and petroleum in the southern Midcontinent, 1998 symposium: OGS Circular 104, p. 71-80.

Hesse, R., and U. Schacht, 2011, Early diagenesis of deep-sea sediments, *in* H. HüNeke and T. Mulder, eds., Deep-Sea Sediments: Amersterdam, The Netherlands, Elsevier, v. 63, p. 557–713.

Hill, G. W., 1984, The Anadarko Basin: a model for regional petroleum accumulations: Technical Proceedings of the 1981 American Association of Petroleum Geologists Mid-Continent Regional Meeting, p. 1-23.

Howell, D. G., and W. R. Normark, 1982, Sedimentology of submarine fans, *in* P. A. Scholle and D. Spearing, eds., Sandstone depositional environments: American Association of Petroleum Geologists Memoir 31, p. 365-404.

Johnson, K. S., 1989, Geologic evolution of the Anadarko Basin, in K. S. Johnson, ed., Anadarko Basin Symposium, 1988: Norman, Oklahoma, Oklahoma Geological Survey Circular 90, p. 3–12.

Johnson, K.S., 1991, Geologic overview and economic importance of Late Cambrian and Ordovician rocks in Oklahoma, *in* K.S. Johnson, ed., Late Cambrian-Ordovician geology of the southern Midcontinent, 1989 symposium: Norman, Oklahoma, Oklahoma Geological Survey Circular 92, p. 3–14.

Karis, A. M., 2015, Stratigraphy and reservoir characteristics of the Desmoinesian Granite Wash (Marmaton Group), Southern Anadarko Basin: Master's thesis, University of Oklahoma, Norman, Oklahoma, 88 p.

Kushner, B.E., G. S. Soreghan, and M. J. Soreghan, 2022, Late Paleozoic cratonal sink: Distally sourced sediment filled the Anadarko Basin (USA) from multiple source regions: Geosphere, v. 18, no. 6, p. 1831–1850.

Kuykendall, M. D., and R. D. Fritz, 2001, Misener Sandstone of Oklahoma: AAPG Search and Discovery Article #10018, 74 p.

Leary, R. J., P. Umhoefer, M. E. Smith, and N. Riggs, 2017, A three-sided orogen: a new tectonic model for Ancestral Rocky Mountain uplift and basin development: Geology, v. 45, no. 8, p. 735–38.

LoCricchio, E., 2012, Granite Wash play overview, Anadarko Basin: Stratigraphic framework and controls on Pennsylvanian Granite Wash production, Anadarko Basin, Texas and Oklahoma. AAPG Search and Discovery #110163, adapted from oral presentation at forum: Discovery Thinking, at AAPG Annual Convention and Exhibition, Long Beach, California, USA, April 22-25, 2012, 43 slides.

Lowe, D. R., 1976, Subaqueous liquefied sediment flows and their deposits: Sedimentology, v. 23, no. 3, p. 285-308.

Lowe, D. R., and R. D. LoPiccolo, 1974, The characteristics and origins of dish and pillar structures: Journal of Sedimentary Petrology, v. 44, no. 2, p. 484-501.

Lyday, J. R., 1985, Atokan (Pennsylvanian) Berlin Field: Genesis of recycled detrital dolomite reservoir, deep Anadarko Basin, Oklahoma: American Association of Petroleum Geologists Bulletin, v. 69, no. 11, p. 1931-1949.

Marsh, S., and A. Holland, 2016, Comprehensive fault database and interpretive fault map of Oklahoma, Oklahoma Geological Survey Open File Report OF2-2016, 15 p.

McGowen, J. H., 1971a, Alluvial fans and fan deltas: depositional models for some terrigenous clastic wedges: American Association of Petroleum Geologists Bulletin, vol. 55, no. 1, p. 155.

McGowen, J. H., 1971b, Gum Hollow fan delta, Nueces Bay, Texas: The University of Texas at Austin, Bureau of Economic Geology Report of Investigations, no. 69, 91 p.

McLennan, S. M., and S. R. Taylor, 1980, Geochemical standards for sedimentary rocks: trace element data for U.S.G.S. standards SCo-1, MAG-1, and SGR-1: Chemical Geology, v. 29, p. 333-343.

McPherson, J. G., G. Shanmugam, and R. J. Moiola, 1987, Fan-deltas and braid deltas: varieties of coarse-grained deltas: Geological Society of America Bulletin, v. 99, no. 3, p. 331-340.

Middleton, G.V., and M. A. Hampton, 1973, Sediment gravity flows: Mechanics of flow and deposition *in* G.V. Middleton and A.H. Bouma, eds., Turbidites and Deep Water Sedimentation, Pacific Section, Society of for Sedimentary Geology, Los Angeles, 38 p.

Mitchell, J. R., 2011, Horizontal drilling of deep Granite Wash reservoirs, Anadarko Basin, Oklahoma and Texas: The Shale Shaker, v. 2, no. 2, p. 118-167.

Montañez, I.P., and C. J. Poulsen, 2013, The late Paleozoic ice age: an evolving paradigm: Annual Review of Earth and Planetary Sciences, v. 41, p. 629–656.

Moore, G. E., 1979, Pennsylvanian Paleogeography of the southern Mid-Continent, *in* Pennsylvanian sandstones of the Mid-Continent: Tulsa Geological Society Special Publication, no. 1, p. 2-12.

Mutti, E., and F. Ricci Lucchi, 1972, Turbidites of the northern Apennines: Introduction to facies analysis (English translation by T.H. Nilson, 1978): International Geology Review, v. 20, p. 125-166.

Parks, M., 2011, Depositional setting and porosity evaluation in Upper Desmoinesian Granite Wash, Buffalo Wallow Field, Hemphill County, Texas: unpublished Master's thesis, Oklahoma State University, Stillwater, Oklahoma, 138 p.

Perry, W. J., 1989, Tectonic evolution of the Anadarko Basin region, Oklahoma: Washington, DC, US Geological Survey Bulletin 1866-A, 19 p.

Philp, R. P., L. Li, and T. X. Nguyen, 2016, Characterization of Granite Wash oils from western Oklahoma and eastern Texas Panhandle: The Shale Shaker, v. 67, no. 4, p. 136-157.

Pittman, E. D., 1979, Porosity, diagenesis, and productive capability of sandstone reservoirs: SEPM Special Publication 26, p. 159-173.

Poppe, L. J., V. F. Paskevich, J. C. Hathaway, and D.S. Blackwood, 2001, A laboratory manual for x-ray powder diffraction: U.S. Geological Survey Open File Report 01-041.

Rascoe, B., and F. J. Adler, 1983, Permo-carboniferous hydrocarbon accumulations, Mid-Continent, U.S.A: American Association of Petroleum Geologists Bulletin, v. 67, no. 6, p. 979-1001.

Rothkopf, B., D. J. Christiansen, H. Godwin, and A. R. Yoelin, 2011, Texas panhandle Granite Wash Formation: horizontal development solutions: paper presented at the SPE Annual Technical Conference and Exhibition, Denver, Colorado, USA, October, 2011.

Sahl, H. L., 1970, Mobeetie Field, Wheeler County, Texas: The Shale Shaker, v. 20, p. 107-115.

Shanmugam, G., 2016, Submarine fans: a critical retrospective (1950-2015): Journal of Paleogeography, v. 5., no. 2, p. 110-184.

Shanmugam, G., 2021, Gravity flows: debris flows, grain flows, liquefied/fluidized flows, turbidity currents, hyperpycnal flows, and contour currents, *in* Mass Transport, Gravity Flows, and Bottom Currents: Downslope and Alongslope Processes and Deposits, Amsterdam, Netherlands, Elsevier, 608 p.

Shanmugam, G. and R. J. Moiola, 1988, Submarine fans: characteristics, models, classification, and reservoir potential: Earth Science Reviews, v. 24, p. 383-428.

Shelby, J. M., 1980, Geologic and economic significance of the upper Morrow Chert Conglomerate reservoir of the Anadarko Basin: Journal of Petroleum Technology, v. 32, p. 489-495.

Thomas, W. A., 2014, The Southern Oklahoma transform-parallel intracratonic fault system, *in* Suneson, N. H., ed., Igneous and Tectonic History of the Southern Oklahoma Aulacogen: Oklahoma Geological Survey Guidebook 38, p. 375-387.

Tunin, Z. T., 2020, Detrital zircon geochronology and provenance analysis of The Desmoinesian (Middle Pennsylvanian) Bartlesville and Red Fork Sandstones, Cherokee Platform and Anadarko Basin, Oklahoma, Master's thesis, Oklahoma State University, Stillwater, Oklahoma, 86 p.

Turko, M., 2019, Structural analysis of the Wichita Uplift and structures in the southeast Anadarko Basin, southern Oklahoma, doctoral dissertation, University of Oklahoma, Norman, Oklahoma, 172 p.

Ulmer-Scholle, D. S., P. Scholle, J. Schieber, and R. Raine, 2014, A color guide to the petrography of sandstones, siltstones, shales and associated Rocks: Tulsa, Oklahoma, American Association of Petroleum Geologists, 526 p.

Walker, R. G., 1978, Deep-water sandstone facies and ancient submarine fans: models for exploration for stratigraphic traps: American Association of Petroleum Geologists Bulletin, v. 62, no. 6, p. 932-966.

Webster, R. E., 1980, Evolution of Southern Oklahoma Aulacogen: Oil and Gas Journal, v. 78, no. 7, p. 150-172.

Wei, Y., and J. Xu, 2016, Granite Wash tight gas reservoir, *in* Ma, Y. Z., and S. A. Holditch, 2016, eds., Unconventional oil and gas resources handbook: Gulf Professional Publishing, p. 449–473.

Wentworth, C. K., 1922, A scale of grade and class terms for clastic sediments: The Journal of Geology, v. 30, no. 5, p. 377-392.

Wickham, J. S., 1978, The Southern Oklahoma Aulacogen, *in* J S. Wickham and R. Denison, Structural style of the Arbuckle region: Geological Society of America South-central Section Field Trip Guidebook 3, p. 8-41.

Wilson, M. D., and E. D. Pittman, 1977, Authigenic clays in sandstones: recognition and influence on reservoir properties and paleoenvironmental analysis: Journal of Sedimentary Petrography, v. 47, no. 1, p. 3-31.

Ye, H., L. Royden, C. Burchfiel, and M. Schuepbach, 1996, Late Paleozoic deformation of interior North America: The greater Ancestral Rocky Mountains: American Association of Petroleum Geologists Bulletin, v. 80, no. 9, p. 1397–1432.

APPENDICES

APPENDIX A: KICKING BIRD #1-20 CORE PHOTOGRAPHS

Core Depth: 12,760.0 – 12,769.9 feet

Core Depth: 12,770.0 – 12,779.9 feet

Core Depth: 12,780.0 – 12,789.9 feet

Core Depth: 12,790.0 – 12,799.9 feet

Core Depth: 12,800.0 – 12,809.9 feet

Core Depth: 12,810.0 – 12,814.5 feet

APPENDIX B: KICKING BIRD #1-20 PETROLOG

Depth (Ft)	Sorting: Poor	Sorting: Moderate	Sorting: Good	Lithology	Color	Sed. Structures
12760			X	Sh	Gray	Laminated Sh
		X		Ss		Laminated Ss with interbedded Sh, rippled, lenses of mud
12761						
						Laminated Ss with interbedded Sh, planar
12762			X	Sh	D. gray	
			X	Ss	L. gray	
			X	Sh	D. gray	
			X	Ss	L. gray	
			X	Sh	D. gray	
12763		X		Ss	L. gray	FUS, lenses of mud at base
			X			
12764			X	Sh	D. gray	Laminated Sh
		X		Ss	L. gray	
			X	Sh	D. gray	
		X		Ss	L. gray	Lenses of mud
						Laminated with interbedded Sh
12765						
			X	Sh	Black	Interbedded Ss
		X		Ss	L. gray	Mud laminae
			X	Sh	D. gray	
12766						
		X		Ss	L. gray	
			X	Sh	D. gray	Planar laminated Sh
				Ss	L. gray	Mud laminae
			X	Sh	D. gray	Planar laminated Sh
12767		X		Ss	L. gray	Mud laminae

													X	Sh	D. gray	Planar laminated Sh
												X		Ss	L. gray	Mud laminae
												X		Ss	D. gray	Interbedded Sh and Ss, planar, Sh laminae
														Sh		
										12768		X		Ss	L. gray	
													X	Sh	Black	Interbedded Ss
												X		Ss	L. gray	
													X	Sh	D. gray	
												X		Ss	L. gray	Mud laminae
										12769						
													X	Sh	D. gray	Laminated
												X		Ss	L. gray	
													X	Sh	D. gray	Laminated
										12770		X		Ss	L. gray	Mud laminae
													X	Sh	D. gray	
												X		Ss	L. gray	Mud laminae
										12771						
												X		Ss	D. gray	Interbedded Sh, planar
														Sh		Interbedded Ss, rippled
												X		Ss	L. gray	
										12772						
														Sh	Gray	Interbedded Ss
												X		Ss	L. gray	Mud laminae
										12773						Mud laminae, rippled
												X		Ss	Gray	
													X	Sh	D. gray	
										12774		X		Ss		Sh with interbeds of Ss
												X		Ss	L. gray	Rippled Ss
										12775						FUS
												X		Ss		

										12776		X		Ss	L. gray	FUS
															D. gray	Laminted with Sh interbeds
										12777		X		Ss	L. gray	Mud laminae
										12778				Sh	D. gray	
														Ss	L. gray	Mud laminae
													X	Sh	D. gray	Sand laminae
										12779		X		Ss	L. gray	
												X		Sh	D. gray	Interbedded Ss
												X		Ss	L. gray	Soft sediment deformation, interbedded Sh
										12780			X	Ss	L. gray	Interbedded Sh, burrow
												X		Ss	Gray	Rippled mud laminae
										12781		X		Ss	D. Gray	Interbedded Sh
												X		Ss	Gray	Mud laminae
													X	Sh	D. gray	Planar interbedded Ss
										12782		X		Ss	Dray	
													X	Sh	D. gray	Planar interbedded Ss
												X		Ss	Gray	
										12783		X		Sh Ss	D. gray	Interbedded Ss and Sh, planar
												X		Ss	L. gray	Mud laminae
												X		Ss Sh	D. gray	Rip-up clasts Crossbedding
										12784	X			Ss	D. gray	Rip-up clasts, Cross bedding
												X		Ss	L. gray	

													X	Sh	D. gray	
										12785				Ss	D. gray	Crossbedded mud Laminae
												X				
													X	Sh	D. gray	Planar, interbedded coarse Ss
										12786		X		Ss	Gray	Planar, interbedded Sh
Missing Core																
																Mud laminae, crossbedded
										12787		X		Ss	Gray	Mud laminae, planar
													X	Sh	D. gray	
												X		Ss		Planar, interbedded Sh
										12788				Ss	L. gray	
														Sh	D. gray	Planar, interbedded Ss
												X		Ss	Gray	
														Sh	D. gray	
														Ss	Gray	Mud Rip-up clasts
										12789						
													X	Sh	D. gray	
																FUS
												X		Ss	Dray	
										12790						
													X	Sh	Black	
																Planar interbedded Sh and mud laminae
												X		Ss	Gray	
										12791						
													X	Sh	D. gray	Planar, Interbedded Ss
																Sh Rip-up clasts
										12792		X		Ss	Gray	
																Planar, Interbedded Ss
													X	Sh	D. gray	
										12793		X		Ss		Planar, Interbedded Sh
													X	Sh		Planar, Interbedded Ss
												X		Ss	Gray	Rippled mud laminae

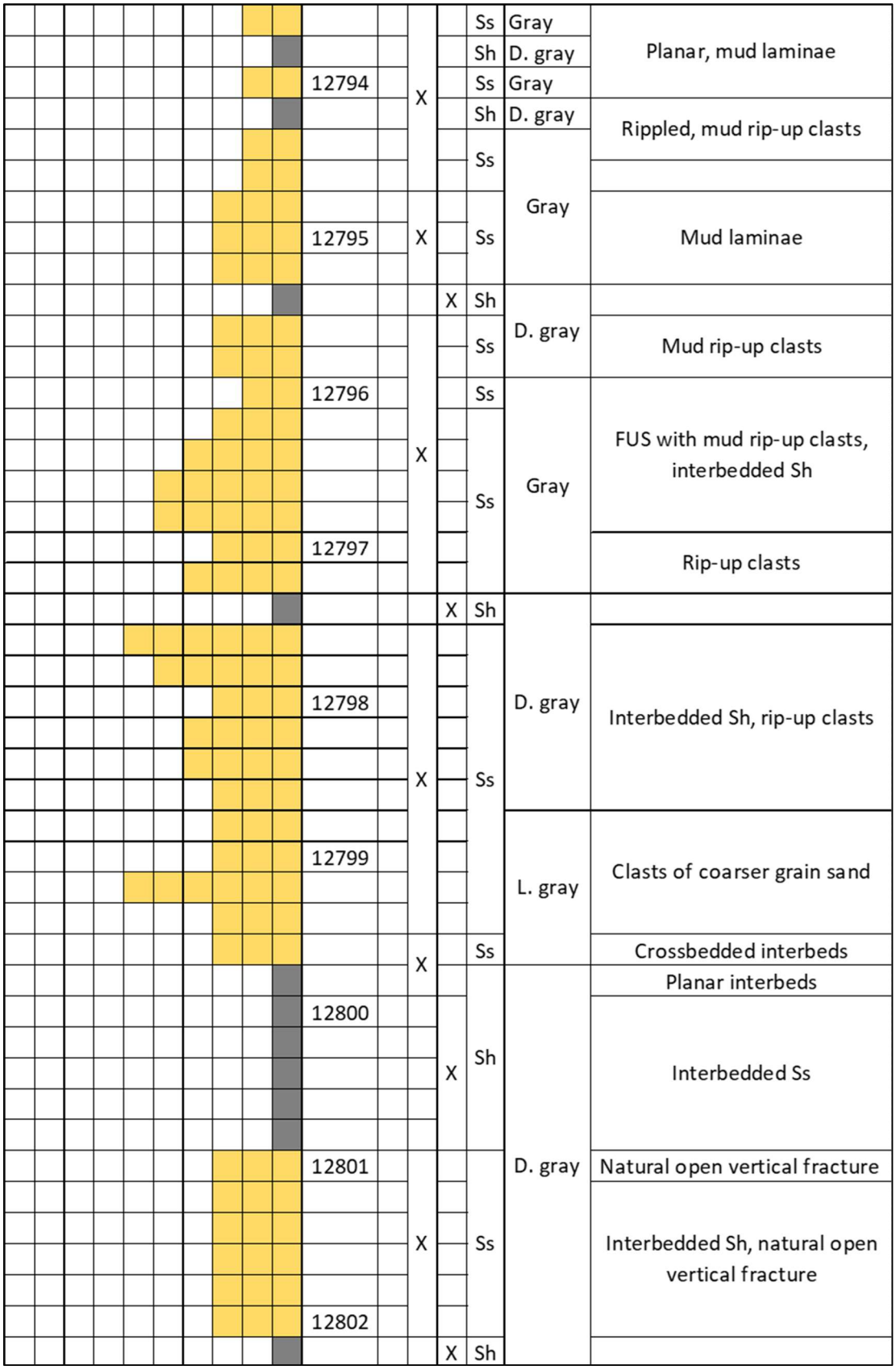
12794
12795
12796
12797
12798
12799
12800
12801
12802
X
Ss
Sh
Gray
D. gray
L. gray
Planar, mud laminae
Rippled, mud rip-up clasts
Mud laminae
Mud rip-up clasts
FUS with mud rip-up clasts, interbedded Sh
Rip-up clasts
Interbedded Sh, rip-up clasts
Clasts of coarser grain sand
Crossbedded interbeds
Planar interbeds
Interbedded Ss
Natural open vertical fracture
Interbedded Sh, natural open vertical fracture

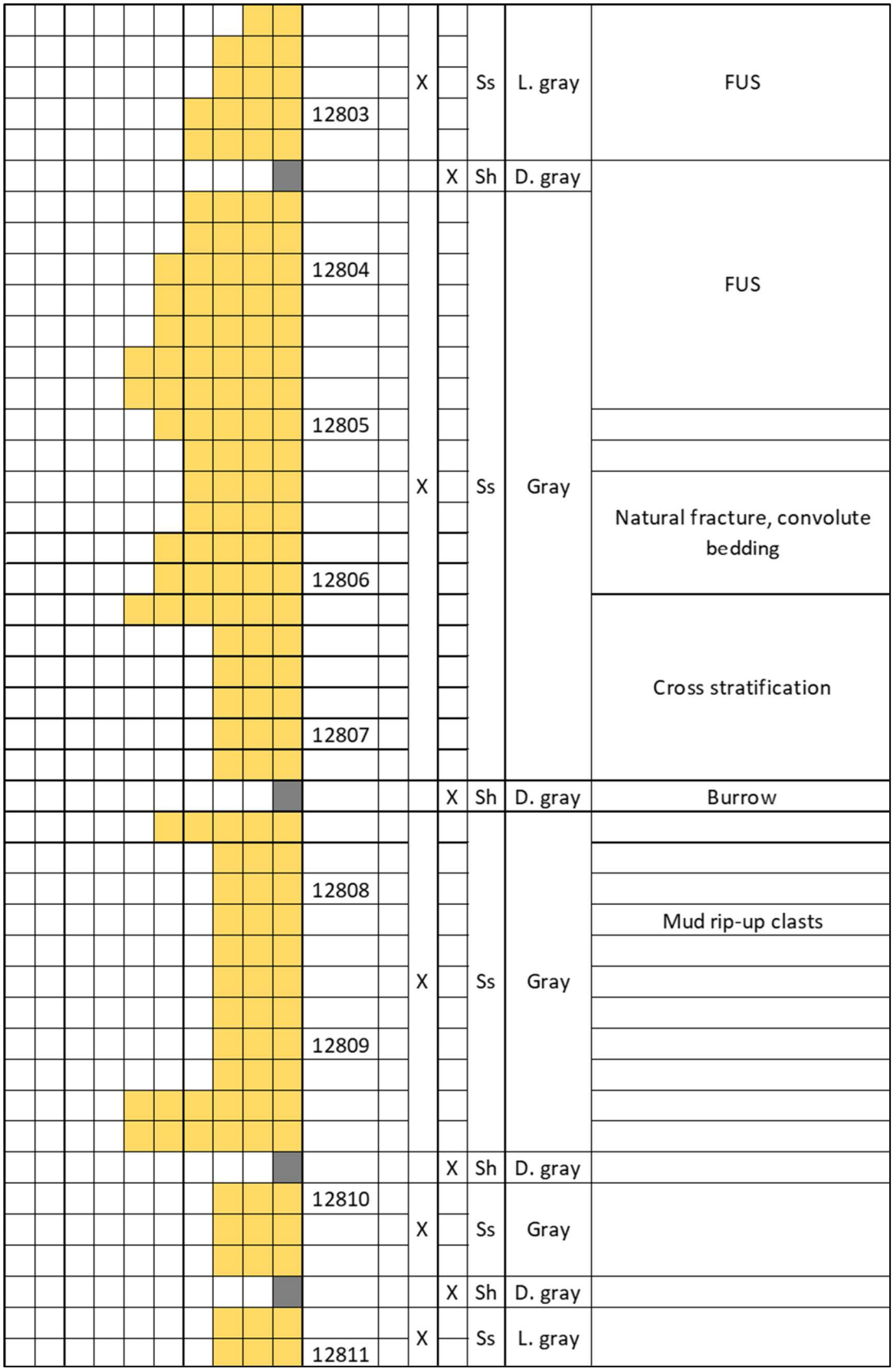
12803
12804
12805
12806
12807
12808
12809
12810
12811
X
Ss
L. gray
FUS
X
Sh
D. gray
FUS
X
Ss
Gray
Natural fracture, convolute bedding
Cross stratification
X
Sh
D. gray
Burrow
X
Ss
Gray
Mud rip-up clasts
X
Sh
D. gray
X
Ss
Gray
X
Sh
D. gray
X
Ss
L. gray

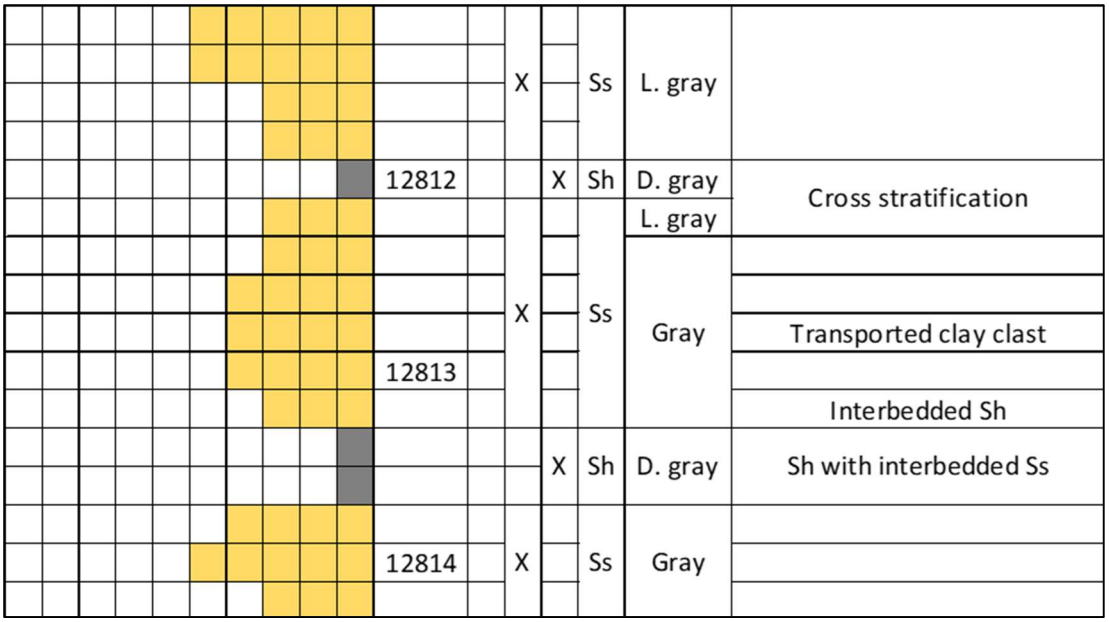
X
Ss
L. gray
12812
X
Sh
D. gray
Cross stratification
L. gray
X
Ss
Gray
Transported clay clast
12813
Interbedded Sh
X
Sh
D. gray
Sh with interbedded Ss
12814
X
Ss
Gray

APPENDIX C: GRANT MEEK #236-1 CORE PHOTOS

Core Depth: 11,333.0 – 11,342.9 feet

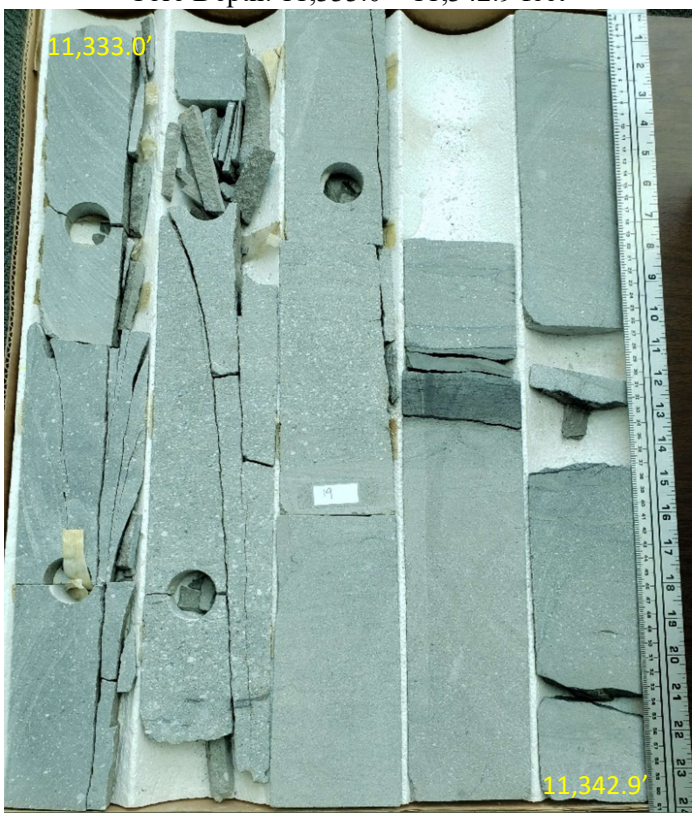

Core Depth: 11,343.0 – 11,352.9 feet

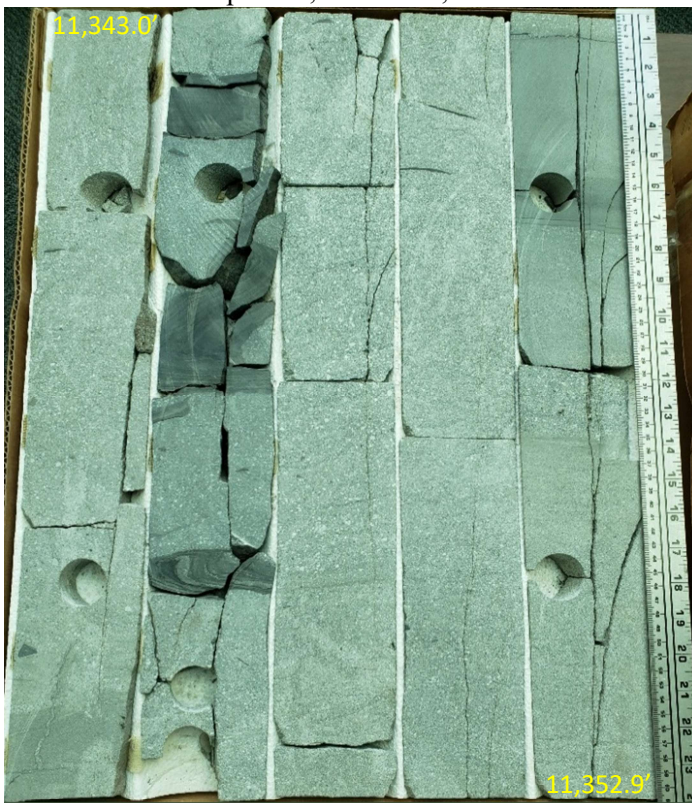

Core Depth: 11,353.0 – 11,362.9 feet

Core Depth: 11,363.0 – 11,362.9 feet

Core Depth: 11,373.0 – 11,382.8 feet

Core Depth: 11,383.4 – 11,392.9 feet

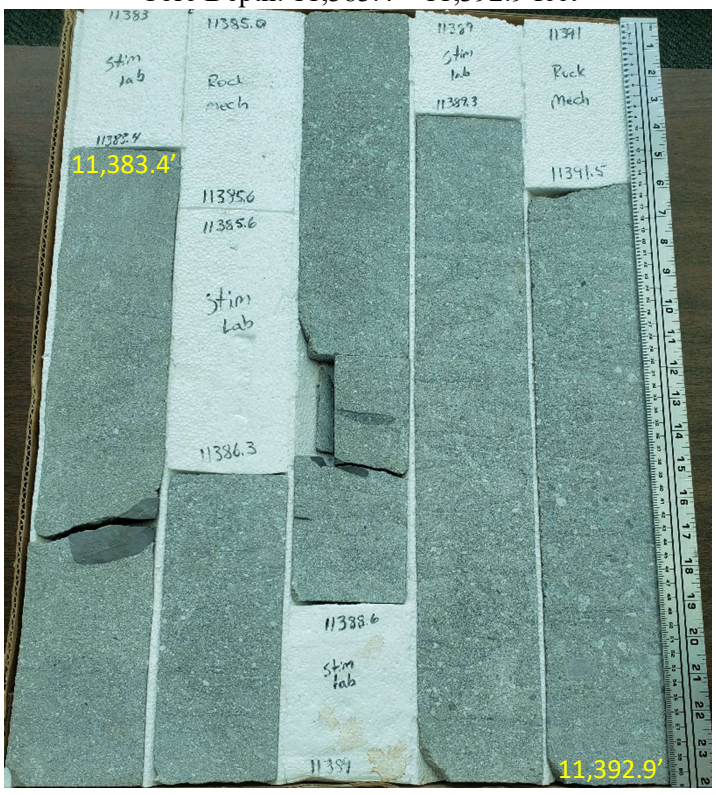

Core Depth: 11,393.4 – 11,402.9 feet

Core Depth: 11,403.0 – 11,412.9 feet

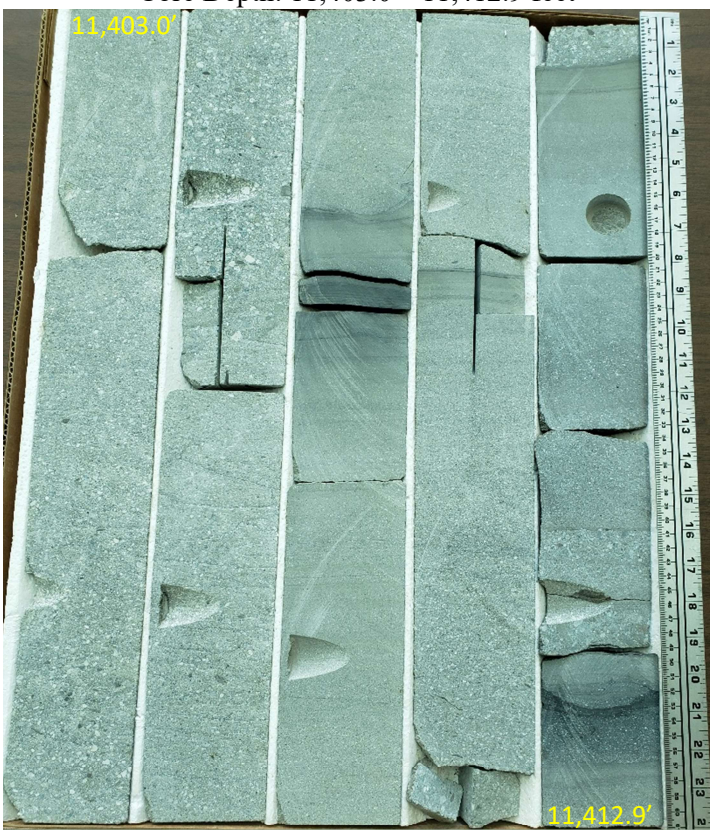

Core Depth: 11,413.0 – 11,422.2 feet

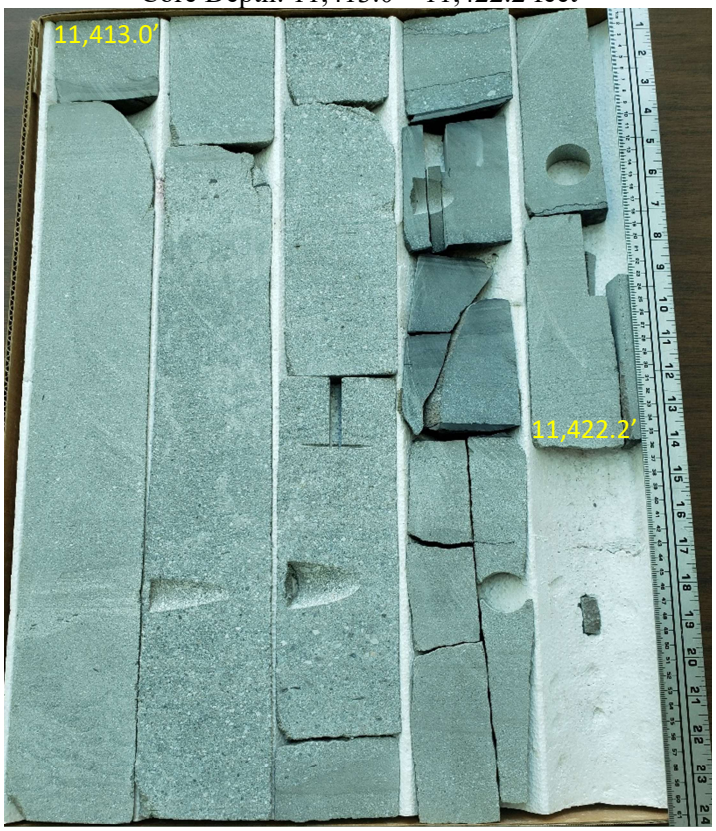

APPENDIX D: GRANT MEEK #236-1 PETROLOG

Gravel			Sand					Mud		Depth	Sorting			Lithology	Color	Sed. Structures
Boulder	Cobble	Pebble	VC Sand	C Sand	M Sand	F Sand	VF Sand	Silt	Clay	(Ft)	Poor	Moderate	Good			
										11333				Ss	Gray	
														Ss	Gray	
												X		Ss	Gray	
														Ss	Gray	
														Ss	Gray	
										11334				Ss	Gray	
														Ss	Gray	
												X		Ss	Gray	
														Ss	Gray	
														Ss	Gray	
										11335				Ss	Gray	
														Ss	L. gray	
												X		Ss	L. gray	
														Ss	L. gray	
														Ss	L. gray	
										11336				Ss	L. gray	Dish and pillar structures
														Ss	L. gray	Dish and pillar structures
											X			Ss	L. gray	Dish and pillar structures
														Ss	L. gray	Flat mud clasts
														Ss	L. gray	Flat mud clasts
										11337		X		Ss	L. gray	FUS
													X	Ss	L. gray	Sharp planar contact
														Ss	L. gray	Dish and pillar structures
												X		Ss	L. gray	Dish and pillar structures
														Ss	L. gray	Dish and pillar structures
										11338				Ss	L. gray	FUS
													X	Ss	L. gray	Sharp planar contact
														Ss	L. gray	
												X		Ss	L. gray	
														Ss	L. gray	Planar mud laminae, FUS
Missing Core: 11,339.0- 11,339.7'																
												X		Ss	Gray	Lenses of finer sand
										11340			X	Ss	D. gray	Mud clasts
												X		Ss	L. gray	Dish and pillar structures
														Ss	L. gray	

												X		Ss	L. gray	
														Ss	L. gray	
										11341				Ss	L. gray	FUS
												X		Ss	L. gray	Sharp planar contact
														Ss	L. gray	
														Ss	L. gray	
												X		Ss	L. gray	FUS
Missing Core: 11,342.1- 11,342.3'																
														Ss	L. gray	
												X		Ss	L. gray	
														Ss	L. gray	FUS, mud clasts
														Ss	L. gray	Sharp planar contact
										11343				Ss	L. gray	
														Ss	L. gray	
												X		Ss	L. gray	Dish and pillar structures
														Ss	L. gray	Mud clasts
														Ss	L. gray	
										11344				Ss	L. gray	
											X			Ss	L. gray	
														Ss	L. gray	Large (0.5") angular clast
														Ss	L. gray	Sand dike/pillar structure
												X		Ss	L. gray	Sharp planar contact
										11345		X		Ss	L. gray	Mud clasts
													X	Sh	D. gray	Sand dike/pillar structure
												X		Ss	L. gray	Flat mud clasts
														Ss	L. gray	Cross-bedded sand laminae
													X	Sh	D. gray	
										11346				Sh	D. gray	Planar mud laminae
												X		Ss	L. gray	
														Ss	L. gray	Flat mud clasts
													X	Sh	D. gray	Soft sediment deformation
												X		Ss	L. gray	Sharp planar contact
										11347				Ss	L. gray	Mud clasts
														Ss	L. gray	
												X		Ss	L. gray	
														Ss	L. gray	Dish and pillar structures
														Ss	L. gray	Dish and pillar structures
										11348				Ss	L. gray	Dish and pillar structures
														Ss	L. gray	Mud clasts
												X		Ss	L. gray	Dish and pillar structures
														Ss	L. gray	FUS
														Ss	L. gray	Sharp planar contact
										11349		X		Ss	L. gray	Flat planar mud clasts
														Ss	L. gray	

															Ss	L. gray	
															Ss	L. gray	
															Ss	L. gray	
										11350					Ss	L. gray	
												X			Ss	L. gray	
															Ss	L. gray	Mud clasts
															Ss	L. gray	Dish and pillar structures
															Ss	L. gray	
										11351					Ss	L. gray	FUS
														X	Ss	L. gray	Stylolite at sharp contact
															Ss	Gray	
												X			Ss	L. gray	
													X		Ss	L. gray	Planar mud laminae, sharp contact
										11352					Ss	L. gray	
															Ss	L. gray	Sharp planar contact
												X			Ss	L. gray	
															Ss	L. gray	Dish and pillar structures
															Ss	L. gray	FUS
										11353					Ss	L. gray	Dish and pillar structures
															Ss	L. gray	Dish and pillar structures
												X			Ss	L. gray	Dish and pillar structures
															Ss	L. gray	Dish and pillar structures
															Ss	L. gray	Dish and pillar structures
										11354					Ss	L. gray	Dish and pillar structures
															Ss	L. gray	Dish and pillar structures
												X			Ss	L. gray	Sharp planar contact
															Ss	L. gray	Mud clasts
															Ss	L. gray	FUS
										11355					Ss	L. gray	
															Ss	L. gray	
												X			Ss	L. gray	
															Ss	L. gray	
															Ss	L. gray	
										11356		X			Ss	L. gray	
															Ss	L. gray	
															Ss	L. gray	
												X			Ss	L. gray	Mud clasts
															Ss	L. gray	
										11357					Ss	L. gray	Mud clasts
												X			Ss	L. gray	FUS
														X	Ss	Gray	Sharp planar contact
															Ss	L. gray	Planar mud laminae
												X			Ss	L. gray	
										11358					Ss	L. gray	

														Ss	L. gray	
												X		Ss	L. gray	
														Ss	L. gray	Sharp planar contact
														Ss	L. gray	Cemented fracture
										11359				Ss	L. gray	Planar mud laminae
														Ss	L. gray	
												X		Ss	L. gray	
														Ss	L. gray	Stylolite, sharp angular contact
														Ss	L. gray	
										11360				Ss	L. gray	
														Ss	L. gray	Stylolite, sharp planar contact
												X		Ss	L. gray	
														Ss	L. gray	Sharp angular contact
														Ss	Gray	Stylolite
										11361		X		Ss	Gray	Sharp planar contact
													X	Sh	Black	
														Ss	L. gray	
												X		Ss	L. gray	
														Ss	L. gray	Sharp angular contact
										11362				Ss	L. gray	
														Ss	L. gray	
												X		Ss	L. gray	Stylolite, sharp angular contact
														Ss	L. gray	Stylolite,sharp angular contact
														Ss	L. gray	
										11363				Ss	L. gray	
												X		Ss	L. gray	
														Ss	L. gray	Stylolite, sharp angular contact
														Ss	L. gray	
													X	Sh	Black	Sharp planar contact
										11364				Ss	L. gray	
														Ss	L. gray	Sharp planar contact
												X		Ss	L. gray	
														Ss	L. gray	
														Ss	L. gray	Dish and pillar structures
										11365				Ss	L. gray	Dish and pillar structures
														Ss	L. gray	Dish and pillar structures
												X		Ss	L. gray	Dish and pillar structures
														Ss	L. gray	Mud clasts
														Ss	L. gray	Dish and pillar structures
										11366				Ss	L. gray	Dish and pillar structures
														Ss	L. gray	Dish and pillar structures
												X		Ss	L. gray	Dish and pillar structures
														Ss	L. gray	Dish and pillar structures
														Ss	L. gray	Dish and pillar structures

										11367		X		Ss	L. gray	FUS
														Ss	L. gray	Sharp planar contact
														Ss	L. gray	
														Ss	L. gray	Sharp planar contact
														Ss	L. gray	
Missing Core: 11,367.9- 11,369.2'																
												X		Ss	L. gray	
														Ss	L. gray	
														Ss	L. gray	Sharp angular contact
														Ss	L. gray	
										11370		X		Ss	L. gray	Sharp planar contact
														Ss	L. gray	Dish and pillar structures
														Ss	L. gray	Dish and pillar structures
														Ss	L. gray	Dish and pillar structures
														Ss	L. gray	Dish and pillar structures
										11371		X		Ss	L. gray	
														Ss	L. gray	
														Ss	L. gray	
														Ss	L. gray	
														Ss	L. gray	
										11372		X		Ss	L. gray	
														Ss	L. gray	FUS
														Ss	L. gray	Sharp angular contact
														Ss	L. gray	
														Ss	L. gray	Dish and pillar structures
										11373		X		Ss	L. gray	Dish and pillar structures
														Ss	L. gray	FUS
														Ss	L. gray	Sharp planar contact
														Ss	L. gray	
														Ss	L. gray	
										11374		X		Ss	L. gray	Dish and pillar structures
														Ss	L. gray	Dish and pillar structures
														Ss	L. gray	Dish and pillar structures
														Ss	L. gray	Dish and pillar structures
														Ss	L. gray	FUS
										11375		X		Ss	L. gray	Sharp angular contact
														Ss	L. gray	Dish and pillar structures
														Ss	L. gray	Dish and pillar structures
														Ss	L. gray	Dish and pillar structures

												X		Ss	L. gray	Dish and pillar structures
										11376				Ss	L. gray	Dish and pillar structures
														Ss	L. gray	Dish and pillar structures
												X		Ss	L. gray	Dish and pillar structures
														Ss	L. gray	Dish and pillar structures
														Ss	L. gray	Dish and pillar structures
										11377				Ss	L. gray	Dish and pillar structures
														Ss	L. gray	Dish and pillar structures
												X		Ss	L. gray	Dish and pillar structures
														Ss	L. gray	Dish and pillar structures
														Ss	L. gray	Dish and pillar structures
										11378				Ss	L. gray	Dish and pillar structures
														Ss	L. gray	Dish and pillar structures
												X		Ss	L. gray	Dish and pillar structures
														Ss	L. gray	FUS
														Ss	L. gray	
										11379				Ss	L. gray	
														Ss	L. gray	Stylolite at planar contact
												X		Ss	L. gray	Dish and pillar structures
														Ss	L. gray	Dish and pillar structures
														Ss	L. gray	Dish and pillar structures
										11380				Ss	L. gray	Dish and pillar structures
														Ss	L. gray	Dish and pillar structures
												X		Ss	L. gray	Dish and pillar structures
														Ss	L. gray	FUS
														Ss	L. gray	Sharp angular contact
										11381				Ss	L. gray	
														Ss	L. gray	Dish and pillar structures
												X		Ss	L. gray	Dish and pillar structures
														Ss	L. gray	Dish and pillar structures
														Ss	L. gray	Dish and pillar structures
										11382				Ss	L. gray	Dish and pillar structures
												X		Ss	L. gray	
														Ss	L. gray	FUS
													X	Sh	D. gray	Sharp angular contact
Missing Core: 11,382.8- 11,383.4'																
														Ss	L. gray	
												X		Ss	L. gray	
														Ss	L. gray	Dish and pillar structures
										11384				Ss	L. gray	Dish and pillar structures
												X		Ss	L. gray	
														Ss	L. gray	

												X		Ss	L. gray	
														Ss	L. gray	FUS
Missing Core: 11,385.0- 11,386.3'																
												X		Ss	L. gray	Dish and pillar structures
														Ss	L. gray	
														Ss	L. gray	
														Ss	L. gray	
										11387		X		Ss	L. gray	
														Ss	L. gray	Dish and pillar structures
														Ss	L. gray	FUS
														Ss	L. gray	Sharp angular contact
														Ss	L. gray	Dish and pillar structures
										11388		X		Ss	L. gray	Large planar mud clasts
														Ss	L. gray	Large planar mud clasts
														Ss	L. gray	FUS
Missing Core: 11,388.6- 11,389.3'																
												X		Ss	L. gray	Dish and pillar structures
														Ss	L. gray	Dish and pillar structures
														Ss	L. gray	Dish and pillar structures
														Ss	L. gray	Dish and pillar structures
										11390		X		Ss	L. gray	Dish and pillar structures
														Ss	L. gray	Dish and pillar structures
														Ss	L. gray	Dish and pillar structures
														Ss	L. gray	Dish and pillar structures
														Ss	L. gray	Dish and pillar structures
Missing Core: 11,391.0- 11,391.5'																
												X		Ss	L. gray	Dish and pillar structures
														Ss	L. gray	Dish and pillar structures
										11392		X		Ss	L. gray	Dish and pillar structures
														Ss	L. gray	Dish and pillar structures
														Ss	L. gray	
														Ss	L. gray	
														Ss	L. gray	
Missing Core: 11,393.0- 11,393.4'																

Missing Core: 11,393.0- 11,393.4'																
												X		Ss	L. gray	
														Ss	L. gray	Large planar mud clasts
										11394				Ss	L. gray	
														Ss	L. gray	Stylolite, small mud clast
												X		Ss	L. gray	
														Ss	L. gray	
														Ss	L. gray	
										11395				Ss	L. gray	
														Ss	L. gray	
												X		Ss	L. gray	
														Ss	L. gray	
														Ss	L. gray	
										11396				Ss	L. gray	Sharp angular contact
														Ss	L. gray	Dish and pillar structures
												X		Ss	L. gray	Dish and pillar structures
														Ss	L. gray	Dish and pillar structures
														Ss	L. gray	Dish and pillar structures
										11397				Ss	L. gray	Dish and pillar structures
														Ss	L. gray	
												X		Ss	L. gray	
														Ss	L. gray	
														Ss	L. gray	
										11398				Ss	L. gray	
														Ss	L. gray	
												X		Ss	L. gray	
														Ss	L. gray	
														Ss	L. gray	
										11399				Ss	L. gray	
														Ss	L. gray	
												X		Ss	L. gray	Sharp angular contact
														Ss	L. gray	
														Ss	L. gray	
										11400				Ss	L. gray	Dish and pillar structures
														Ss	L. gray	Dish and pillar structures
												X		Ss	L. gray	Dish and pillar structures
														Ss	L. gray	Dish and pillar structures
														Ss	L. gray	
										11401				Ss	L. gray	
														Ss	L. gray	
												X		Ss	L. gray	
														Ss	L. gray	Sand dike/pillar structure
														Ss	L. gray	Sharp angular contact
										11402		X		Ss	L. gray	

														Ss	L. gray	
												X		Ss	L. gray	Fluid escape features
														Ss	L. gray	Fluid escape features
														Ss	L. gray	Fluid escape features
										11403				Ss	L. gray	
														Ss	L. gray	
												X		Ss	L. gray	
														Ss	L. gray	
														Ss	L. gray	
										11404				Ss	L. gray	
														Ss	L. gray	
												X		Ss	L. gray	
														Ss	L. gray	
														Ss	L. gray	
										11405				Ss	L. gray	
														Ss	L. gray	
												X		Ss	L. gray	
														Ss	L. gray	
														Ss	L. gray	Sharp angular contact
										11406				Ss	L. gray	
														Ss	L. gray	Stylolite
												X		Ss	L. gray	Dish and pillar structures
														Ss	L. gray	Dish and pillar structures
														Ss	L. gray	
										11407				Ss	L. gray	
														Ss	L. gray	Sharp angular contact
												X		Ss	L. gray	Dish and pillar structures
														Ss	L. gray	Flame structure
														Ss	L. gray	Thin planar mud beds
										11408				Ss	L. gray	
														Ss	L. gray	
												X		Ss	L. gray	
														Ss	L. gray	
														Ss	L. gray	
										11409				Ss	L. gray	
														Ss	L. gray	Dish and pillar structures
												X		Ss	L. gray	
														Ss	L. gray	Sharp angular contact
														Ss	L. gray	Thin planar mud beds
										11410				Ss	L. gray	
														Ss	L. gray	
												X		Ss	L. gray	
														Ss	L. gray	Mud clasts
														Ss	L. gray	

										11411		X		Ss	L. gray	
														Ss	L. gray	Sharp angular contact
														Ss	L. gray	Thin planar mud beds
														Ss	L. gray	
														Ss	L. gray	
										11412		X		Ss	L. gray	
														Ss	L. gray	
														Ss	L. gray	
														Ss	L. gray	Sharp angular contact
														Ss	L. gray	
										11413		X		Ss	L. gray	
														Ss	L. gray	
														Ss	L. gray	Sharp angular contact
														Ss	L. gray	
														Ss	L. gray	
										11414		X		Ss	L. gray	
														Ss	L. gray	
														Ss	L. gray	
														Ss	L. gray	Dish and pillar structures
														Ss	L. gray	
										11415		X		Ss	L. gray	Mud clasts
														Ss	L. gray	Thin planar mud beds
														Ss	L. gray	Dish and pillar structures
														Ss	L. gray	
														Ss	L. gray	
										11416		X		Ss	L. gray	Dish and pillar structures
														Ss	L. gray	
														Ss	L. gray	
														Ss	L. gray	
														Ss	L. gray	
										11417		X		Ss	L. gray	
														Ss	L. gray	
														Ss	L. gray	
														Ss	L. gray	
														Ss	L. gray	
										11418		X		Ss	L. gray	
														Ss	L. gray	
														Ss	L. gray	Sharp angular contact
														Ss	L. gray	
														Ss	L. gray	
										11419		X		Ss	L. gray	Stylolite
														Ss	L. gray	Sharp angular contact
														Ss	L. gray	
														Ss	L. gray	

												X		Ss	L. gray	
										11420			X	Sh	D. gray	
														Ss	L. gray	Stylolite
												X		Ss	L. gray	
														Ss	L. gray	
														Ss	L. gray	
										11421				Ss	L. gray	
														Ss	L. gray	
												X		Ss	L. gray	
														Ss	L. gray	Stylolite
														Ss	L. gray	Mud laminae
										11422		X		Ss	L. gray	Dish and pillar structures
End of core: 11,422.2'																

APPENDIX E: FILLINGIM #88-2 CORE PHOTOS

Core Depth: 11,402.0 – 11,409.9 feet

Core Depth: 11,410.0 – 11,419.8 feet

Core Depth: 11,420.3 – 11,427.9 feet

Core Depth: 11,429.0 – 11,436.9 feet

Core Depth: 11,437.0 – 11,445.9 feet

Core Depth: 11,446.0 – 11,452.9 feet

Core Depth: 11,453.0 – 11,459.9 feet

Core Depth: 11,460.0 – 11,463.9 feet

APPENDIX F: FILLINGIM #88-2 PETROLOG

Gravel			Sand					Mud		Depth	Sorting			Lithology	Color	Sed. Structures
Boulder	Cobble	Pebble	VC Sand	C Sand	M Sand	F Sand	VF Sand	Silt	Clay	(Ft)	Poor	Moderate	Good			
										11402			X	Sh	D. gray	Bioturbation
														Sh	D. gray	Bioturbation
														Ss	Gray	Sharp planar contact
												X		Ss	Gray	
														Ss	Gray	
										11403				Ss	Gray	
														Ss	Gray	
												X		Ss	Gray	Planar mud laminae
														Ss	Gray	Planar mud clasts
														Ss	Gray	FUS
										11404			X	Sh	D. gray	Bioturbation
														Ss	Gray	Planar mud laminae
												X		Ss	Gray	
														Ss	Gray	
														Ss	Gray	FUS
										11405			X	Sh	D. gray	
														Ss	Gray	
												X		Ss	Gray	
														Ss	Gray	FUS
														Sh	D. gray	Sand dike/pillar structure
										11406				Ss	Gray	Planar mud laminae
														Ss	Gray	
												X		Ss	Gray	
														Ss	Gray	Dish and pillar structures
														Ss	Gray	
										11407				Ss	Gray	
														Ss	Gray	
												X		Ss	Gray	
														Ss	Gray	
														Ss	Gray	
										11408				Ss	Gray	
														Ss	Gray	
												X		Ss	Gray	
														Ss	Gray	
														Ss	Gray	
										11409				Ss	Gray	
												X		Ss	Gray	
														Ss	Gray	

														Ss	Gray	
											X			Ss	Gray	
									11410					Ss	Gray	
														Ss	Gray	
											X			Ss	Gray	
														Ss	Gray	
														Ss	Gray	
									11411					Ss	Gray	FUS
														Ss	Gray	Sharp angular contact
											X			Ss	Gray	Sharp angular contact
														Ss	Gray	Mud clast
														Ss	Gray	Dish and pillar structures
									11412					Ss	Gray	Dish and pillar structures
														Ss	Gray	Dish and pillar structures
											X			Ss	Gray	
														Ss	Gray	
														Ss	Gray	
									11413					Ss	Gray	
														Ss	Gray	
											X			Sh	D. gray	Sharp angular contact
														Ss	Gray	Planar mud laminae
														Ss	Gray	Planar mud laminae
									11414					Ss	Gray	
														Ss	Gray	Planar mud laminae
											X			Ss	Gray	
														Ss	Gray	Dish and pillar structures
														Ss	Gray	FUS

Missing core: 11,415.0- 11,417.8'

									11418					Ss	Gray	Planar mud laminae
											X			Ss	Gray	

														Ss	Gray	Dish and pillar structures
												X		Ss	Gray	Dish and pillar structures
														Ss	Gray	Dish and pillar structures
										11419		X		Ss	Gray	Dish and pillar structures
														Ss	Gray	FUS
													X	Sh	D. gray	Flame structure
												X		Ss	Gray	
														Ss	Gray	Planar mud laminae
										11420				Ss	Gray	Dish and pillar structures
														Ss	Gray	FUS
												X		Ss	Gray	Sharp planar contact
														Ss	Gray	Planar mud laminae
														Ss	Gray	
										11421				Ss	Gray	
														Ss	Gray	
												X		Ss	Gray	
														Ss	Gray	
														Ss	Gray	
										11422				Ss	Gray	
														Ss	Gray	FUS
												X		Ss	Gray	Sharp planar contact
														Ss	Gray	Planar mud laminae
														Ss	Gray	
										11423				Ss	Gray	Dish and pillar structures
														Ss	Gray	
												X		Ss	Gray	
														Ss	Gray	Mud rip-up clasts
														Ss	Gray	
										11424				Ss	Gray	
														Ss	Gray	
												X		Ss	Gray	Planar mud clasts
														Ss	Gray	FUS
												X		Ss	D. gray	Sharp planar contact
										11425				Ss	Gray	
														Ss	Gray	
												X		Ss	Gray	
														Ss	Gray	
														Ss	Gray	
										11426				Ss	Gray	
														Ss	Gray	
												X		Ss	Gray	
														Ss	Gray	
														Ss	Gray	
										11427				Ss	Gray	

														Ss	Gray	FUS
												X		Ss	D. gray	Planar mud laminae
														Ss	Gray	
														Ss	Gray	Planar mud laminae
Missing core: 11,428.0- 11,429.0'																
										11429		X		Ss	Gray	Mud rip-up clasts
														Ss	Gray	FUS
													X	Sh	D. gray	Sand lenses
												X		Ss	Gray	Sharp planar contact
														Ss	Gray	
										11430				Ss	Gray	
														Ss	Gray	
												X		Ss	Gray	
														Ss	Gray	
														Ss	Gray	
										11431				Ss	Gray	
														Ss	Gray	
												X		Ss	Gray	FUS
														Ss	Gray	Sharp planar contact
														Ss	Gray	
										11432				Ss	Gray	
														Ss	Gray	
												X		Ss	Gray	
														Ss	Gray	
														Ss	Gray	
										11433				Ss	Gray	
														Ss	Gray	
												X		Ss	Gray	
														Ss	Gray	Calcite concretion
														Ss	Gray	
										11434				Ss	Gray	
														Ss	Gray	
												X		Ss	Gray	
														Ss	Gray	FUS
												X		Sh	D. gray	Sharp planar contact
										11435				Ss	Gray	Planar mud clasts
														Ss	Gray	
												X		Ss	Gray	Dish and pillar structures
														Ss	Gray	Dish and pillar structures
														Ss	Gray	Dish and pillar structures

										11436		X		Ss	Gray	
													X	Sh	D. gray	Sharp angular contact
												X		Ss	Gray	Planar mud laminae
													X	Sh	D. gray	Sharp planar contact
												X		Ss	Gray	Planar mud laminae
										11437				Ss	Gray	
												X		Ss	Gray	
														Ss	Gray	
														Ss	Gray	FUS
													X	Sh	D. gray	Sharp planar contact
										11438		X		Ss	Gray	Gradual contact
														Ss	Gray	Mud clasts
														Ss	Gray	Planar mud laminae
												X		Ss	Gray	FUS
														Ss	Gray	Sharp planar contact
										11439				Ss	Gray	
												X		Ss	Gray	
														Ss	Gray	FUS
Missing core: 11,439.5- 11,440.0																
										11440			X	Sh	D. gray	
														Ss	Gray	
												X		Ss	Gray	Planar mud laminae
														Ss	Gray	
														Ss	Gray	Mud rip-up clasts
										11441				Ss	Gray	
														Ss	Gray	
												X		Ss	Gray	
														Ss	Gray	
														Ss	Gray	
										11442				Ss	Gray	
														Ss	Gray	
												X		Ss	Gray	Large (2+") round clast
														Ss	Gray	
														Ss	Gray	
										11443				Ss	Gray	FUS
														Ss	Gray	
												X		Ss	Gray	Dish and pillar structures
														Ss	Gray	Dish and pillar structures
														Ss	Gray	Angular mud laminae
										11444				Ss	Gray	FUS
												X		Ss	Gray	Sharp planar contact
														Ss	Gray	Bioturbation
														Ss	Gray	Dish and pillar structures

												X		Ss	Gray	Dish and pillar structures
										11445				Ss	Gray	
														Ss	Gray	Planar mud clasts
												X		Ss	Gray	
														Ss	Gray	Dish and pillar structures
														Ss	Gray	Dish and pillar structures
										11446				Ss	Gray	
														Ss	Gray	
												X		Ss	Gray	
														Ss	Gray	
														Ss	Gray	
										11447				Ss	Gray	
												X		Ss	Gray	
														Ss	Gray	
														Ss	Gray	
												X		Ss	Gray	FUS
										11448			X	Sh	D. gray	
														Sh	D. gray	Sand lenses
												X		Ss	Gray	Planar mud laminae
													X	Sh	D. gray	Sand lenses
												X		Ss	Gray	Wavy angular contact
										11449			X	Sh	D. gray	
														Ss	Gray	Sharp planar contact
												X		Ss	Gray	
														Ss	Gray	
														Ss	Gray	
										11450				Ss	Gray	
														Ss	Gray	
												X		Ss	Gray	
														Ss	Gray	
														Ss	Gray	
										11451				Ss	Gray	
														Ss	Gray	
												X		Ss	Gray	FUS
														Ss	Gray	Wavy planar contact
														Ss	Gray	Planar mud laminae
										11452				Ss	Gray	
														Ss	Gray	
												X		Ss	Gray	
														Ss	Gray	
														Ss	Gray	
										11453				Ss	Gray	
												X		Ss	Gray	
														Ss	Gray	

												X		Ss	Gray	
														Ss	Gray	
										11454				Ss	Gray	Calcite concretions
														Ss	Gray	
												X		Ss	Gray	
														Ss	Gray	Dish and pillar structures
														Ss	Gray	Dish and pillar structures
										11455				Ss	Gray	Dish and pillar structures
														Ss	Gray	Dish and pillar structures
												X		Ss	Gray	
														Ss	Gray	
														Ss	Gray	Dish and pillar structures
										11456				Ss	Gray	
														Ss	Gray	FUS
												X		Ss	Gray	Sharp angular contact
														Ss	Gray	Soft sediment deformation
														Ss	Gray	Mud rip-up clasts
										11457		X		Ss	Gray	
														Ss	Gray	
												X		Ss	Gray	Mud rip-up clasts
														Ss	Gray	
														Ss	Gray	
										11458				Ss	Gray	
														Ss	Gray	
												X		Ss	Gray	
														Ss	Gray	
														Ss	Gray	
										11459				Ss	Gray	
														Ss	Gray	
												X		Ss	Gray	
														Ss	Gray	
														Ss	Gray	
										11460				Ss	Gray	
														Ss	Gray	
												X		Ss	Gray	
														Ss	Gray	
														Ss	Gray	
										11461				Ss	Gray	
														Ss	Gray	
												X		Ss	Gray	
														Ss	Gray	
														Ss	Gray	
										11462		X		Ss	Gray	
														Ss	Gray	Sharp planar contact

												X		Ss	Gray	
													X	Sh	D. gray	Sharp planar contact
												X		Ss	Gray	
										11463				Ss	Gray	
														Ss	Gray	
												X		Ss	Gray	
														Ss	Gray	
														Ss	Gray	

VITA

Autumn M. Graf

Candidate for the Degree of

Master of Science

Thesis: DEPOSITIONAL SETTING AND CONTROLS ON POROSITY DEVELOPMENT IN THE MARMATON GRANITE WASH, SOUTHWESTERN ANADARKO BASIN, WESTERN OKLAHOMA AND TEXAS PANHANDLE

Major Field: Geology

Biographical:

Education:

Completed the requirements for the Master of Science in geology at Oklahoma State University, Stillwater, Oklahoma in May, 2023.

Completed the requirements for the Bachelor of Science in geology at Oklahoma State University, Stillwater, Oklahoma in 2021.

Experience:

Graduate Research Assistant – Boone Pickens School of Geology, Stillwater, Oklahoma, August 2021 to May 2023

Geoscience Intern – EOG Resources, Inc., Oklahoma City, Oklahoma, Summer 2023

Professional Memberships:

American Association of Petroleum Geologists (AAPG), Geological Society of America (GSA), Society for Sedimentary Geology (SEPM), Tulsa Geological Society (TGS)